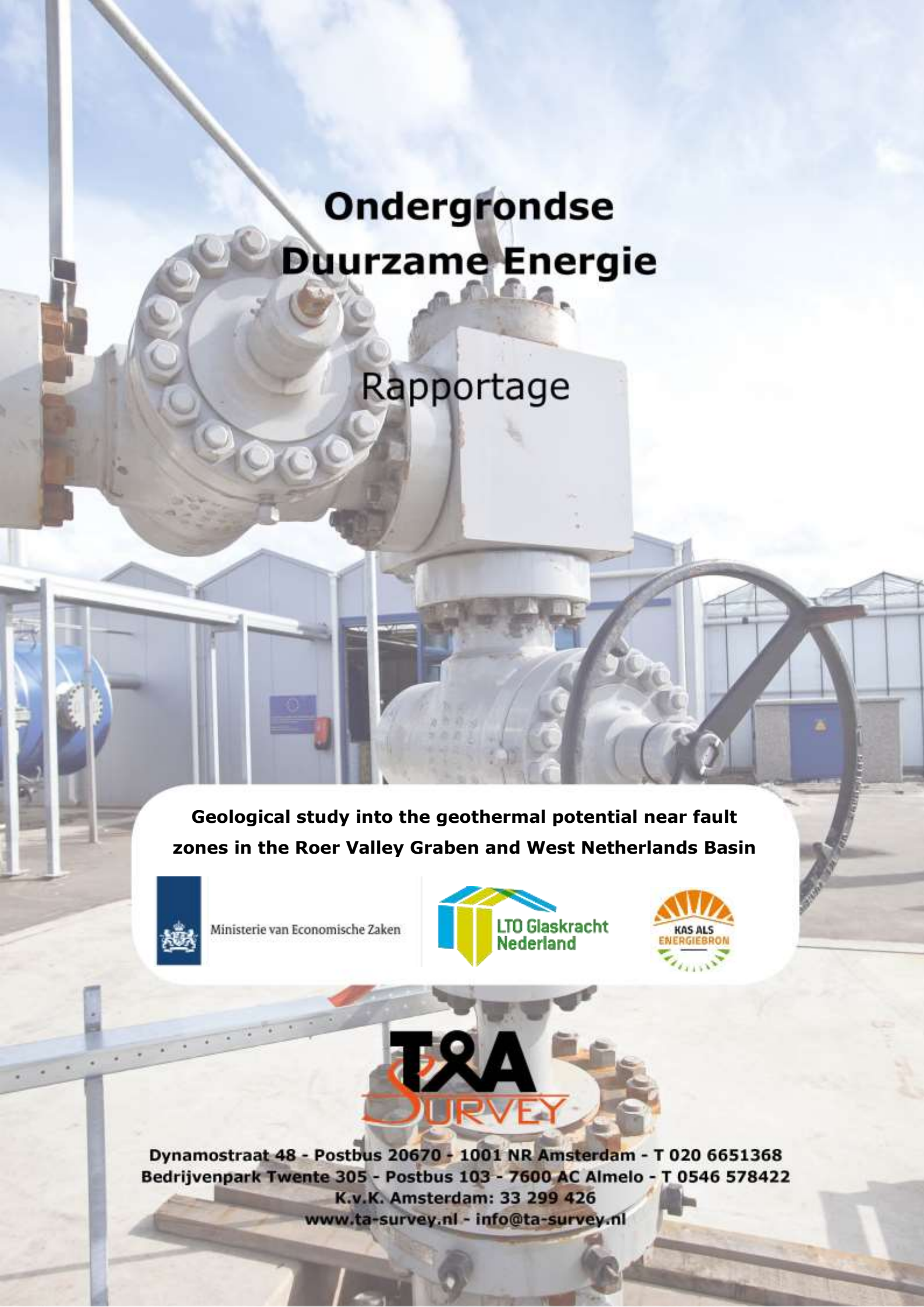

Ondergrondse Duurzame Energie

Rapportage

Geological study into the geothermal potential near fault zones in the Roer Valley Graben and West Netherlands Basin

Ministerie van Economische Zaken

LTO Glaskracht Nederland

KAS ALS ENERGIEBRON

T&A Survey

Dynamostraat 48 - Postbus 20670 - 1001 NR Amsterdam - T 020 6651368
Bedrijvenpark Twente 305 - Postbus 103 - 7600 AC Almelo - T 0546 578422
K.v.K. Amsterdam: 33 299 426
www.ta-survey.nl - info@ta-survey.nl

Geological study into the geothermal potential near fault zones in the Roer Valley Graben and West Netherlands Basin

Report number: ODE6425

Commissioned by:
Kennisagenda Aardwarmte
Dhr. F. Schoof
frank.schoof@fpp-management.nl

Advisor:
T&A Survey BV
Ir. G.A. de Bruin
Postbus 20670
1001 NR AMSTERDAM
Tel: 020 6651368
Fax: 020 6685486
Internet: www.ta-survey.nl
E-mail: debruin@ta-survey.nl

Authors:
MSc D.P.M. Stegers
MSc S. Edelman
Ir. K. Pieterse

Project manager:
Ir. G.A. de Bruin

DATE	STATUS
18-05-2018	V 2.1 - Final

Samenvatting

Deze studie richt zich op afwijkende temperatuurgradiënten nabij (grootschalige) breuksystemen in de ondergrond van het onshore West-Netherlands Basin en de Roer Valley Graben. Er wordt gekeken waar dergelijke anomalieën zich bevinden, hoe deze gekoppeld kunnen worden aan breukstructuren, wat de eigenschappen zijn van gerelateerde breukzones, waar dergelijke temperatuur-anomalieën nog meer te verwachten zijn en wat de potentiële gevolgen kunnen zijn voor (toekomstige) geothermische projecten. Allereerst wordt een inzicht in ondergrondse temperaturen gecreëerd door temperatuurmetingen uit boorgatmetingen te verzamelen. Doordat gesteente afkoelt tijdens het boren onder invloed van de boorspoeling, zal voor een betrouwbare benadering van de gesteentetemperatuur een correctie moeten worden uitgevoerd. Gezien de grootte van de gebruikte dataset in deze studie is hierbij gekozen voor een statistische correctie in plaats van een numerieke correctie. Vervolgens zijn de geothermische gradiënten bepaald en gekarteerd.

Uit de analyse van deze gradiënten is gebleken dat er zowel in exacte als ruimtelijke zin (grote) variatie tussen de verschillende geothermen bestaat. Om deze verschillen te classificeren zijn er drie geothermische gradiëntklassen opgericht, te weten: 1) verlaagde gradiënt [< 29,0 ˚C/km], 2) gemiddelde gradiënt [29,0 - 33,0 ˚C/km] en 3) verhoogde gradiënt [> 33,0˚C/km]. De gradiënten zijn vervolgens geplot op de kaart van het studiegebied. Diverse clusters met gradiënten van eenzelfde klasse konden worden herkend. Vervolgens is het gebied in drie regio's opgedeeld en zijn er per deelgebied één of meerdere well logs en seismische lijnen geanalyseerd en geïnterpreteerd in of nabij breukzones en/of zones met afwijkingen op de standaard geothermische gradiënt [31,3 ˚C/km]. Als laatst zijn de geothermische gradiënten geïnterpoleerd voor een dekkende kaart en zijn er geothermische vermogensberekeningen uitgevoerd voor verschillende gradiënten.

Uit het onderzoek blijkt dat er significante variaties [± >2,0 ˚C/km] op de standaard geothermische gradiënt voorkomen in 66% van alle temperatuurmetingen in het studiegebied. Clustering van deze afwijkingen op de gradiënt lijkt aanwezig. Echter is er geen individuele verklaring gevonden voor deze afwijkingen. Wel lijken er een aantal factoren van invloed te zijn op de afwijking in de geothermische gradiënt, te weten:

1. Aanwezigheid van (openstaande-)breuken en/of een sterk verbreukte zone (*fault damage zone*)
2. Breukactiviteit gedurende de Laat Oligoceen tot recente extensiefase.
3. Strekking van deze breukstructuren
4. Aanwezigheid van dikke, slecht warmtegeleidende gesteentepakketten zoals kleistenen (*thermal blanketing*)

In het oosten van het Roer Valley Graben is een verlaagde geothermische gradiënt waargenomen. Deze afwijking is in een studie van Luijendijk et al. (2012) verklaard door een topografie-gedreven grondwaterstroom. Verhoogde temperaturen in het centrale deel van het studiegebied lijken niet gerelateerd te zijn aan magmatisch gesteente dat is aangeboord in diverse putten in deze regio, gezien de betreffende putten geen significant hogere geothermische gradiënten laten zien.

Tot slot is een potentieel verband ontdekt tussen de geothermische gradiënt en het geothermische vermogen. Onder de standaardwaardes in DoubletCalc resulteert 1˚C/km afwijking op de standaard geothermische gradiënt in een vermogensverandering van 6-7%.

Summary

This study focuses on the deviating temperature gradients near (large-scale) fault systems in the subsurface of the onshore West Netherlands Basin and Roer Valley Graben. We have studied the location of these anomalies, their potential link to fault structures, the properties of related fault zones, the expected location of similar temperature anomalies and the potential consequences for (future) geothermal projects. First, an insight into underground temperatures has been created by collecting temperature data from borehole temperature measurements. Since the rock is cooled down by drilling fluid during the drilling process, it is necessary to carry out a temperature correction. Given the size of the used dataset in this study, we chose a statistical correction instead of a numerical one. Subsequently, the geothermal gradients have been determined and mapped.

The analysis of the geothermal gradients shows a (substantial) exact and spatial variation between the multiple geothermal gradients. To classify these variations, three geothermal gradient classes have been established: 1) reduced gradient [<29.0 ˚C/km], 2) average gradient [29.0 - 33.0 ˚C/km] and 3) increased gradient [>33.0˚C/km].The gradients were plotted on a map of the area of investigation. Various clusters with gradients of the same class can be distinguished. Subsequently, the area was divided into three sub-areas. For each sub-area, at least one well log and seismic line situated in or near fault zones and/or zones with deviations on the standard geothermal gradient [31.3˚C/km] have been analysed and interpreted. Finally, the geothermal gradients have been interpolated for an area-covering map and geothermal power calculations were performed for different gradients.

The analyses indicates significant variations [± > 2.0 ˚C/km] on the standard geothermal gradient in 66% of all temperature measurements in the area of investigation. Clustering patterns of these gradient deviations appear to be present. No individual explanation for these deviations has been discovered, though, a number of factors seem to affect the deviation in the geothermal gradient:

1. Presence of (open) faults and/or a fault damage zone
2. Fault activity during the Late Oligocene to recent extension phase
3. Extent and orientation of these fault structures
4. Presence of thick, poorly heat-conducting rock packages such as claystones (thermal blanketing)

A reduced geothermal gradient has been observed in the eastern part of the Roer Valley Graben. This deviation is explained in a study by Luijendijk et al. (2012), by a topography-driven groundwater flow. The elevated temperatures in the central part of the area do not seem to be linked to magmatic rocks which have found in various wells in this region, since these wells do not show significantly increased geothermal gradients.

Finally, a potential relationship has been discovered between the geothermal gradient and geothermal output power of a doublet. Using the default values in DoubletCalc, 1˚C/km deviation on the standard geothermal gradient results in a power change of 6-7%.

Index

1 Introduction

1.1 Problem definition

In geothermal projects, temperature predictions for subsurface reservoirs are essential. Depth is primarily used for the prediction of subsurface temperatures. For the Netherlands, the average geothermal gradient is determined at 31.3˚C/km (f.e. Bonté et al., 2012). However, the geothermal gradient can differ locally. This appears to be the case in some parts of the Roer Valley Graben, where some wells report geothermal gradients of 35.0 – 38.0˚C/km (Luijendijk et al., 2012). For a conventional system at 2.500 meters, this could result in a positive temperature difference of up to +10-18 ˚C.

It is thought that temperature variations could be related to fault zones, resulting in positive or negative temperature outliers. Water from deeper layers may migrate to shallower levels by density differences, causing positive temperature anomalies. Opposite to this, it may be possible that meteoric water infiltrates from the surface towards deeper layers along permeable fault zones, causing negative temperature anomalies. Both processes can potentially have a significant impact on the performance of nearby geothermal projects. As such, the identification and prognosis of potential temperature anomaly zones would make a significant contribution in geothermal exploration, feasibility and optimization studies for future geothermal systems.

This leads to the main objective for this project:

Investigate deviations of the average geothermal gradient in and nearby regional fault zones in the West Netherlands Basin and Roer Valley Graben.

Dutch:

Deze studie richt zich op afwijkende temperatuur gradiënten nabij (grootschalige-) breuksystemen in de onshore 'West-Netherlands Basin' en de 'Roer Valley Graben'. Er wordt gekeken waar dergelijke anomalieën zich bevinden, hoe deze gekoppeld kunnen worden aan breukstructuren, wat de eigenschappen zijn van gerelateerde breukzones, waar we dergelijke temperatuur anomalieën nog meer kunnen verwachten en wat de potentiële gevolgen kunnen zijn voor geothermische projecten.

Projectdoel:

Onderzoek naar afwijkingen van de gemiddelde geothermische gradiënt in en nabij regionale breukzones in het West Nederland Bekken en de Roer Dal Slenk

1.2 Project goals

Project sub-goals are set up to solve the main problem as defined in the previous paragraph. The following sub-goals are defined:

- Build a subsurface temperature dataset for the study area
- Locate potential temperature anomalies in the onshore part of the West Netherlands Basin (WNB) and Roer Valley Graben (RVG)
- Relate anomalies to large fault zones/networks
- Evaluate fault zones and extrapolate to other locations in the study area
- Assess potential increase in porosity/permeability near large fault zones in reservoir rocks
- Relate anomalies to current and potential future geothermal projects
- Assess effects of anomalies on geothermal output

Temperature anomalies may significantly affect various components of nearby geothermal projects. An increase in the geothermal gradient can have multiple effects:

- Expected geothermal output values can increase significantly, when compared with the application of an average geothermal gradient.
- Steeper gradients may indicate potential shallower geothermal targets, which previously were assessed as being non-suitable. Such targets may also improve business cases, as shallower wells are more cost-effective to drill.
- Steeper gradients may bring more locations in the 100+˚C range, which may be worthwhile for various direct applications in industrial processes and for potential electricity generation
- Lower geothermal gradients may result in lower geothermal output values, which can have drastic consequences in projects where minimal output values are already on the margin of a profitable business case. As such, a better grip on geothermal gradients can provide better insights in the expected associated risks.

Identifying the specific locations of these anomalies is essential for the effects mentioned above.

Note: When planning a geothermal doublet to a fault (zone), the chance of induced seismicity needs to be studied carefully. This study does not focus on the probability or risk of induced seismicity. No recommendation is done on this topic.

1.3 Previous studies

Various studies looked into temperature maps and profiles in the Dutch subsurface (eg. Bonté et al, 2012; Luijendijk et al., 2012, Lipsey et al, 2016, etc.). The study of Luijendijk is of special interest, as it concentrates on subsurface temperatures in the Roer Valley Graben. In his thesis, he addressed temperature profiles of various wells, which did not correspond to the average geothermal gradient

in the Netherlands. Some wells showed lower temperatures and other wells showed significantly higher temperatures, in relation to expected temperatures based on the average geothermal gradient. In addition to the Roer Valley Graben, one of the aims is to what extent these anomalies can be extended towards the West-Netherlands Basin. This would be of high importance, as most Dutch geothermal activities are located in this basin. Extra insights in potential temperature anomalies may have significant impacts to potential projects. Additional publications of special interest are Angemar (2015), Bense (2006), Garibaldi (2010), Loveless (2014) and Vondrak (2016).

Though these studies are meant to get better insights in subsurface temperatures, there are no direct (or only marginal) links to the application of geothermal projects. Additionally, specific relations to nearby faults is not evident everywhere. In our study, we would like to specifically analyse temperature profiles of wells in the West Netherlands Basin/Roer Valley Graben and check whether these anomalies can be related to potential nearby faults. Additionally, available 2D/3D seismic data is consulted to identify the characteristics of the fault zones, in order to see whether similar faults can be recognized in other parts of the basin. If so, it's potentially possible to set-up a map of predicted temperature anomalies.

For the geothermal energy industry formation temperature is of great importance. A small increase in formation temperature already leads to a higher geothermal power output. This geothermal power indicates how much heat demand can be covered, but also determines the amount of SDE+ subsidy. As many geothermal projects have marginal business cases, this effect shouldn't be trivialized and as such, reliable temperature prognoses are of great importance.

1.4 Research area

The research area consists of the onshore part West Netherlands Basin [WNB] and the Roer Valley Graben [RVG]. The provinces of South-Holland, nortwestern part of Brabant and western part of Utrecht are located in the WNB. The RVG stretches from northern Limburg towards the eastern part of the Utrecht province. The NE-SW area between the cities of 's Hertogenbosch and Tiel roughly indicates the gradueal transfer of the basin area of the RVG towards the WNB. Both of the basins have a similar structural NW-SE axis. Figure 1 presents the research area.

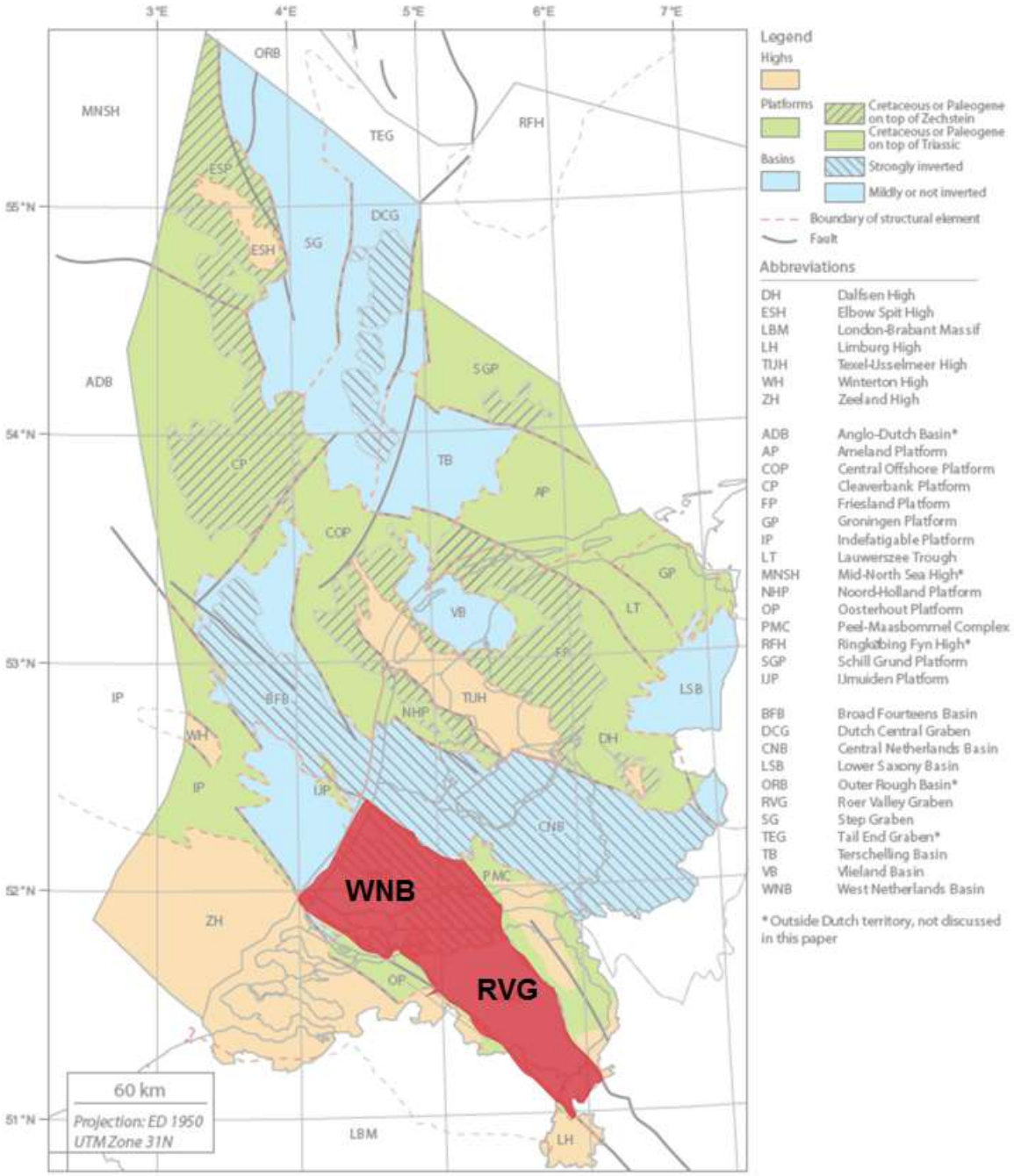

Figure 1 Study area high-lighted in red with the structural elements map of the Netherlands on the background. WNB = West Netherlands Basin, RVG = Roer Valley Graben. Structural elements map edited from Kombrink et al. (2012)

2 Methods

This research project is divided into five phases. The first phase is the data collection phase. In order to investigate a potential relationship between fault structures and temperature anomalies in the research area, a large temperature dataset is required. Multiple datasets are collected during this phase. Subsequently, the temperature dataset is analysed extensively and geothermal gradients are calculated. Prior to the analyses, all temperature data are corrected for disturbance in the measurements. This principle is further discussed in paragraph 2.1.1.

In the second phase, the corrected geothermal gradients are geographically plotted on a map. Anomalies on the average Dutch geothermal gradient are divided into three classes; positive-, negative- and no significant temperature anomalies. In the third phase the potential relationship between geological (fault-) structures and geothermal gradient anomalies is analysed. To assess this relationship, a seismic analysis of multiple lines is performed along wells with temperature data in the RVG and WNB and relating to fault maps. Petrophysical well log evaluation is performed on multiple wells that penetrated faults, along the analysed seismic lines, in order to identify faults in the wells and accordingly evaluate the potential in fault host rock and fault core.

In phase four, temperature anomalies are interpolated without geological steering throughout the WNB and RVG system between wells with available temperature data. In this way, a map is constructed with expected reduced and increased geothermal gradient zones. Multiple geothermal gradient anomaly maps are made with data of wells to specific depths in the geothermal energy window. In the fifth phase, temperature anomalies are related to current and potential future geothermal projects. Specific locations are pointed out with a potential increased geothermal gradient. The temperature anomaly effect on geothermal power output is calculated and described. The next paragraphs describe each of the research steps in detail.

2.1 Data collection

Subsurface temperature data from the area of the West Netherlands Basin and the Roer Valley Graben is collected. Overall, Bottom Hole Temperature [BHT] data is the most abundant temperature data in the region. A BHT is the maximum recorded temperature during a logging run shortly after drilling. Besides BHT data, temperature data from drill stem tests [DST] are also available, albeit much less common. Apart from that, production temperature data from current active geothermal systems in the study area collected.

The main dataset is obtained via dr. Damien Bonte (Utrecht University) and dr. Elco Luijendijk (VU Amsterdam). Both scientists applied different BHT correction methods to determine the original formation temperature. These methods are explained and compared in paragraphs 2.1.2 - 2.1.4. For the specific interest of geothermal doublets, TNO supplied production and temperature data of geothermal systems in and around the study area. For the study, only temperature data from depths over 1000m is used. This is primarily because around this depth the geothermal 'window' starts, for which this study is conducted. An additional database of mud losses was supplied by EBN[1]. Mud losses could provide arguments whether a fault is open and if fluid migration can occur along the fault plane or in the fault zone.

The spatial distribution of wells with temperature data is not even over the study area. Most wells were drilled to hydrocarbon reservoirs in the West Netherlands Basin and western part of the Roer Valley Graben. Only a limited number of wells with temperature data is positioned in the eastern part of the Roer Valley Graben. Figure 2 presents the spatial distribution of wells in and around the study area.

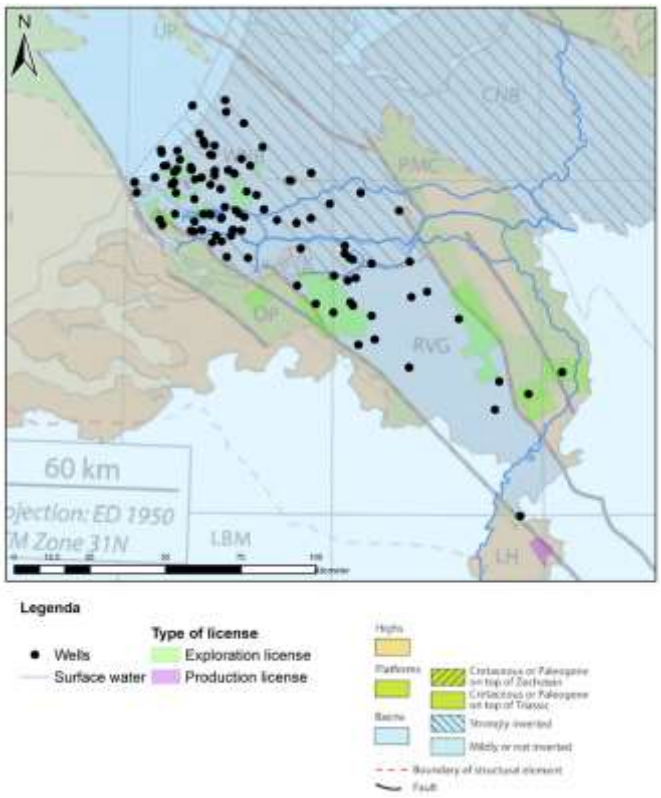

Figure 2: Selection of wells with temperature data in the Roer Valley Graben (RVG) and West Netherlands Basin (WNB) and near basin boundaries. Wells in figure are deeper than 1000 meters. On the background the structural elements map (Kombrink et al., 2012).

[1] Geo-Drilling Event database; personal communication EBN. Q4 2017

2.1.1 Temperature data

For this study a combined temperature database is set up. The temperature dataset from Luijendijk (2012) and Bonté (2012) are obtained. These temperature datasets consist of corrected temperature data from wells that are located in the West Netherlands Basin and the Roer Valley Graben. When it comes to temperature data, several important aspects need to be taken into account:

- Formation temperatures are predominantly measured shortly after drilling. Common sources of temperature data are Bottom Hole Temperature recordings (BHT) and Drill-Stem Tests (DST). BHT data is recorded for short periods of time, whereas DST data is measured over longer periods (f.e. 12 hours). As a result, DST temperature data is considered to be more reliable. However, the amount of BHT data is much higher and as such, both data are consulted.

- In general borehole fluids or drilling mud have an average lower temperature than the ambient formation temperature. When a formation is drilled by a well, drilling mud is circulated in the well during and after drilling. Circulation is done in order to remove the cuttings and clean the wellbore. The relatively cool bore fluid used for circulation will cause cooling of the formation (Bonté et al., 2012).

- Over time, formation temperature will recover from the above mentioned cooling effects. How long this temperature recovery takes, depends on multiple parameters. Examples of these parameters are lithology, depth, permeability and the local geological setting (Bonté et al., 2012; Luijendijk et al., 2012). In relation to BHT data, this is an important aspect: The timing of BHT measurements is not always documented for all measurements. It is important to understand that greater well depths are accompanied with longer tripping times when the drill string is brought to surface and the measuring tool is lowered into the borehole. These longer periods of time between drilling and measuring lead to an already ongoing formation temperature recovery. This results in a depth-varying uncertainty in the temperature measurements.

Luijendijk (2012) and Bonté (2012) use different correction methods for their temperature data. In this paragraph their methods are explained and the outcomes of the temperature corrections are compared. The correction method of Luijendijk is explained first: the Bottom Hole Temperature Recovery Model.

2.1.2 Bottom Hole Temperature Recovery Model

Luijendijk (2012) developed the analytical Bottom Hole Temperature Recovery Model. This model is developed to track the initial formation temperature, after the formation has recovered from cooling by the drill fluid. The BHT Recovery Model simulates the temperature recovery in specific time steps after drilling and circulating of the wellbore. Time series are used to determine the equilibrium between the formation temperature and the drilling fluid temperature (Luijendijk et al., 2012).

The BHT Recovery Model uses a two component mathematical model. A two component model is based on the physics of heat transfer. A study on the accuracy of this method performed on wells in the North Sea Basin concluded that a two component model gives accurate estimates with little to no systematic errors (Hermanrud, 1990; Luijendijk et al., 2012).

The type of two component model that was used in the development of the BHT Recovery Model is based on the heat flow between the drilling fluid and formation (Luheshi, 1983; Shen & Beck, 1986). Luijendijk (2012) created a new numerical finite difference model to solve the 2D heat conduction equation, as presented in equation I. The model uses a 2D grid of 200 columns with a cell size of 1x1cm.

$$\frac{\partial T}{\partial t} = \kappa \nabla^2 T \qquad \text{(I)}$$

In which:

$$\kappa = \frac{K}{\rho C} \qquad \text{(II)}$$

In which the parameters are:

T	Temperature	[˚C]
t	time	[s]
κ	thermal diffusivity	[m^2/s]
K	thermal conductivity	[W/m/K]
ρ	density	[Kg/m^3]
c	heat capacity	[J/Kg/K]

The BHT Recovery Model is calibrated by the Levenberg-Marquant algorithm, which is based on long interval borehole temperature measurements (Luijendijk et al., 2012). The outcome of the model

shows the temperature recovery in a 2D diagram over multiple time steps. Additionally, the models shows the average temperature in the bore hole section as a graph over time. See figure 3d for an example.

The thermal diffusivity given by equation I, represents the bulk thermal conductivity of the rock matrix and the pore-water. To apply the BHT Recovery Model to the BHT-data from selected wells in the Roer Valley Graben, the following parameters were assumed (Luijendijk et al., 2012):

$\boldsymbol{K}_{\text{pore water}}$ = 0,6 W/m/K
$\boldsymbol{\kappa}_{\text{drillingmud}}$ = 1,8×10^{-7} m^2/s

Porosity values were obtained from available density well logs, where calibration was applied by using publicly available porosity data points from cores. If no density log data was available, a depth dependent porosity parameter was assumed. This is described by equation III.

$$\emptyset = \emptyset_{\mathbf{0}} \cdot \boldsymbol{exp}^{-\boldsymbol{cz}} \qquad \text{(III)}$$

With the parameters:

Ø	porosity	[%]
z	depth	[m]
c	porosity depth coefficient	[%/m]
$\boldsymbol{\emptyset_0}$	porosity at surface value	[%]

Values for the porosity at surface ($\boldsymbol{\emptyset_0}$) and the porosity depth coefficient (***c***), were based on values of the southern North Sea area reported by Sclater and Christie (1980). The outcome of the BHT Recovery model is highly influenced by the circulation time of the drilling mud in the bore hole. For the model, an average circulation time of 5 hours is assumed (Luijendijk et al., 2012). Further, the model assumes an average surface temperature of 10˚C for The Netherlands.

The BHT Recovery Model requires an extensive parameter input for the BHT correction estimation. Examples of the input variables are: depth of the BHT value (TVD), type of lithology at recording depth, borehole diameter at this point, drilling mud temperature and the BHT recording time. An example of the output of the BHT Recovery Model from well WWS-01 was provided by Luijendijk (2012) and presented in figure 3. The tests on the BHT Recovery Model concluded a **±5 ˚C** temperature uncertainty range and a **95%** confidence interval for the rock matrix thermal conductivity calculation.

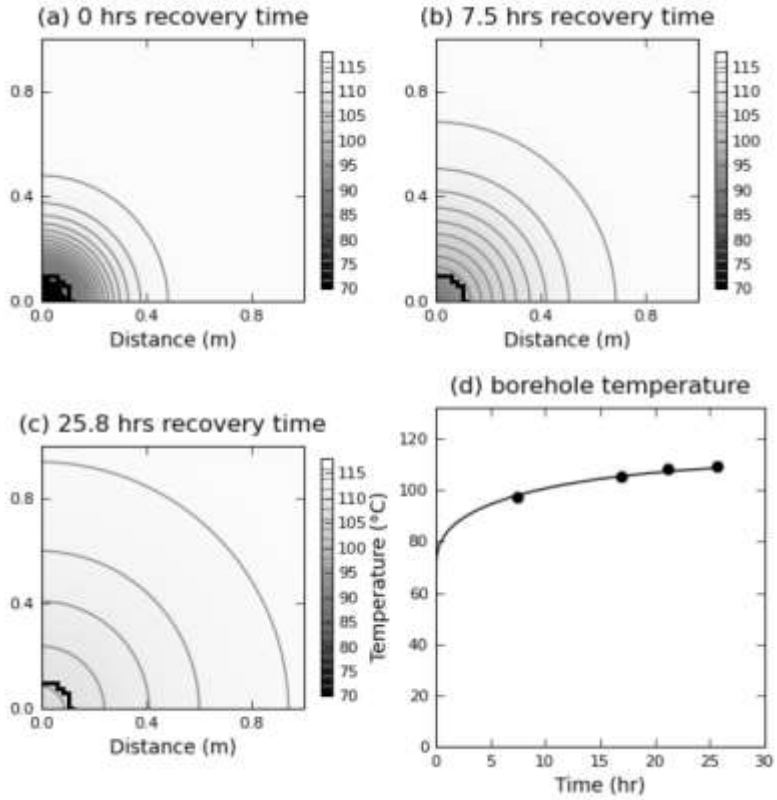

Figure 3: The outcome of the BHT Recovery Model for BHT data of well WWS-01, south of Waalwijk. a) temperature recovery directly after circulation. b) after 7,5 hours of recovery. c) after 25,8 hours of recovery. d) This graph presents evolution of the borehole temperature from the model over time (black line) in respect to the measured borehole temperatures (dots). The temperature recovers most rapidly during the first period after cooling. After: Luijendijk (2012)

2.1.3 AAPG BHT correction

Bonté (2012) uses the AAPG correction method to track initial formation temperatures from BHT recordings. The AAPG correction method has a statistical origin. It is based on a dataset of over 10.000 North American wells, with around 20.000 BHT values (Bonté et al., 2012). Selected BHT data was compared with DST data and by statistical means an equation was developed with four parameters. These parameters are location dependent and are initially setup for two regions in the United States. See table 1 for the values that were developed for the West Texas and Louisiana regions. Additionally, Bonté developed a set of parameters applicable to the Dutch subsurface which he used in his subsurface temperature model (Bonté et al., 2012; Bonté et al., in prep). The AAPG equation to determine the BHT correction is presented in equation IV (Deming, 1989).

$$\Delta T = az + bz^2 + cz^3 + dz^4 \qquad \text{(IV)}$$

Table 1: The AAPG correction method values for West Texas and Louisiana (Deming (1989)). For the Netherlands a specific set of parameters is determined (Bonté et al.; in prep).

Area	a	b	C	d
West Texas	-1.169×10^{-3}	-4.689×10^{-7}	6.609×10^{-10}	-8.312×10^{-14}
Louisiana	4.926×10^{-3}	2.164×10^{-6}	-7.628×10^{-10}	4.950×10^{-14}
The Netherlands	-6.234×10^{-3}	6.618×10^{-6}	-1.731×10^{-9}	1.235×10^{-13}

The uncertainty of the AAPG statistical method is tested at **±10 ˚C**, but requires less input parameters as the analytical method (Bonté et al., 2012).

2.1.4 Comparison of BHT correction methods

To determine the difference between both BHT correction methods, BHT data from two wells is compared. The BHT data of the wells is first corrected by the analytical model (Luijendijk, 2012) and secondly corrected via the statistical AAPG method (Deming, 1989; Bonté et al., 2012; Bonté et al., in prep). In the AAPG correction method the values applicable to the Dutch subsurface are used, as developed by Bonté et al. (in prep). For this comparison the wells Kerkwijk-01 [KWK-01] and Waalwijk South-01[WWS-01] are selected. Results of both BHT correction methods are presented in table 2.

Table 2: Comparison between analytical and statistical BHT correction methods for wells KWK-01 and WWS-01. $BHT_{analytical}$ values after Luijendijk (2012). The AAPG correction relates to the method of Bonté (Bonté et al., in prep). DST data is an extrapolated temperature to the depth of the BHT-data. After: Luijendijk (2012)

Well	Depth [m]	BHT_0 [˚C]	Corrected $BHT_{analytical}$ [˚C]	Corrected BHT_{aapg} [˚C]	DST depth [m]	DST temperature [˚C]
KWK-01	2683.44	103.9	119.2	107.8		
WWS-01	3054.02	116.9	116.3	113.1	2744	119

The DST data is an extrapolated value to the depth of the BHT temperatures, using a linear geothermal gradient and a surface temperature of 10 ˚C. Overall, the two statistically corrected BHT values are lower in respect to the analytically corrected BHT values. The correction method of Luijendijk (2012) is very detailed and requires many parameters in comparison with the AAPG method that was applied by Bonté (2012). As a result, the Luijendijk (2012) analytical method is hard

to apply on larger temperature datasets. However, the analytical model has a lower uncertainty in corrected BHT value and matches better with DST recordings (Bonté et al., 2012). Though the statistical AAPG correction method with the adopted values for The Netherlands possesses a slightly higher uncertainty, it is more efficient when working with larger data sets. Since a larger data set is also used in this research project, the statistical AAPG BHT correction method is applied to the BHT data.

2.1.5 Geothermal gradient

The geothermal gradient is the average temperature increase per depth unit, with an average surface temperature of 10˚C in The Netherlands. The BHT data is corrected via the statistical AAPG method as explained in paragraph 2.1.3. Geothermal gradients calculated from the analytically corrected BHT measurements are on average significantly higher (35,9 ˚C/km; Luijendijk et al., 2012) in relation to the statistically corrected BHT values (31,3˚C/km; Bonté et al., 2012). One has to keep in mind that the dataset of Luijendijk is much smaller in respect to the dataset of Bonté. Additionally the study area of Luijendijk is restricted to the RVG and parts of the WNB, whereas the dataset of Bonté relates to the complete Dutch subsurface. However, the differences do indicate that the standard 31,3 ˚C/km geothermal gradient varies in the Netherlands.

2.1.6 Temperature data active geothermal systems

Temperature data of active geothermal systems in the study area is also obtained, after personal consult with TNO-AGE . The obtained temperature data of the current active geothermal systems have the advantage of temperature measurements over a longer track of time. As a result, cooling effects related to drilling activities will be negligible. The database contains three types of temperature data: maximum production temperature, average production temperature and temperature data from initial test activities after drilling. The wells are divided in two groups: one with production temperatures and one with test temperatures. Wells with both data types are not available. The database does not include additional information on the type of testing and/or the production history of the geothermal system.

It’s difficult to obtain a specific geothermal gradient for the various wells, due to various reasons. Perforation heights of reservoirs range from 53 meters to 884 meters for the various wells. The measured temperature is a mix from formation water from this whole screen interval. One option is to simply apply the mid perforation depth to the observed temperatures. However, reservoir qualities of the reservoir will very likely vary in depth. If higher transmissivities in the top part of the

reservoir are responsible for the main flow of produced formation water, observed temperatures will be a bit lower. The reverse situation with higher transmissivities at the base would give similar issues. In a situation where the perforation reservoir is limited (eg. <50 meters), this effect is limited. However, a height difference of 100 meters could already lead to ~3 ˚C in temperature difference.

For comparison reasons, the geothermal gradients based on mid perforation depth of the test temperature data and the average production temperature data are included in the results chapter.

Note: In agreement with the operators, the data of the various systems have been anonymously processed in this report. As such, the data is not merged with the BHT/DST-database.

2.2 Geographically mapping of temperature anomalies

In this phase the temperature anomalies on the geothermal gradients in the onshore area of the WNB and RVG are geographically plotted on a map. In the first place we'd like to know whether the temperature data indicate an increased or decreased temperature anomaly at the various wells, or whether there is no significant deviation from the average geothermal gradient at all. The standard deviation of the dataset is calculated at ~4,1 ˚C/km, which would lead in big offsets to the prognosed and observed temperatures. However, temperature prognoses on half of the standard deviation, would already have a significant impact on temperature prognosis and indirectly the related geothermal energy output. For example, a system with an average geothermal gradient at 3000m has an expected temperature of 103,3˚C, whereas temperatures could be as low as 97,3 ˚C with a reduced geothermal gradient of 29,1˚C/km. An increased geothermal gradient of 33,1 ˚C/km would lead to temperatures of 109,3˚C encountered at equal depths.

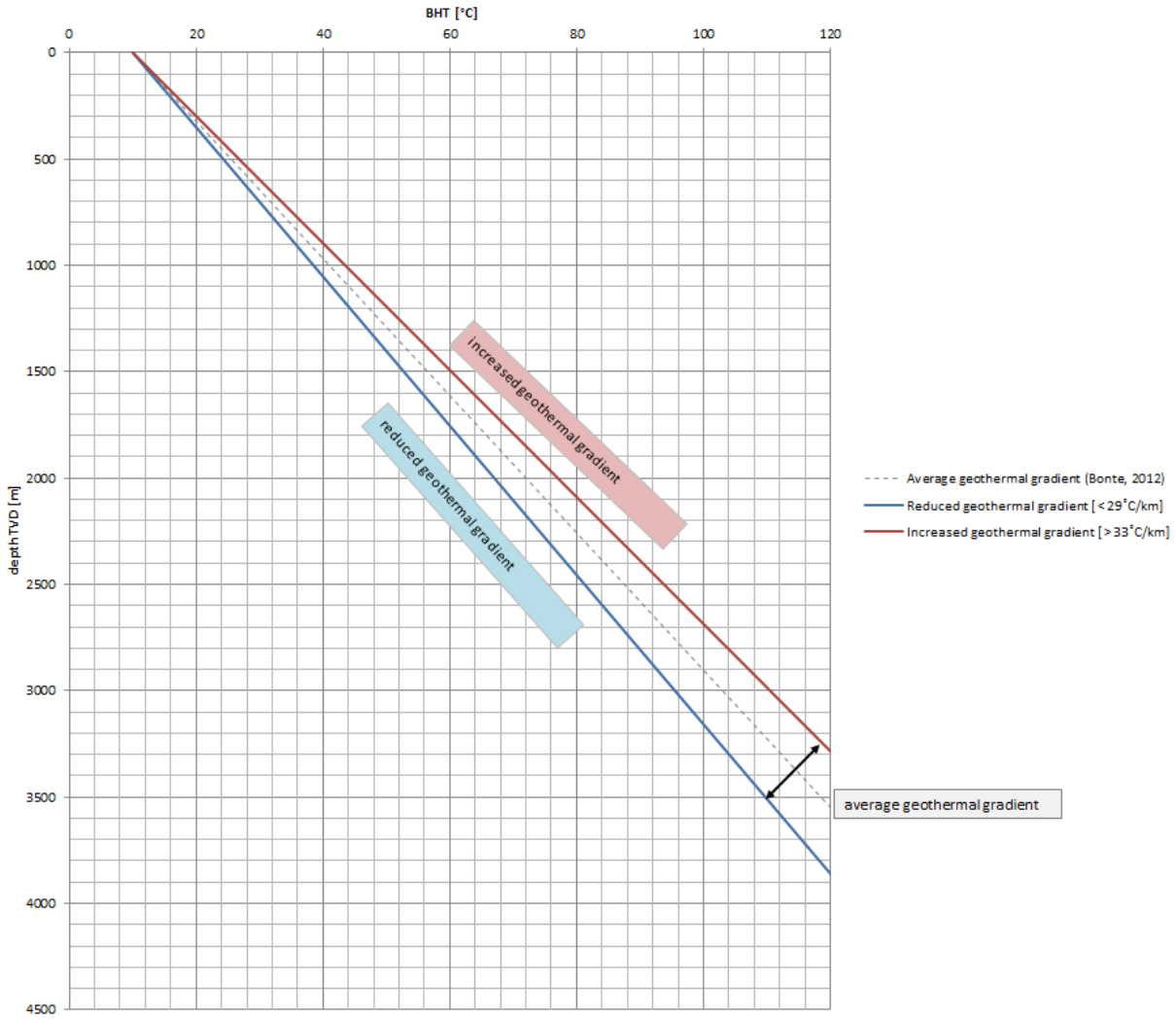

Figure 4: Geothermal gradient classification diagram. Each temperature data point (BHT_{corr} or DST) can be plotted in this diagram and indicates in which group it is classified.

As such, 2˚C/km spreading on the total geothermal gradient and is seen as a significant influence on the geothermal energy output. This leads to three classes which mark the character of the temperature anomaly, if present. All geothermal gradients between 29˚C/km - 33˚C/km are classified as average. Gradients less than 29˚C/km are classified as reduced geothermal gradients (blue). Geothermal gradients exceeding 33˚C/km indicate increased gradients (red). Figure 4 presents the boundaries of the various classifications. Aside the plotted temperature profile, the average geothermal gradient for the Dutch subsurface (Bonté et al., 2012) is plotted by a dashed line in the diagram.

2.3 Relate temperature anomalies to geology

Geothermal gradients vary between wells. Sudden temperature rises or drops can even be observed within a well. Several examples will be presented to indicate the potential temperature variations in a well. Besides deviations in the general geothermal gradient per well, lithological differences can also affect subsurface temperatures. To observe these effects, the lithostratigraphic interval is determined for every corrected temperature data point in which it is measured. Next the temperature data is converted to a geothermal gradient and sorted per lithostratigraphic unit.

After accumulating the geothermal gradients, they are extrapolated throughout the WNB and RVG, resulting in maps of the geothermal gradient covering the study area. Fault structures are plotted on top and potential relations between the geological frame work and the potential presence of geothermal gradient anomalies is analysed.

Next, seismic lines around these clusters of wells are analysed and interpreted to gain insight in the geological structures. In this way the well paths and the depths at which the BHT's are measured are evaluated. Fault structures are analysed and information from the geothermal gradient anomalies is combined with information from the mud-losses dataset.

2.4 Fault zones

Seismic and petrophysical analysis is conducted to investigate the potential relation and predictability of temperature anomalies and fault structures from well logs. In this study, various cluster of wells with significant (varying) anomalies on the average geothermal gradient are selected. Multiple logs from wells drilled in/through fault (zone)s in these different clusters are examined on increased porosities and/or permeabilities. Porosity calculations are mainly based on availability density logs. The petrophysical analysis can potentially indicate high(er) or low(er) porosities in or nearby fault zone, which may be a first indication on potential fault transmissivity and/or the presence of a fault damage zone. First, an explanation on fault damage zones is given below.

2.4.1.1 Damage zone

A fault structure in a host rock can be divided into two components, the damage zone and fault core (Bense et al., 2013). In general the fault core is positioned in the centre of a fault damage zone and the width of this zone is the maximum measured distance between the two edges of the damage zone perpendicular to the fault plane. The fault damage zone is the part of the fault zone with an

increased fracture density. Fractures can potentially improve permeability significantly and allow fluid flow. A fault zone is schematically presented in figure 5.

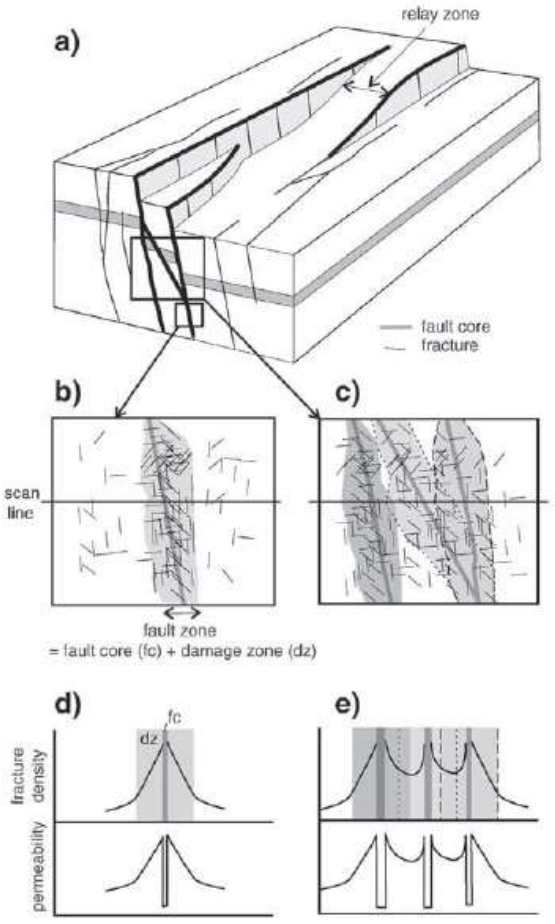

Figure 5: a-e Schematic presentation of a fault zone with the elements of a fault core, a fault damage zone and a relay zone. A relay zone refers to any such rock volume between kinematically related fault segments. Source: Walsch et al. (1999) Childs et al. (2009); Chester and Logan (1990); Caine et al. (1996); Faulkner et al. (2010); Bense et al. (2013)

Even when a fault core is closed, a fault damage zone around the fault can still create fracture based permeability (Garibaldi et al., 2010). The fault damage zone is represented by an ellipse-shaped zone around the fault that contains a significantly higher fault density in comparison to the host rock directly at the fault plane. The presence and extent of the fault damage zone depends on multiple factors like clay content in the host rock and the vertical offset of a fault (Bense et al., 2013). In clay bearing lithologies, the offset of the fault needs to be higher by higher clay content to create a fault damage zone. For example, a fault in a host rock with 0% clay content and a vertical offset can have a 100m broad damage zone, whereas a host rock with 20% clay content and a fault with a similar vertical offset will only have a damage zone of 3 to 5m (Houwers et al., 2015).

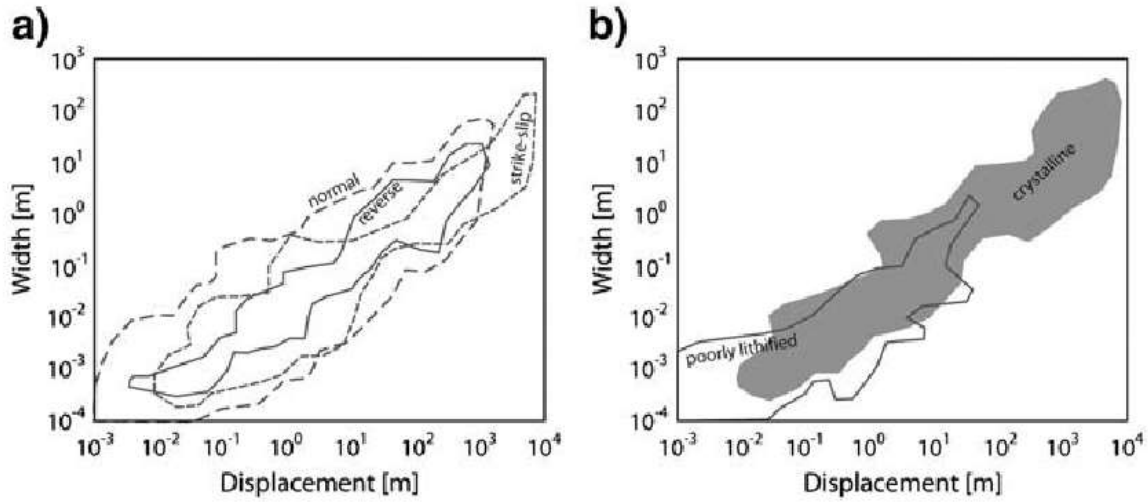

Figure 6 Relationship between fault thickness and fault displacement (a) between different fault types and (b) for poorly lithified and crystalline rocks. After: Childs et al. (2009)

The relationship between fault displacement and the width of a damage zone is researched by many scientists. Childs (2009) and Bense (2013) created a diagram that correlates this relationship for different types of faults, respectively normal-, reverse- or strike-slip faults (see fig. 6a). The same type of relation between fault damage zone width and fault displacement for poorly lithified rocks and crystalline rocks is presented in figure 6b. The figures indicate that the associated lithologies at the fault and the type of fault, both affect the width of a fault zone.

The extension of the fault damage zone is highly dependent on multiple factors. The most important factors are the types of rock cut by a fault and the size and orientation of the local stress field. Sandstones nearly always have a more brittle character in respect to claystones. Therefore, the extension of a fault damage zone in a sandstone is larger with respect to a claystone. Figure 7 presents the fault damage zone in different lithologies, accompanied by an indication of the variation in permeability increase over these rocks. The permeability ellipses give a good indication of the preferential and non-preferential flow path orientations. Since the main target in the study area relate to lithified siliciclastic rocks, figure 20b is of special interest. It clearly indicates that the damage zone can play a significant role in the fluid flow along the fault zone.

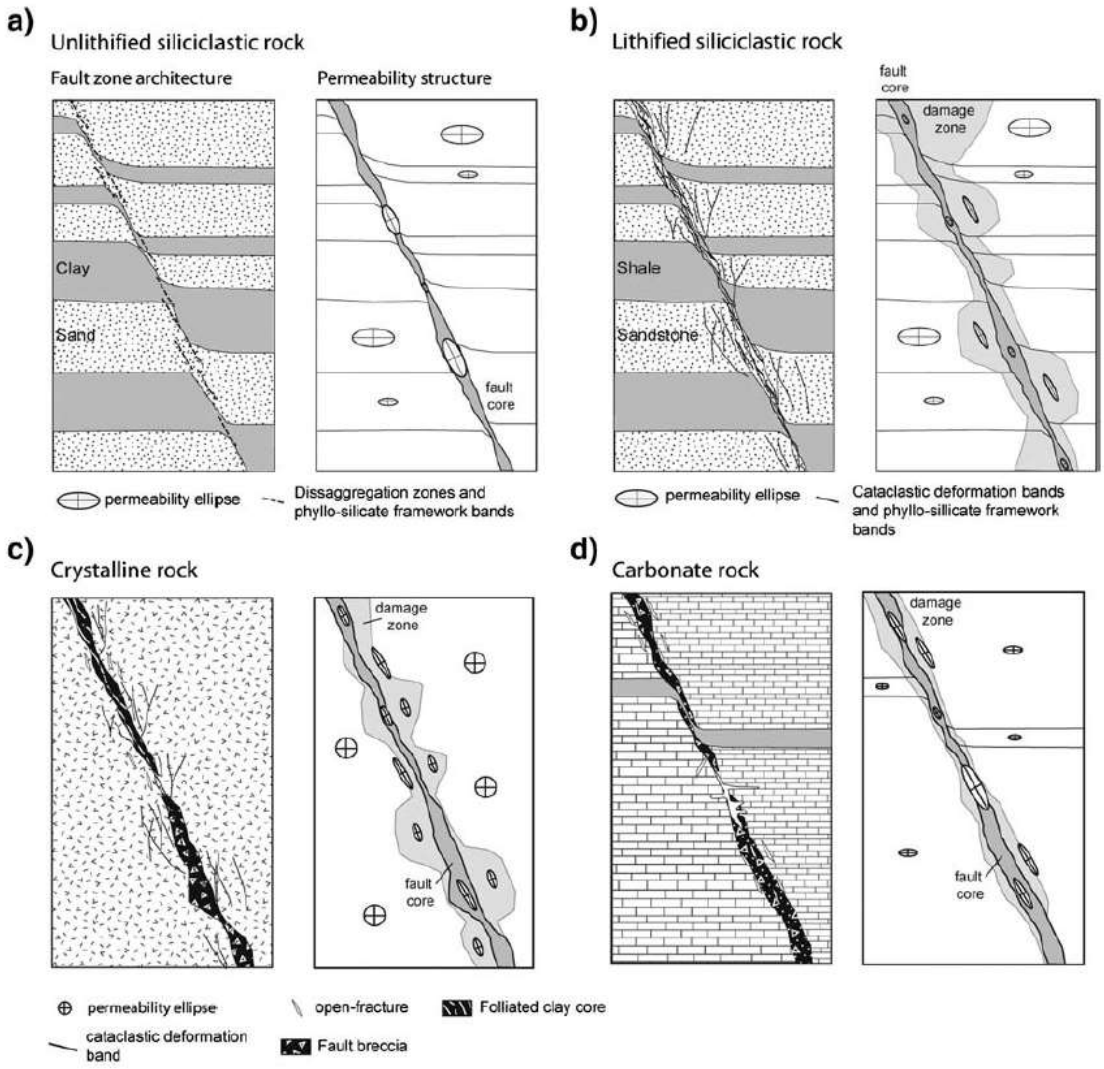

Figure 7a-d: Fault damage zone width varying per lithology (after Bense et al., 2013)

Lithologies around the fault core also have an effect on onather important process related to fault sealing: cataclasis. Cataclasis is a process in which the grains of the faulted formations are grinded along the fault plane (also see fig. 7c). The formed 'paste' of crushed sediments, called fault gouge, can result in a very fine grainsize, which has the potential to make the original lithology impermeable, resulting in potential fault sealing. Whether cataclasis occurs and whether a fault is sealing is very complex to answer. Examples of parameters that help to determine whether or not a fault is sealing are listed below:

- Fault offset (vertical) and fault type (extensional, compressional, strike-slip)
- Lithological characteristics on both sides of the fault
- Formation water flow
- Occurrence of cementation
- Depth, which leads to the hydrostatic pressure and ambient temperature

- Pressure difference between the compartments on both sides of the fault
- Direction of regional (paleo)stressfield versus fault orientation

The orientation of a fault in a specific stress regime may also reveal if a fault is expected to be opened or not (Bense et al., 2013; Loveless, 2014). In case of the West Netherlands Basin, different stress regimens have affected the geology over time during the multiple tectonic events (for example Ziegler et al., 1990; Van Balen et al., 2002; Houwers et al., 2015), making this a complex parameter.

The combination of so many parameters makes the prediction whether a fault is open or closed difficult. A cataclastic gouge can form over a range of development stages with different sealing properties. Roughly, cataclasis can only occur in normal faults at great depths and in reverse faults at nearly all depth intervals, because it requires a mix of high stress normal to the fault plane and shear movement (Nieuwland, 2012; Bense et al., 2013).

2.5 Effects of temperature anomalies on geothermal power output

To assess the effects of deviating of thermal anomalies on geothermal power output, calculations are performed in the latest version of DoubletCalc[1] to translate these variations in geothermal gradient into geothermal power output for multiple scenarios. Subsequently, a link is made between temperature anomalies and potential future geothermal projects.

[1] DoubletCalc V1.4.3

3 Results

In the following paragraphs the results of the temperature data analysis are discussed.

3.1 Geothermal gradients active systems

The temperature database of the active geothermal systems incorporates temperature data of 21 wells, relating to 11 geothermal systems. The data and the associated geothermal gradients are presented in table 3. The average geothermal gradient of the production temperatures relates to 30.4 ˚C/km and is slightly higher in relation to the temperatures measured during testing: 29.7 ˚C/km. Differences in geothermal gradients between injection and production well of the same geothermal system vary between 0.2 - 7.7 ˚C/km. In three systems the difference is higher than 5 ˚C/km. As the average distance between production and injection wells at reservoir level is normally roughly 1.5 km, this is quite an unexpected difference. All three systems are located in different parts of the study area and as such, the differences cannot be related to a specific part in the study area. Part of an explanation may lie in different ways of testing. Another explanation may relate to the perforation reservoir height, as these three systems all have more than 200 meters of perforation reservoir height. Though these reasons seem feasible, additional information is necessary for a proper analysis.

Table 3 Temperature data of current geothermal systems in the study area, divided by test temperatures (left) and average production temperatures (right). Geothermal gradients are related to mid perforation depths.

Ttest	Mid perforation depth	Geothermal Gradient
°C	m TVDss	°C/km
55.0	1570	**28.7**
52.0	1750	**24.0**
62.0	1786	**29.1**
67.0	1825	**31.2**
80.0	2115	**33.1**
76.1	2133	**31.0**
74.0	2174	**29.4**
75.0	2240	**29.0**
89.4	2240	**35.4**
87.5	2315	**33.5**
84.0	2374	**31.2**
86.5	2426	**31.5**
88.5	2830	**27.7**

Tavg	Mid perforation depth	Geothermal Gradient
°C	mTVDss	°C/km
60.0	1635	**30.6**
63.9	1840	**29.3**
74.3	2069	**31.1**
69.4	2181	**27.3**
76.0	2230	**29.6**
72.3	2259	**27.6**
85.6	2373	**31.9**
84.3	2433	**30.5**

The geothermal gradients based on production and test temperatures are (anonymously) plotted in the geothermal gradient classification diagram (figure 8). Though the systems do not show extreme temperature gradients, a variation in gradients is clearly present. Most of the geothermal production temperatures lie within the 29-33˚C/km bandwidth. Systems producing from depths between 1500-2000m are positioned slightly below the average geothermal gradient, whereas production temperatures from reservoirs deeper as 2000m tend to reveal a broader range in respect to the average geothermal gradient.

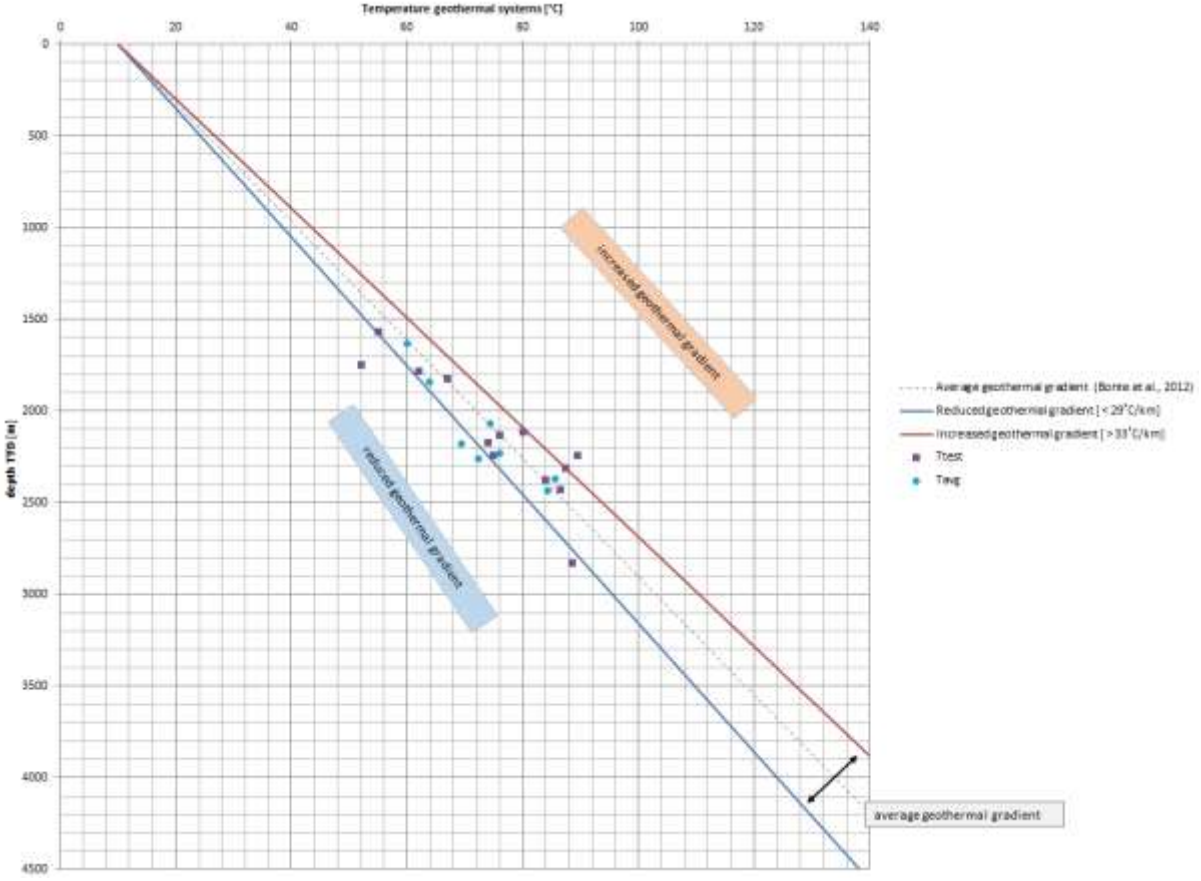

Figure 8: Geothermal gradients of active geothermal installations in the WNB and RVG. Data relates to test temperatures (purple) and average production temperatures (blue). Source: Personal consult TNO-AGE

3.2 Geothermal gradients BHT-DST

Geothermal gradients are calculated for every well in the database. All raw BHT temperature data is corrected with the AAPG statistical BHT correction method prior to analysis (see paragraph 2.1). In the Netherlands, the average geothermal gradient is determined at 31,3˚C/km (Bonté et al., 2012). Though various basins can have deviations to this average gradient, average geothermal gradients in the study area resulted in similar average geothermal gradients at various depth intervals (see table 4).

Table 4 Total temperature dataset sorted by depth interval. The average gradient per interval closely resembles the national average gradient of 31,3 ˚C/km.

	All wells	Wells > 1000m	Wells > 2000m	Wells > 3000m	Unit
Number of temperature measurements	429	369	211	44	-
Average geothermal gradient	30,8	30,7	31,3	31,3	˚C/km

However, individual temperature measurements can deviate significantly from the average geothermal gradient. This is recognized by the authors of the datasets and translated into uncertainty ranges (Bonté et al., 2012; Luijendijk et al., 2012). One of the goals of this study is to locate the geographical locations of these temperature anomalies. Though an individual measurement may relate to the outer boundary of the proposed uncertainty range, clustering of multiple positive or negative thermal anomalies may give a good indication of local to regional deviations.

All temperature data from wells deeper than 1000m are plotted in the geothermal gradient classification diagram (see paragraph .2.). This resulted in the distribution as presented in figure 9. The blue zone corresponds with a decreased geothermal gradient, the red zone with an increased geothermal gradient. The white zone indicates the average geothermal gradient, respectively < 29,0˚C/km and > 33,0˚C/km (also see paragraph 2.2).

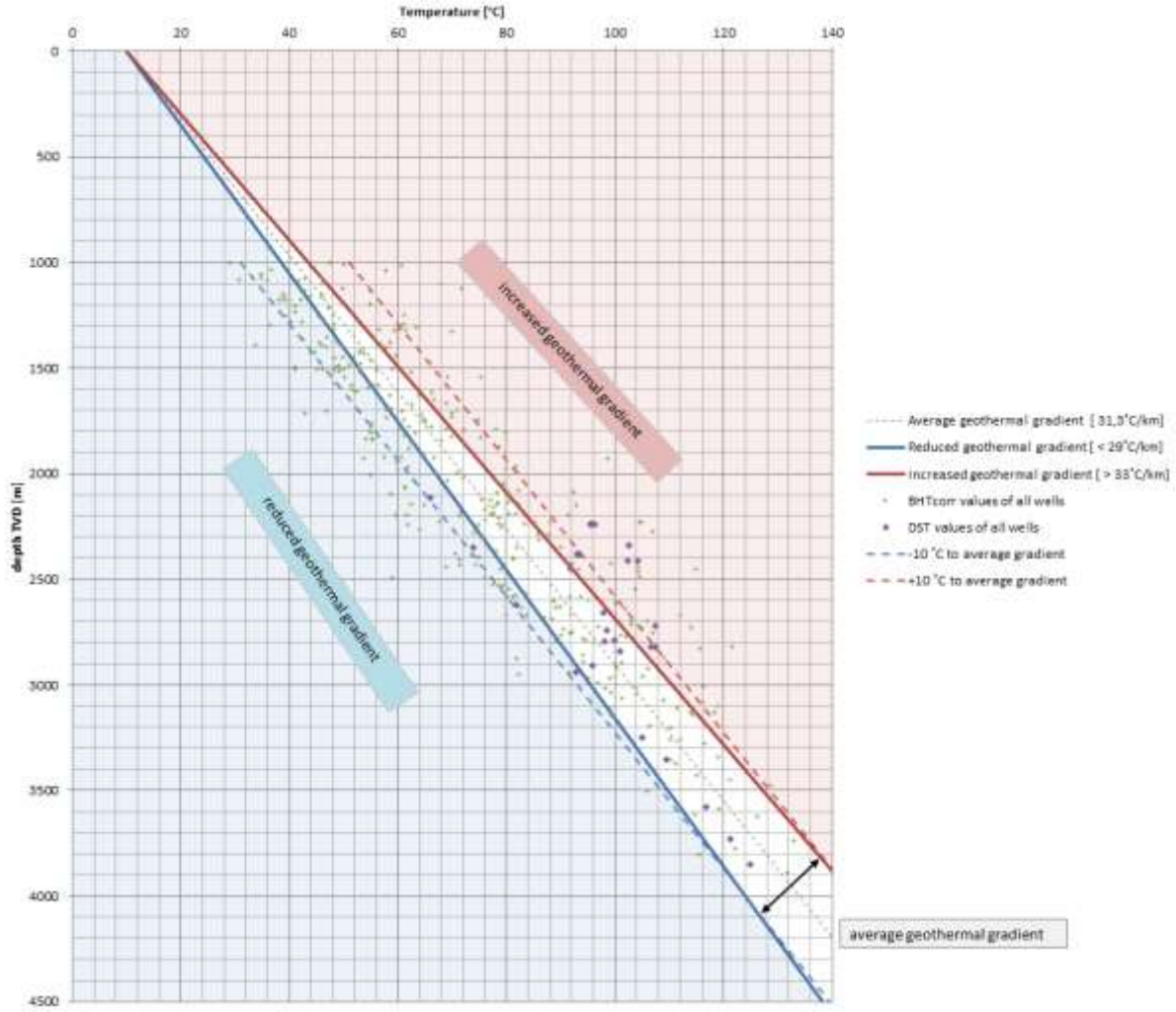

Figure 7: All 369 $BHT_{corrected}$ (green) and DST values (purple) from wells deeper then 1000m in the RVG or WNB are plotted in the classification diagram. The area above the increased geothermal gradient boundary is highlighted red, the area below the reduced geothermal gradient boundary is marked blue.

The total temperature data distribution of the BHT and DST data from wells located in the WNB or RVG that were used for this study, is presented in figure 9. As can be observed a significant amount of BHT and DST data lie outside the average geothermal gradient zone (±68 %). A large part of this still lies within the uncertainty range defined by Bonté (2012), stated at ±10˚C fixed offset (dashed lines). Nevertheless, approximately a third of all analysed wells falls inside the defined average geothermal gradient zone. Increased and decreased values also relate to roughly a third of the complete dataset. The distribution of the BHT data is presented in the diagram of figure 10.

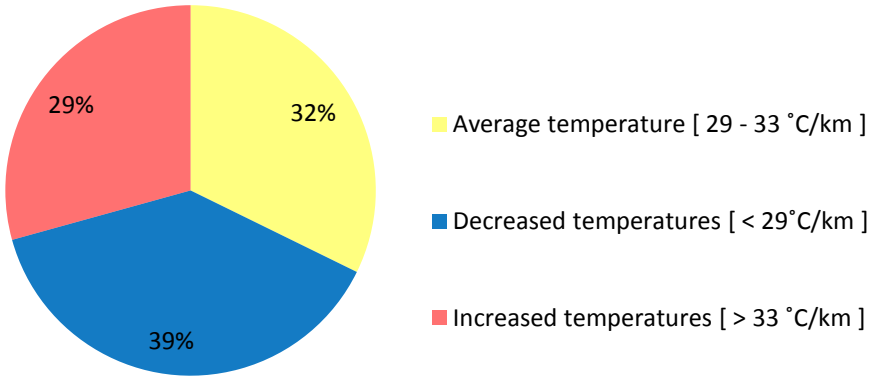

Figure 8: Percentile distribution of all temperature data points from wells deeper than 1000m.

In order to give an indication of the geothermal gradient curvatures and characteristics of the calculated geothermal gradients classes, four example wells are selected and plotted in the following section: BRTZ-01, SPK-01, WWK-01 and AND-02 (figures 11-14). Besides geothermal classification, selection is also based on amount of data points per well and on the specific curvature of the gradient. Most wells have temperature data measured in various stratigraphic intervals. Formation tops along the well path are defined in the diagrams.

SUB-CONCLUSION: The geothermal gradients of temperature data points in the study area indicate a high variability in the subsurface of the WNB and RVG. As such, the average Dutch geothermal gradient of ~31.3˚C/km should be considered as a very broad temperature guideline for this area. However, many uncertainties exist in the reliability of the subsurface temperature data.

3.2.1 BRTZ-01

The geothermal gradient is calculated from the available BHT data of the Barendrecht-Ziedewij well (BRTZ-01), see figure 11. The calculated gradient is nearly similar to the average geothermal gradient and temperature increases linearly over depth. The calculated geothermal gradient for BRTZ-01 is 31.0˚C/km. This lies entirely inside the average geothermal gradient zone and shows only a minor positive deviation around the top of the Lower Germanic Trias Group. This may be caused by insulating effects of the claystones in the Upper Triassic and Lower Jurassic.

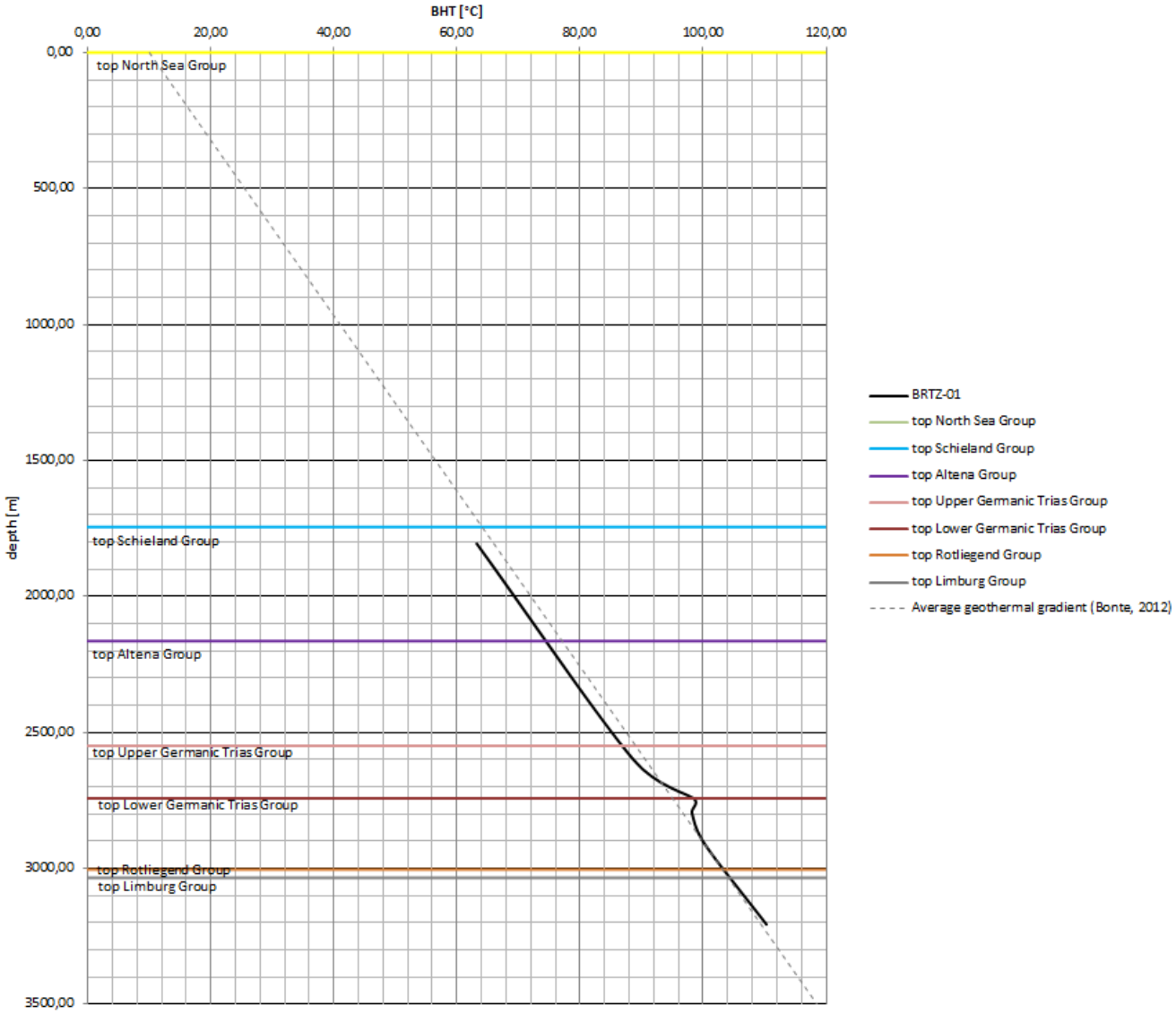

Figure 9: The geothermal gradient for the BRTZ-01 well (Barendrecht-Ziedewij-1).

3.2.2 SPK-01

The temperatures measured in Spijkenisse-01 well increase over depth as described by the plotted temperature profile (fig. 12). The geothermal gradient is slightly reduced over the entire length compared to the average geothermal gradient. The average linear gradient was calculated at 28,1˚C/km. This average gradient lies below the defined average geothermal gradient zone. Though, a turning point in the temperature profile can be observed around the top Schieland- / top Altena Group where after an increase in geothermal gradient occurs.

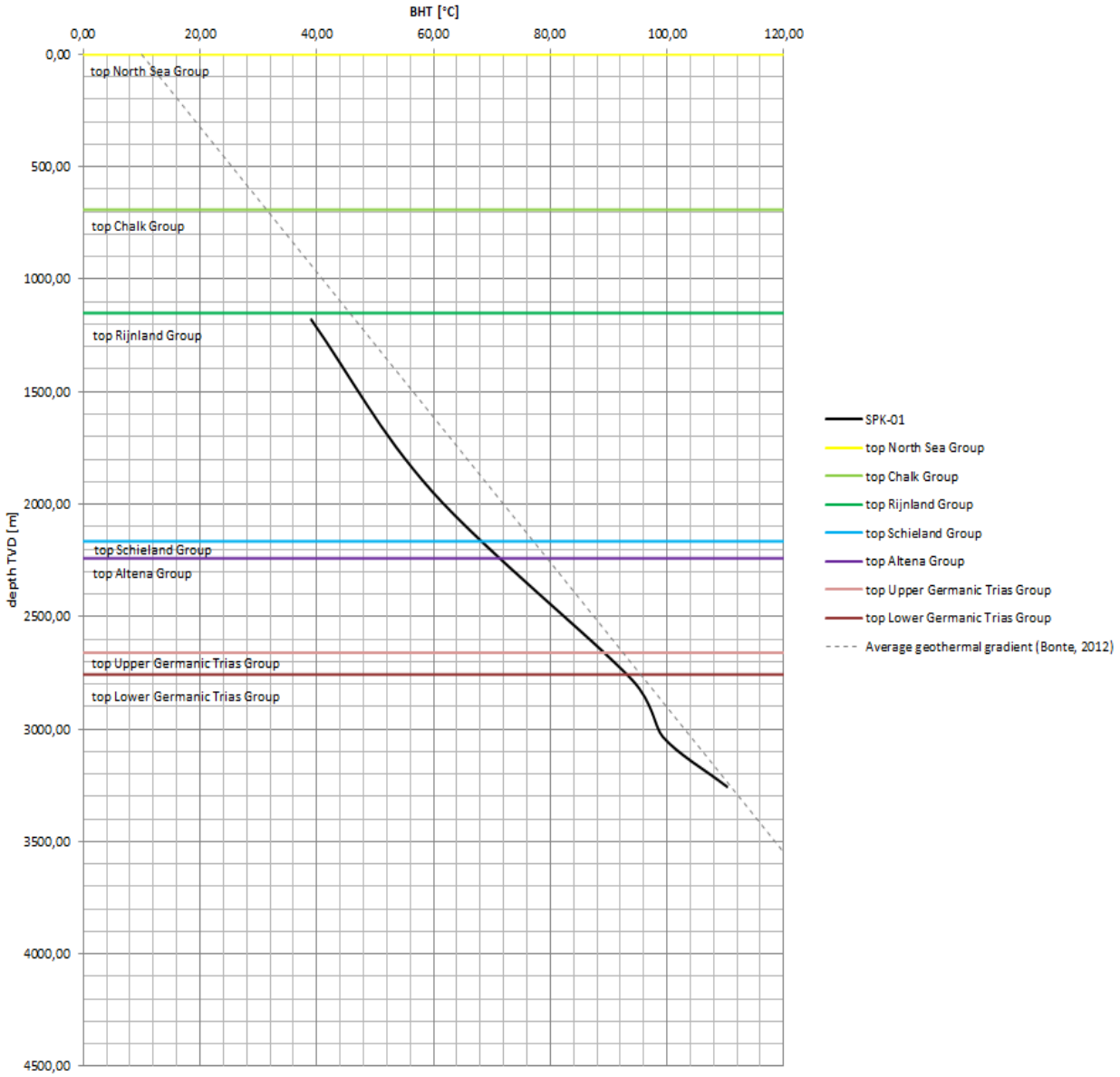

Figure 10: The temperature profile for the SPK-01 well (Spijkenisse-1) with the encountered formation tops plotted.

3.2.3 WWK-01

In contrast to the previous wells, the Waalwijk-01 [WWK-01] well temperature profile shows an irregular pattern for the temperature increase over depth (fig. 13). A linear geothermal gradient flattens out the curvature, but might be less applicable and hosts higher error amplitudes. Overall the temperature gradient lies significantly above the average geothermal gradient for the Dutch subsurface. The flattened linear geothermal gradient for this well is 37.4˚C/km. This results in a classification as significantly increased geothermal gradient. The major temperature increase in occurs inside the Aalburg Formation of the Altena Group. This lithostratigraphic group comprises predominantly of claystones. Further seismic analysis is performed to investigate the geological structure at this location. The result of this analysis is presented in paragraph 3.5.4.

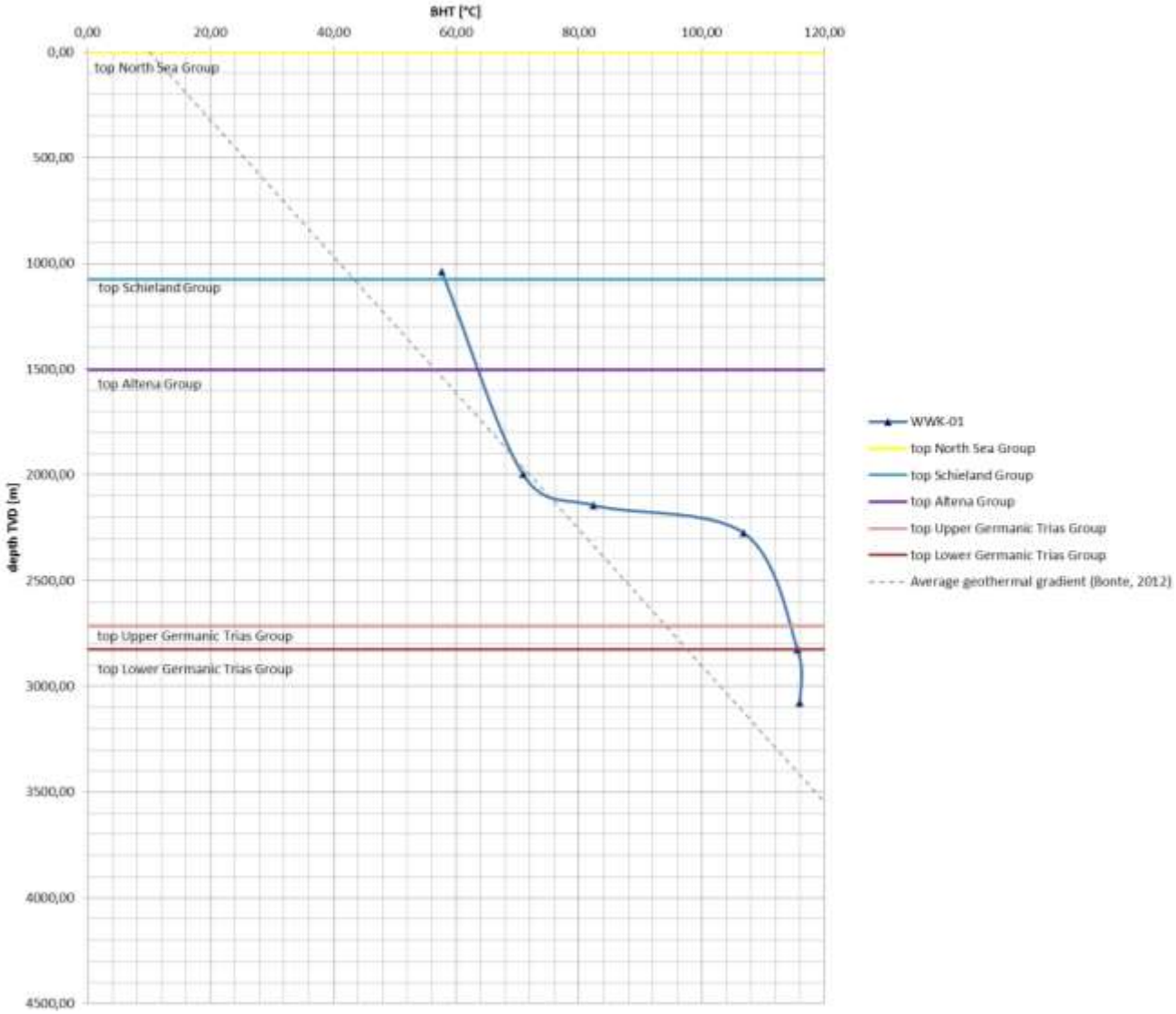

Figure 11: Temperature profile of WWK-01 (Waalwijk-1) well. The profile shows a more irregular profile.

3.2.4 AND-02

The calculated geothermal gradient for well Andel-02 [AND-02] shows the opposite of the gradient that was calculated for Waalwijk-01. The AND-02 temperature profile is positioned below the average geothermal gradient, with a calculated linear gradient of 23,0˚C/km (fig. 14). This is a significantly reduced geothermal gradient. Further seismic analysis is performed on this structure. The results are presented in paragraph 3.5.4.

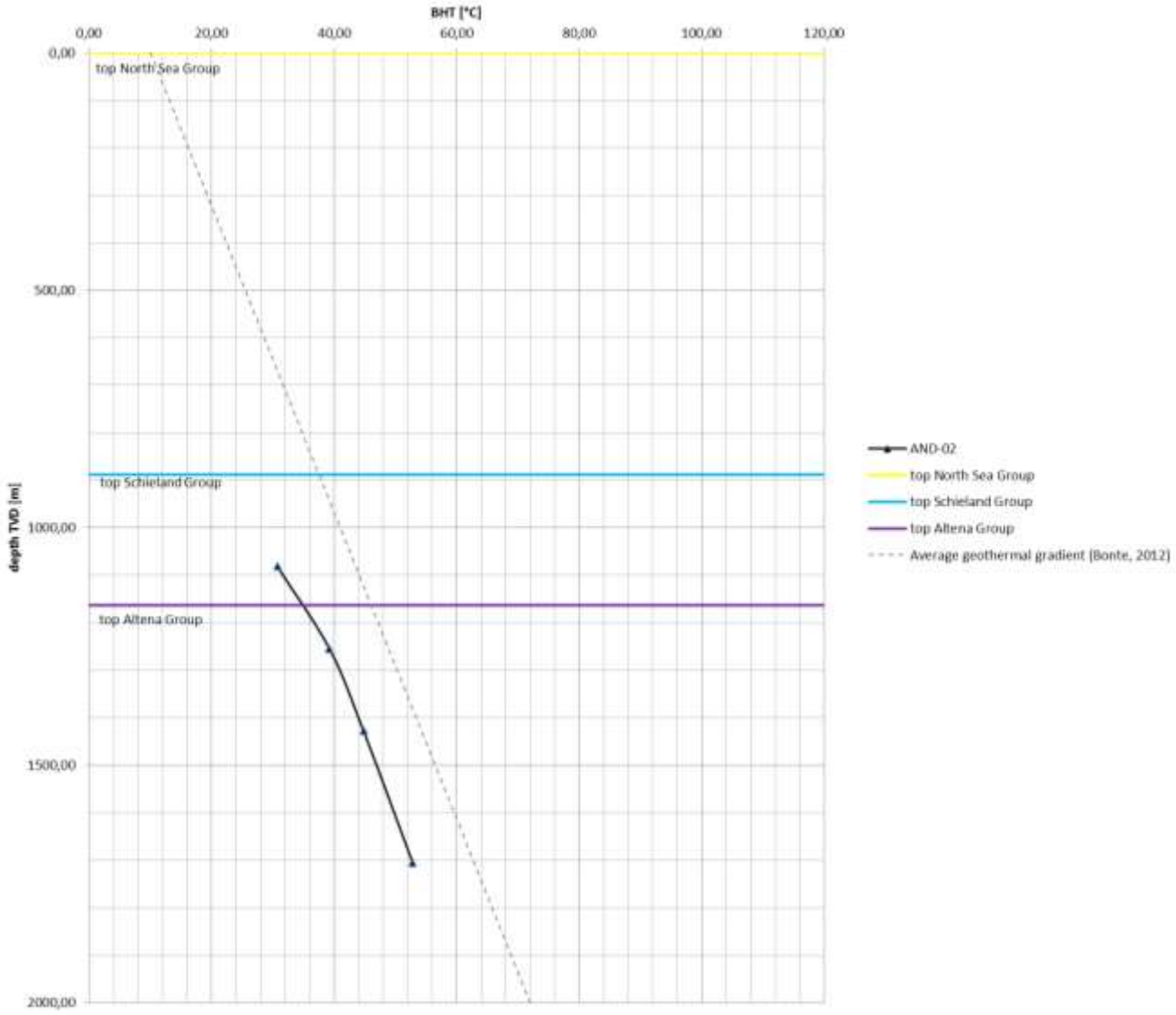

Figure 12: The temperature profile over depth for the AND-02 well (Andel-02). The formation tops encountered by the well are plotted in the diagram.

3.3 Formation dependent geothermal gradient

The distribution of geothermal gradients per stratigraphic interval is presented in the diagram of figure 15.

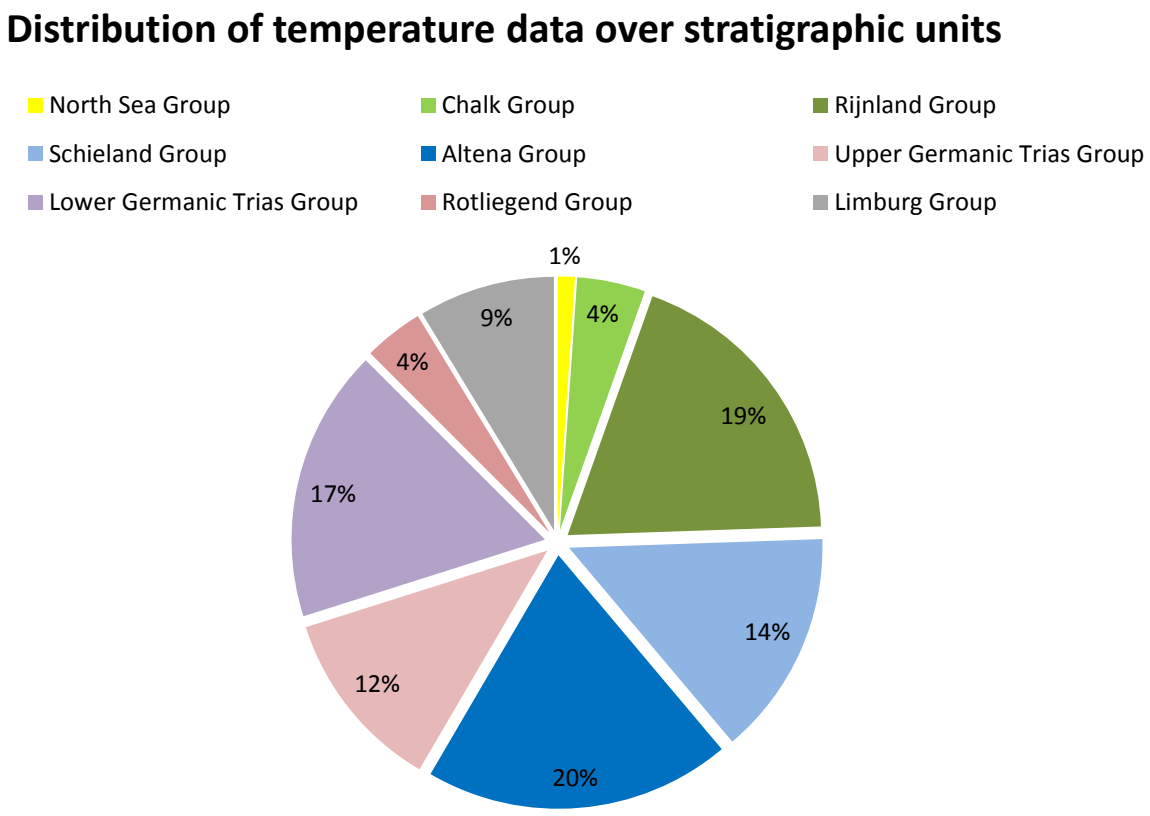

Figure 13: The relative distribution of temperature measurements over multiple stratigraphic units for which individual geothermal gradients were determined. Stratigraphic units as defined in the stratigraphic nomenclature (van Adrichem Boogaert et al., 1997).

The relative distribution of the temperature data points over the various stratigraphic units is non-equal. Specifically the North Sea-, Rotliegend- and Chalk Groups have a limited number of data points in the data set of the West Netherlands Basin and Roer Valley Graben. Table 5 presents the number of data points per stratigraphic interval of the 369 temperature data points, the average geothermal gradient over all data points measured in the specific stratigraphic units and the standard deviation of these. A graphic presentation of the comparison between the average geothermal gradient per stratigraphic unit and the overall average geothermal gradient is given in figure 16. The green bars present the calculated geothermal gradient per lithostratigraphic unit and the red bars indicate the average geothermal gradient of 31,3˚C/km (Bonté et al., 2012).

Table 5: The subdivision of geothermal gradients from stratigraphic groups. Geothermal gradients are based on 369 temperature data points divided over 129 wells in the WNB or RVG with at least one temperature measurement.

Stratigraphic unit	Number of data points/geothermal gradients	Average Geothermal gradient [˚C/km]	Standard deviation Geothermal gradients
North Sea Group	*4*	32,7	9.5
Chalk Group	*16*	35,1	9.9
Rijnland Group	*70*	29,8	5.6
Schieland Group	*53*	28,6	4.4
Altena Group	*72*	29,3	4.8
Upper Germanic Trias Group	*43*	33,8	4.7
Lower Germanic Trias Group	*64*	32,3	3.3
Rotliegend Group	*14*	31,4	2.4
Limburg Group	*32*	30,1	2.7
Total	*368*		

The calculated average geothermal gradients between the different stratigraphic intervals indicate clear differences. The geothermal gradients in the North Sea Group and the Chalk Group indicate higher increased geothermal gradients, though this may also be related to low amounts of data and a high spread in the temperature data when looking at the standard deviation. The standard deviation of the stratigraphic formation decreases further down, indicating that the calculated gradients have a lower spread in temperature range. The sandstones in the Rijnland and Schieland Groups are one of the main geothermal target reservoirs in western part of the WNB. The calculated average geothermal gradients for the Rijnland and Schieland Groups are respectively 29.8˚C/km and 28.6˚C/km. This is relatively low in comparison to the 31,3˚C/km geothermal gradient.

In contrast to these reduced geothermal gradients, sediments in the Triassic relate to a slightly increased average geothermal gradient of 33,8 and 32,3˚C/km for respectively the Upper and Lower Germanic Trias Group. Potential causes of these values might relate to sediment heat conductivity, known as thermal blanketing (Blackwell et al., 1989; Ter Voorde et al., 1994). This is discussed in paragraph 5.2.

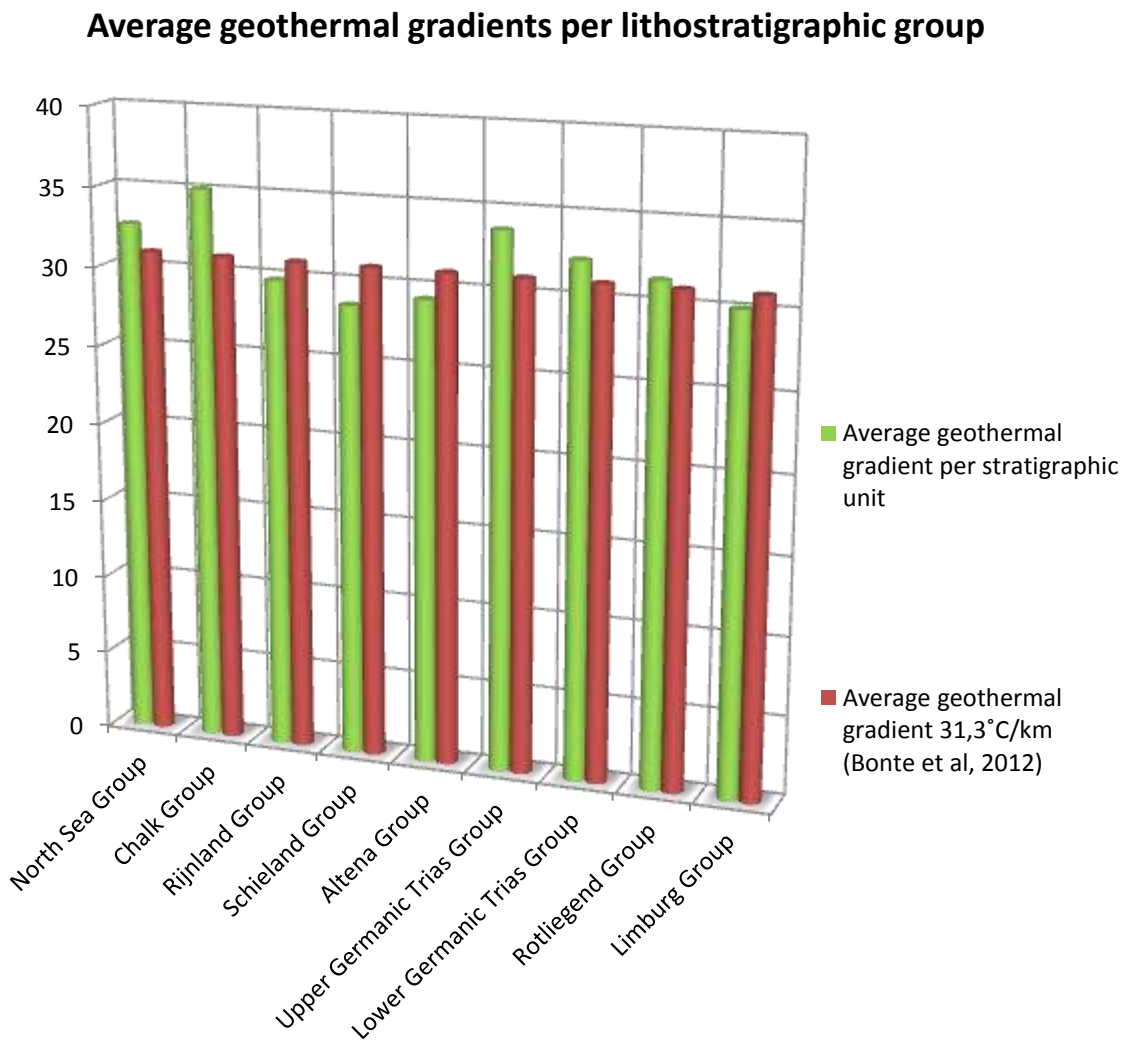

Figure 14: The average geothermal gradients per lithostratigraphic group shows various offsets in comparison with the average geothermal gradient in the Netherlands.

SUB-CONCLUSIONS:

1) Calculated geothermal gradients for measurements in the Schieland Group are significantly lower
2) Temperature gradients in the Triassic indicate significantly higher calculated geothermal gradients

3.4 Geothermal gradients map

In order to gain insight in the spatial distribution of potential temperature anomalies, calculated average geothermal gradients are plotted on a map together with the fault structures (See figure 17). The blue, yellow and red colours relate to the specific classification of the obtained geothermal gradients (see paragraph 2.2). The fault network map was obtained from the Dutch Oil and Gas portal (NLOG) and is based on a regional interpration. The faults are described by multiple attributes that indicate if the fault truncates stratigraphies of specific ages. This map is applied to gain insight in the orientation and dip of fault structures in the WNB and RVG, where truncations with younger ages are lighter in colour. Hence, a N-S trending pink line 'left' of a dark red line indicates that the fault dips towards the east.

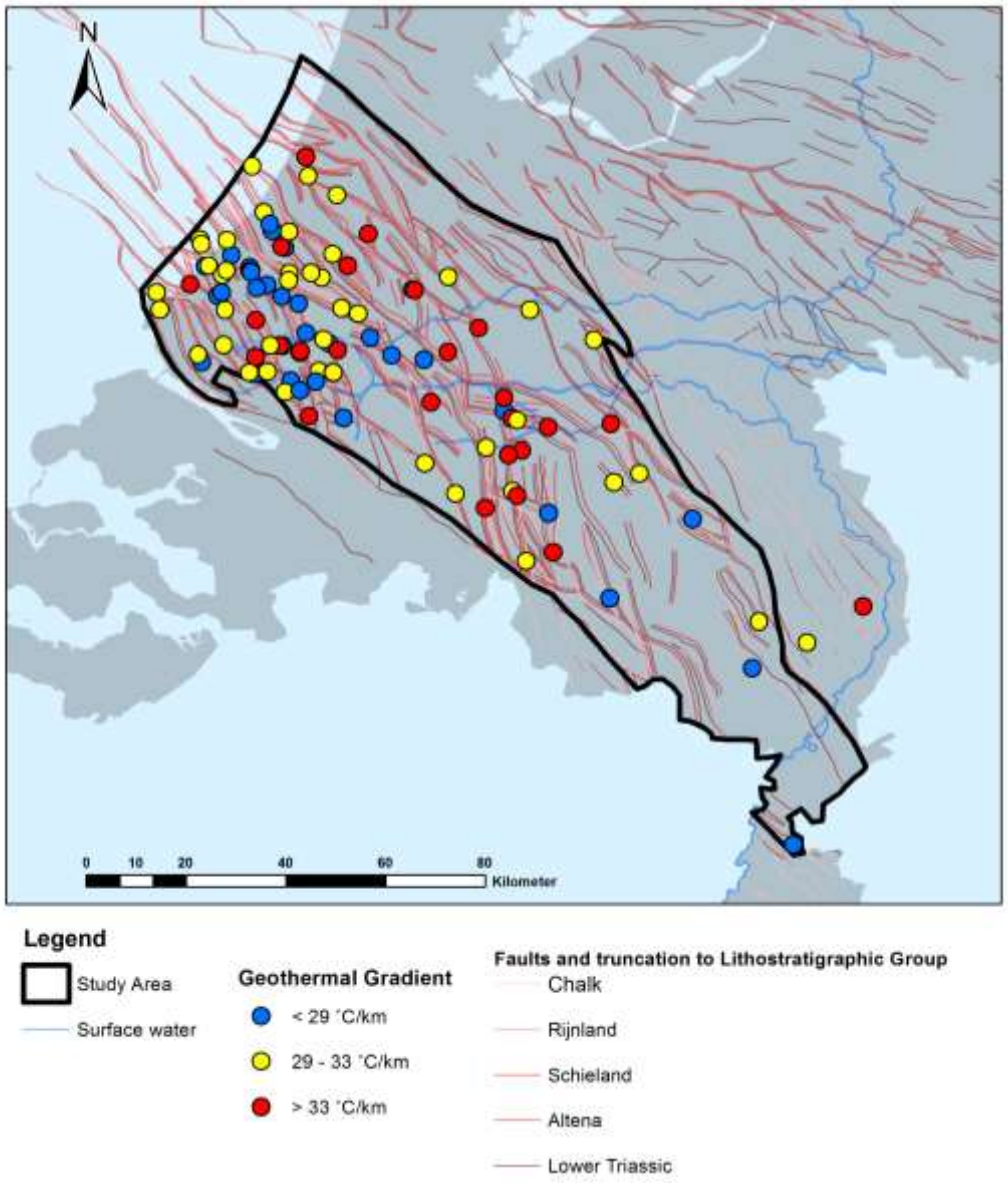

Figure 15: Presentation of the calculated geothermal gradient per well divided into three gradient classes. The plotted fault network on the background shows in overall structural setting.

3.5 Bottom hole temperatures wells >2000m and >3000m

The conventional geothermal window is roughly between 1500-3500 meter, the geothermal gradients of wells towards these depths give a better representation in relation to geothermal activities. The two maps below present the wells with geothermal gradient of wells deeper as 2000 meter (Figure 18) and wells drilled deeper than 3000 meter (Figure 19). Though the amount of temperature data in these figures is less in respect to the whole database (eg. Figure 15), the distribution of the three classes of geothermal gradients remains roughly the same, implying that depth does not directly indicates whether a geothermal gradient is increased or reduced.

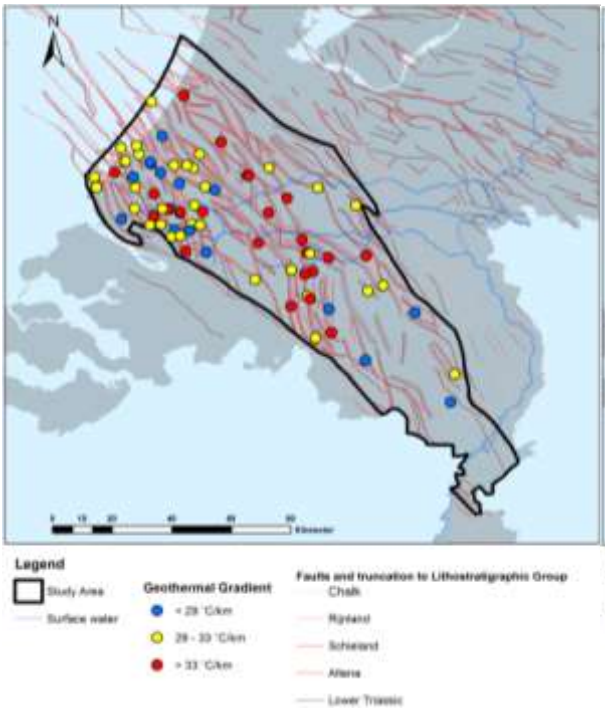

Figure 16: Average geothermal gradient map of wells deeper as 2000m.

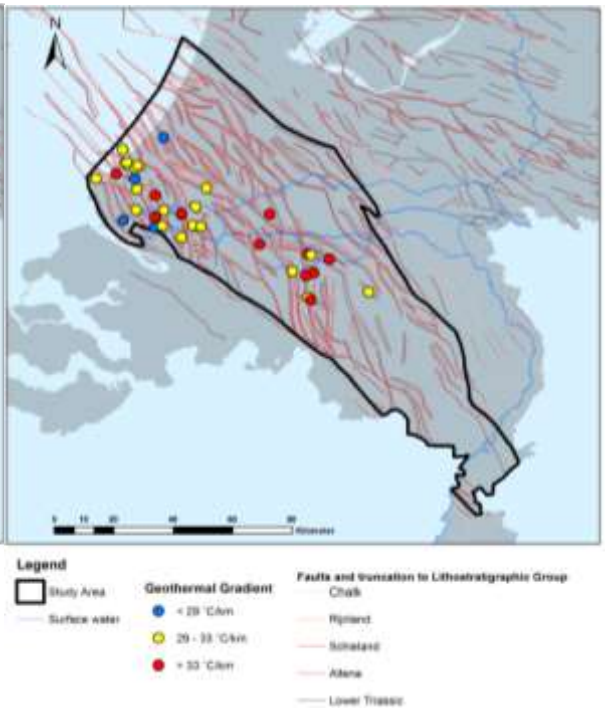

Figure 17: Average geothermal gradient map of wells deeper as 3000m.

The temperature data appears to indicate zones of equal geothermal gradient anomalies with specific trends. In the first map (figure 18) a zone of significantly increased geothermal gradients is clearly visible, stretching from the upper northwest towards the centre of the study area. Remarkably, this appears to correlate with the NNW-SSE fault trend in the central part of the study area, which slightly deviates from the general NW-SE trend. This phenomenon is further discussed in chapter 5. In the south-western part of the WNB a higher density of wells presents a greater variety in geothermal gradients. However, when geothermal gradients of similar anomaly classes are correlated to each other, parallel to the overall fault trend in the area, WNW-ESE trending zones appear. Figure 20 presents the visual anomalies related to the wells deeper as 2000 meter. Note that the anomalies are based on a visual interpretation. The wells in the northern part of the WNB with

increased geothermal gradients are not displayed in figure 19 anymore, since they do not reach 3000 meter. The geothermal gradients of equal classes are not correlated in the south-eastern part of the study area, due to the low amount of data in this area. This increased uncertainty makes it difficult to correlate the data points. However, the zones in figure 20 clearly illustrate the potential relation of geothermal anomalies to regional fault structures. In the next paragraphs an attempt is made to relate faults to temperature anomalies.

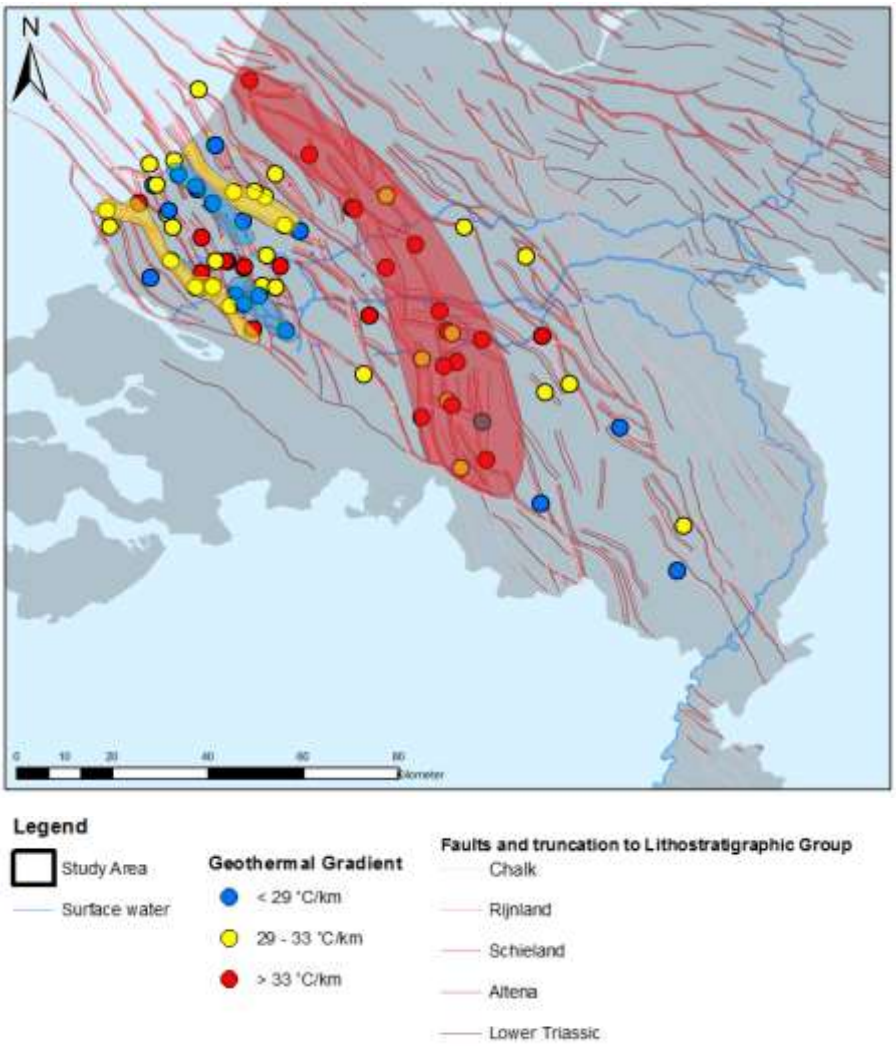

Figure 18: Presentation of geothermal gradient anomaly zonation, based on a visual interpolation. Zonation colours are equal to those of the geothermal gradient anomaly (red zone – increased gradients; blue zones – decreased gradients; yellow zone – average gradients).

SUB-CONCLUSION: Geothermal gradients appear to follow zones that relate to geological trends.

3.6 Relate faults to temperature anomalies

3.6.1 Three regions

For more in-detail investigation on the discovered temperature anomalies the study area is divided into three regions. Respectively: region A, B and C (see figure 21). The regions are presented in figure 21.

- *Region A* covers the West Netherlands Basin and has the highest density of data points. An analysis over the area indicates an approximate equal amount of negative- (blue), neutral- (yellow) and positive temperature anomalies (red).
- *Region B* is situated over the eastern part of the West Netherlands Basin and the western part of the Roer Valley Graben. The region covers less data points in regards to region A. Overall, this area contains mainly positive temperature anomalies in comparison to region A. The highest density of data points is situated in the central and south-eastern part of the region, east of 's-Hertogenbosch.
- *Region C* is characterized by its larger size and the low density of data points. Overall, the map indicates relatively more negative temperature anomalies in relation to the other two regions.

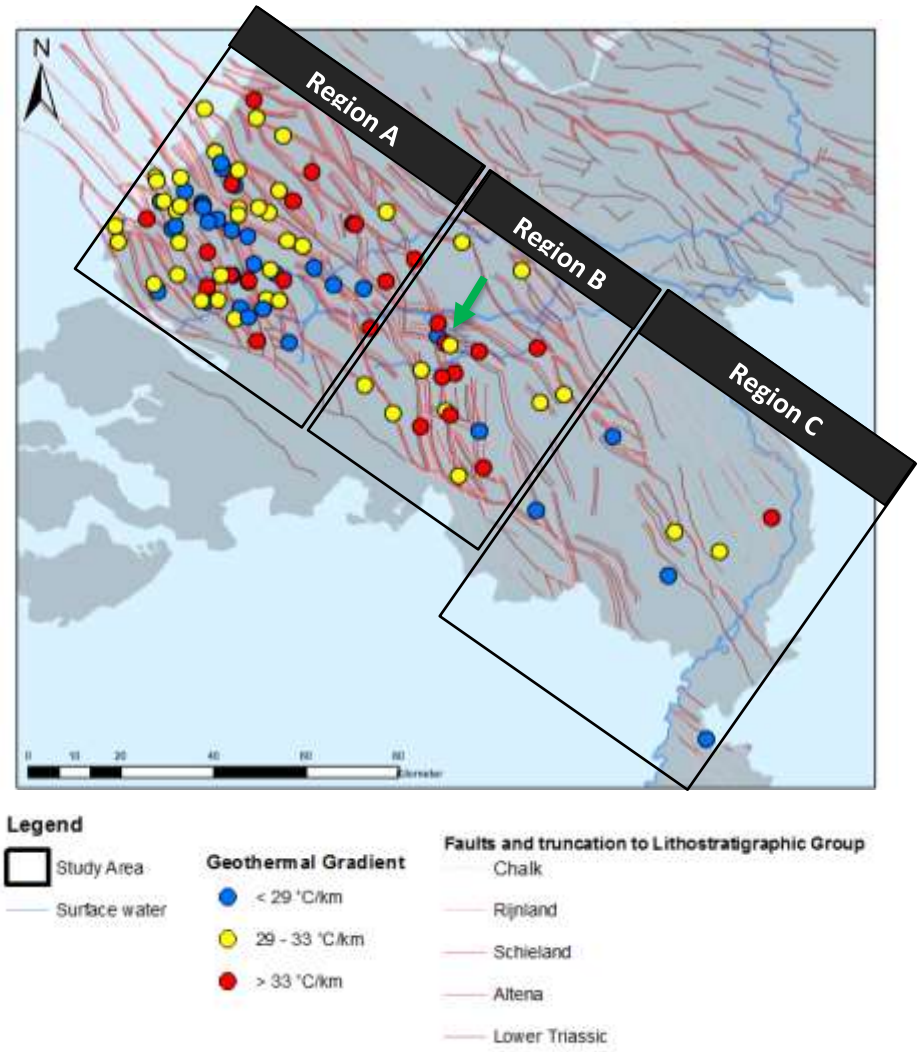

Figure 19: The three regions inside the study area.

For each of these regions multiple seismic sections were interpreted and multiple wells are petrofysically evaulated. Zones of high interest are the areas with significant increased or decreased temperature anomalies, located at (relatively) short distance from each other. An example is the central part region B (green arrow). Two increased-, one average- and one decreased geothermal gradient are located at a few square kilometres. These wells are also positioned inside a high density fault belt as noticed in paragraph 3.5.

3.6.2 Petrophysical evaluation

Identification of a fault within a borehole is possible in various ways. One of the most obvious one is a doubling or missing part of a stratigraphic interval, which could be the result of a normal or reverse fault. Another indication of faults are losses of drilling fluids during the drilling process. Though losses can be the result of penetrating a very porous reservoir, it's also possible that losses occur at a fault. This could result in a technical failure of the well.

Analysis of available logs of the borehole may also assist in fault identification. The presence of a fault in a borehole may result in a sudden change of various logs. For example: the caliper log registers the geometrical shape of the borehole. When a fault is penetrated, the formation around the fault is often non-stable, which can result in partial borehole collapse. If this is the case, the size of the borehole at the fault location is slightly bigger in respect to the diameter of the drilling bit, which can potentially lead to a sudden offset in the borehole diameter size in the caliper log. Additionally, porosity logs may show an anomaly due to the sudden 'increase' in porosity (in this case, an open hole). In the upcoming section, such sudden spikes in the logs are studied in various wells in the study area. Additionally, the formations near the faults are analysed for increased and/or decreased reservoir properties. Initially faults indicated on composite well logs and/or on the lithostratigraphic columns have been taken into account. Seismic data was also consulted for the potential presence of faults in wells and at what approximate stratigraphic interval and depth.

3.6.2.1 Well selection

In this petrophysical study several wells were examined where faults are identified and/or expected. Public available regional fault maps provided by TNO (www.nlog.nl), have been consulted for a first estimation to determine which wells are in the close vicinity of a fault. Additionally, an attempt has been made to apply a good distribution over the study area. The selected wells are shown in the map below (figure 22). The selected wells have also been analysed on seismic data to assess the presence and the approximate depth of faults (see paragraph 3.6.3).

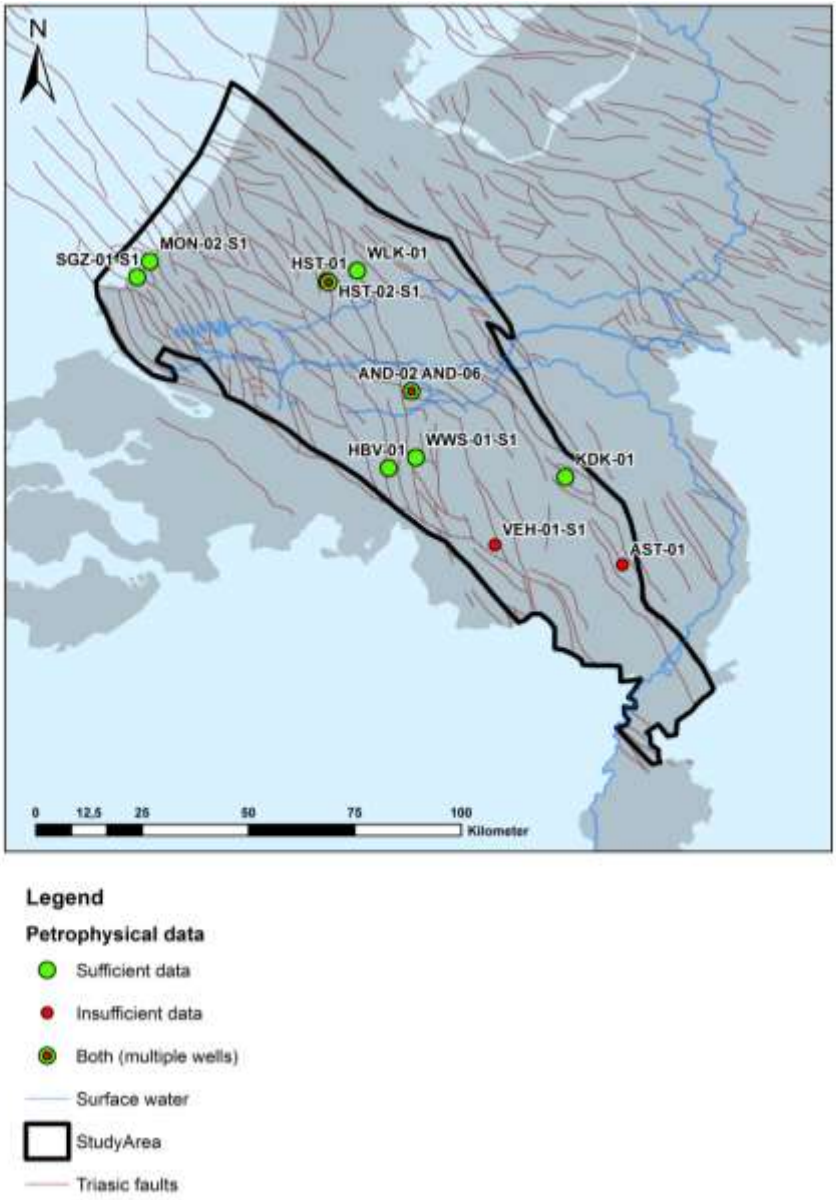

Figure 20 Location of the selected wells for the petrophysical analysis. Wells with insufficient and/or poor quality of log data are marked with a red dot.

In the Roer Valley Graben, the amount of available wells is limited. Of three selected wells near fault zones, only one well provided suitable data for the petrophysical analysis: Keldonk-1 (KDK-01). Some wells are relatively old and as a result these wells often lack sufficient logs and/or the quality of the logs is not suited for the aims of the petrophysical evaluation. For example: for Haastrecht-1 (HST-01) only a limited caliper log; a spontaneous potential log (SP) and few resistance logs are available. For well Andel-2 (AND-02) only vintage analogue logs are available. Consequently, these wells could not be analysed.

To assess the presence and effects on a borehole, three logs have been consulted: gamma ray (GR), the density log (RHOB) and the caliper log. The gamma ray is used to distinguish between sand- and claystones and additionally is used as a reference log. To assess the effects of the fault on the porosities of potential sandstone reservoir, the density log is consulted. Though other logs like the sonic (DT or neutron porosity (NPHI) can also indicate porosities, the density log is specifically tailored for calculating porosities in sandstone reservoir. When available the caliper log is used to check if potential higher porosity values are caused by a sudden increase in borehole diameter, which could be the result of partial borehole collapse related to a fault. In that case, the high porosity basically directly relates to the measurement of a 'gap' in the borehole. In table 6 an overview of the available logs per selected well is presented.

Table 6 Overview of the available logs for the selected wells. Logs may only be available at specific intervals of the borehole.

Well Name	Well Code	Gamma ray	Caliper log	Density log	Suitable for study
Andel-2	**AND-02**				
Andel-6	**AND-06**	x	x	x	x
Asten-1	**AST-01**				
Huibeven-1	**HBV-01**	x	x	x	x
Haastrecht-1	**HST-01**		x		
Haastrecht-2-Sidetrack1	**HST-02-S1**	x	x	x	x
Keldonk-1	**KDK-01**	x		x	x
Monster-2-Sidetrack1	**MON-2-S1**	x	x	x	x
's-Gravenzande-1-Sidetrack1	**SGZ-01-S1**	x	x	x	x
Veldhoven-1	**VEH-01**		x		
Willeskop-1	**WLK-01**	x	x	x	x
Waalwijk South-1-sidetrack1	**WWS-01-S1**	x	x	x	x

3.6.2.2 Log Analysis

Depth corrections

For the analysis, a small correction needs to be applied to take differences between drillers depth (DD) and loggers depth (LD) into account. The cable where the logging equipment is attached will extend during the logging job in a different way to the normal drill pipes, which leads to a small difference between the LD and reported AH depths. As such, if core data was available, a correction has been applied to correlate the cores to the correct lithologies according to the logs. Another correction to the logs was applied at overlapping intervals of different drill sections, which usually occurs around casing shoes.

Porosity calculation

As the study relates to a bulk evaluation at different stratigraphic levels, assumptions need to be made in the porosity calculations. The presence of gas and oil in the area should normally also be accounted for. However, for the current evaluation, the focus is set on identification of faults in the logs. As such, the overall matrix rock density is assumed at 2,65 g/cm³ and for brine density 1,05 g/cm³ is applied. The value for rock density is a common value which relates to the average density of clean sands. Though there are always impurities in sandstones, like clay and/or concretions, it's impractical to compensate for the specific matrix rock density in detail. The same applies for brine density, which also varies in the subsurface. As the current study focuses on overall indications of improved/decreased reservoir properties, standard values are applied. As a result the calculated porosities only give an indication of the porosities, in order to compare different intervals with each other.

The following formula has been applied to calculate the porosity:

$$\boldsymbol{\rho_{bulk\ density} = \phi * \rho_{brine} + (1 - \phi) * \rho_{matrix}} \qquad \text{(V)}$$

In which the parameters are:

$\boldsymbol{\rho_{bulk\ density}}$	= combination rock and fluid density (density log)	[g/cm³]
$\boldsymbol{\rho_{brine}}$	= brine density (assumed 1,05 g/cm³)	[g/cm³]
$\boldsymbol{\rho_{matrix}}$	= matrix rock density (assumed 2,65 g/cm³)	[g/cm³]
$\boldsymbol{\phi}$	= porosity	[-]

3.6.2.3 Results

As indicated, possible identification of a fault on logs, may be related to a sudden decrease in the density log and/or a sudden increase in the caliper log. In figure 23 an example is visible for well AND-06. However, faults are not always visible in the logs. In figure 24 this is visualized for well HST-02-S1. Though multiple faults are reported in the CWL of this well, the logs do not show any indications of this.

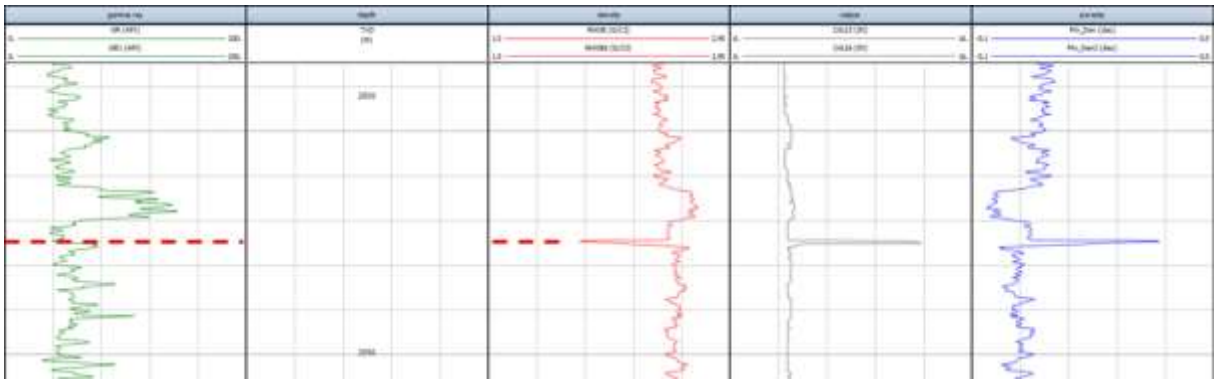

Figure 21 Well AND-06: from left to right gamma ray log (green), density log (red), caliper log (grey) and calculated porosity (blue). The sudden increase in caliper and porosity, indicates a fault at 2520 m (dashed line).

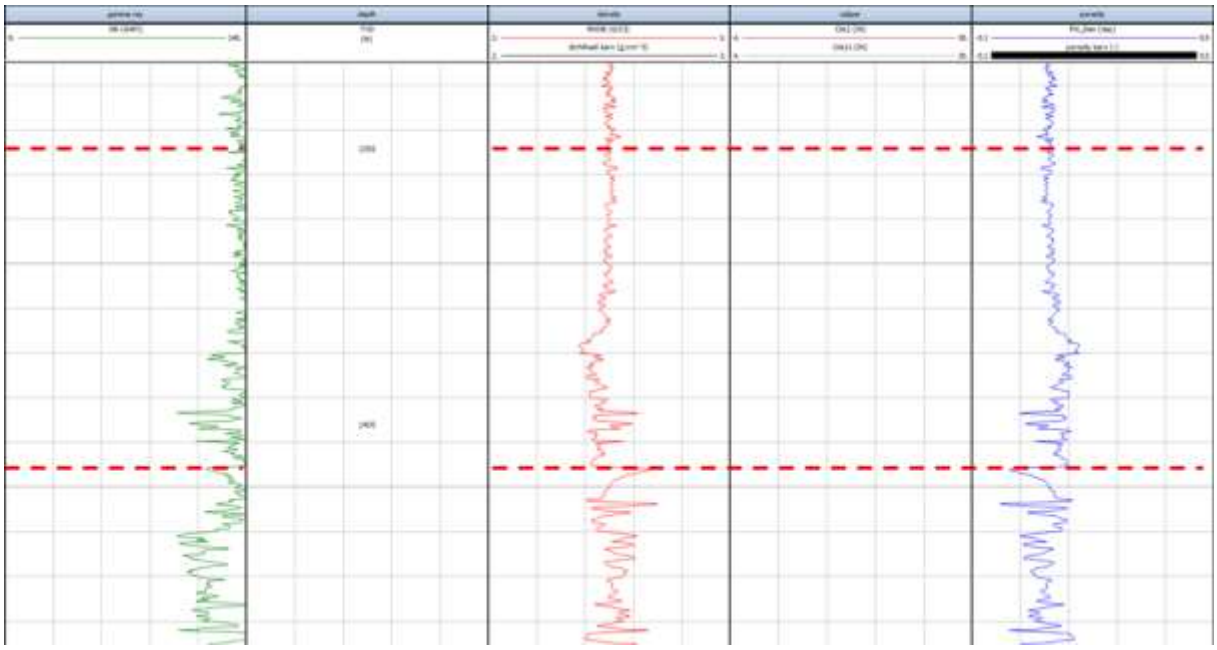

Figure 22 Well HST-02-S1: According to the CWL, multiple faults are present in the well, including at depths 1350 m and 1410 m TVD (dashed lines). However, these faults are not visible on the logs. Note that no caliper log is available at these depths.

Region A-west: SGZ-01-S1 and MON-02-S1

Both wells are located in the Westland area approximately four kilometres from each other and target the same Triassic sandstone reservoirs. Both wells also report faults: In SGZ-01-S1 at 2905 m AH at the base of the Schieland Group; in MON-02-S1 a fault is reported at 2660 m AH. For SGZ-01-S1 insufficient logs are available to recognize this fault in the logs. In MON-02-S1 the fault is visible in the logs at the base of the Sleen Formation at 2660 m TVD (see figure 25).

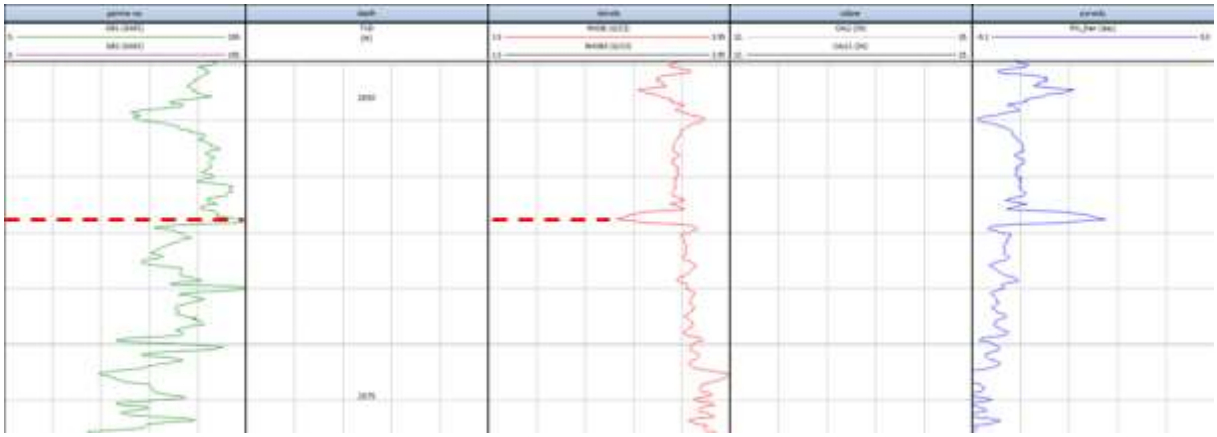

Figure 23 Well MON-02-S1: the sudden drop in the density log at 2660 m TVD (dashed line) indicates the presence of a fault.

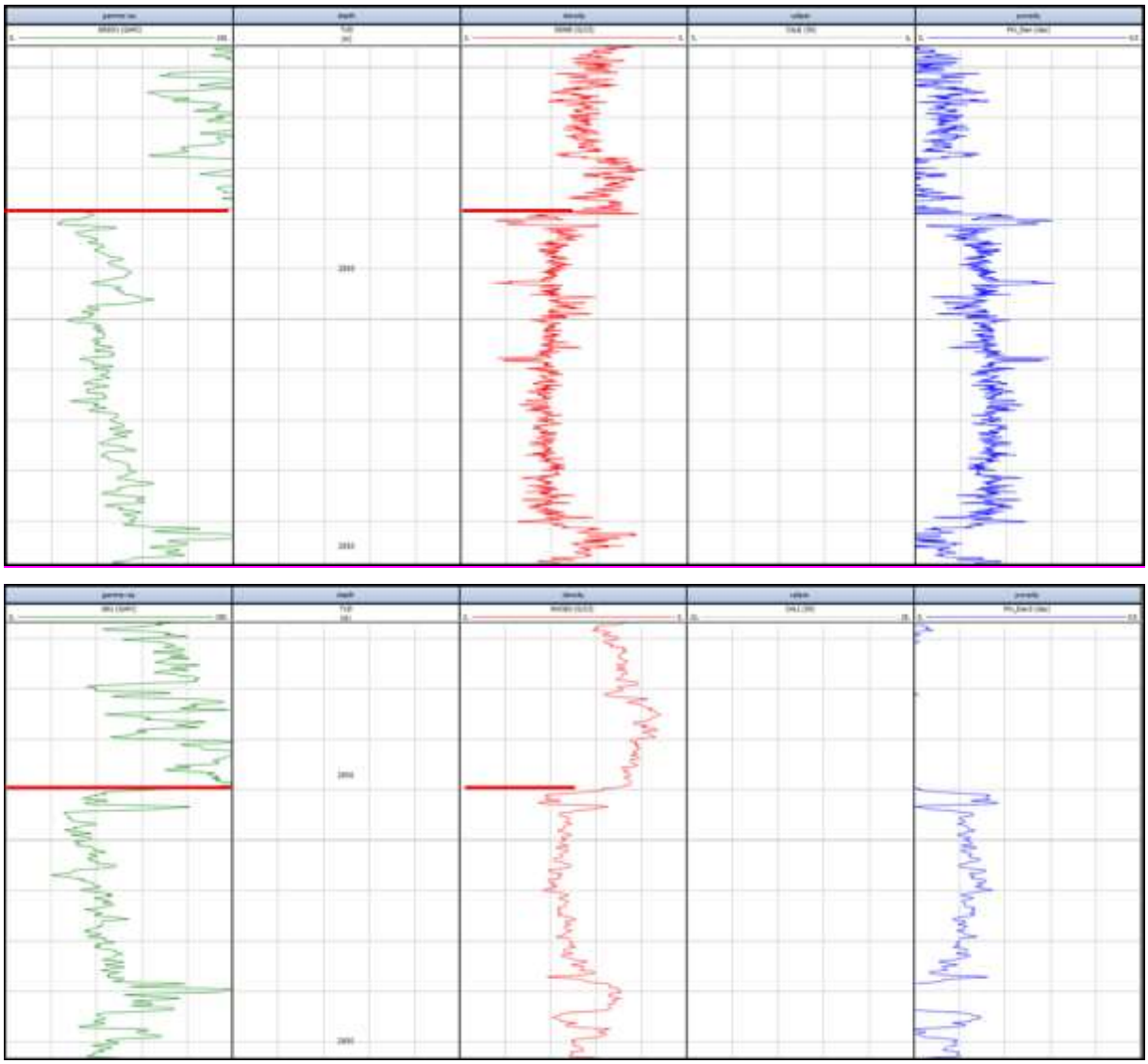

Figure 24 Calculated porosities of the Hardegsen in SGZ-01-S1 (upper figure) and MON-02-S1 (lower figure). Red line indicates top Hardegsen.

Region A-north: HST-02-S1 and WLK-01

Well HST-02-S1 and WLK-01 are both located in the northern part of the WNB. In both wells faults are reported in the borehole. In HST-02-S1 these faults are not visible on the logs (see figure 24). In WLK-01 a reverse fault is reported in the Aalburg Formation. At the fault zone a porosity increase can be seen, though the caliper does not show any significant change at that depth (see figure 27). However, just above and below the caliper log shows distorted zones (purple lines), which also relates to increases in porosity. At the red line, low densities are reported with high porosities, however the caliper does not show a sudden increase. All together this part of the well appears to indicate the damage zone of the fault, within an interval of approximately 25 meters. The highest porosities (up to 15 to 20%) are related to a clayey formation according to the GR, which indicates a

potential open fault. Interestingly enough, no specific losses are reported in the well. This would indicate that though the hole may be open at the borehole itself, the fault appears to be closed just away from the fault, as otherwise drilling fluids would very likely have been lost.

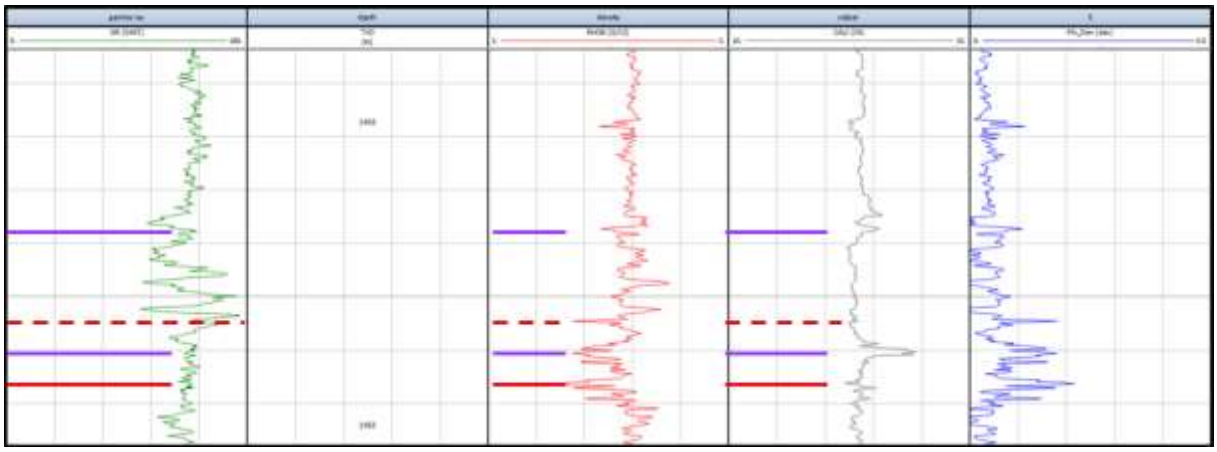

Figure 25 Well WLK-01: the fault plane is reported at the dashed line. Just above and below the fault, the caliper log shows a distorted zone (purple lines). Red line indicates low densities, though caliper does not show a sudden increase.

Region B-south: HBV-01

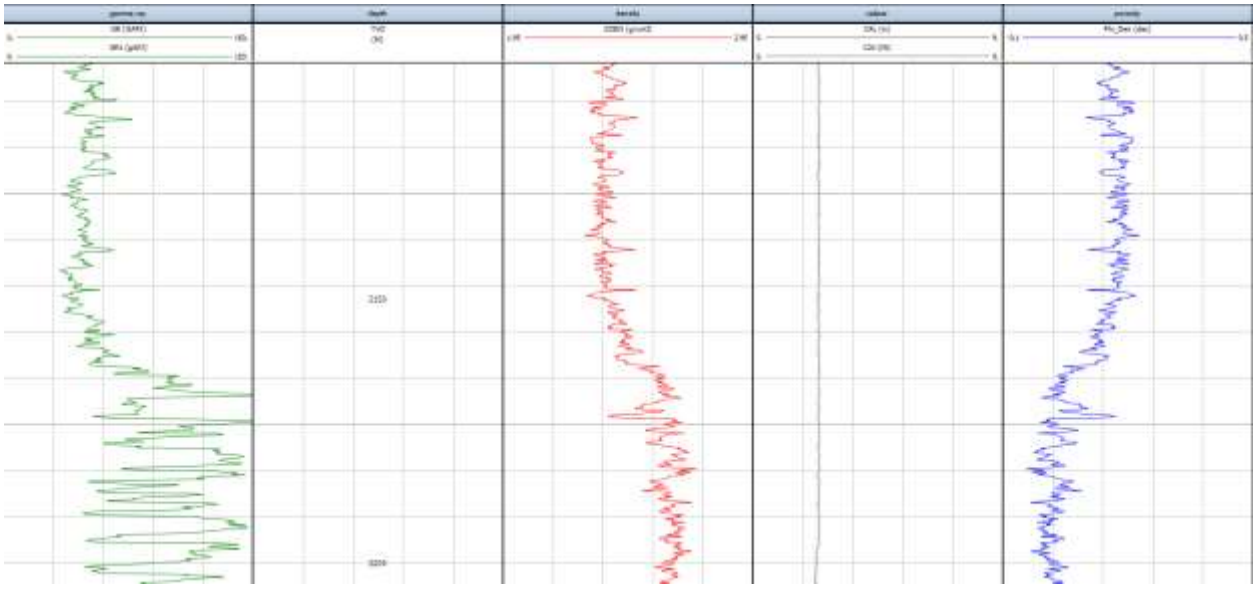

Figure 26 HBV-01 fault at 2170 m: Sudden increase in porosity with no change in the caliper log.

In well HBV-01 a fault is reported at 2170 m. In figure 28 the fault at 2170 m doesn't have a change in the caliper log. However, the porosity is so much higher that this could potentially relate to the fault. A potential explanation is that the present lithology was stable enough to prevent from collapsing.

Region B-Center: AND-02 and AND-06

In the center of region B wells AND-02 and AND-06 are located close to each other, though both wells indicate different geothermal gradient with respectively 23.0 and 37.5 'C/km. However, Andel-02 did not penetrate the Triassic sandstone reservoir, which acts as the reservoir of the Andel gas field. The structural map of the field already indicates multiple faults in the reservoir (see figure 29). The trajectory of AND-06 is located close to a normal fault at reservoir level. Within the well, eight normal faults are reported throughout the well between 1410 and 2630 m TVD, within the Werkendam Formation and the Triassic interval. The faults in the Triassic interval (five) very likely relate to the mapped normal fault. In the Triassic interval the various logs indicate sudden drops and increases at these depths, which correspond to the interpreted faults (see figure 30). However, the interval above and below the faults do not indicate significant increased or decreased reservoir qualities, according to calculated porosities. This appears to indicate that the faults do not have a direct effect on reservoir properties. In the well significant losses are reported at the Triassic interval, which is an additional argument indicating that the faults are potentially open.

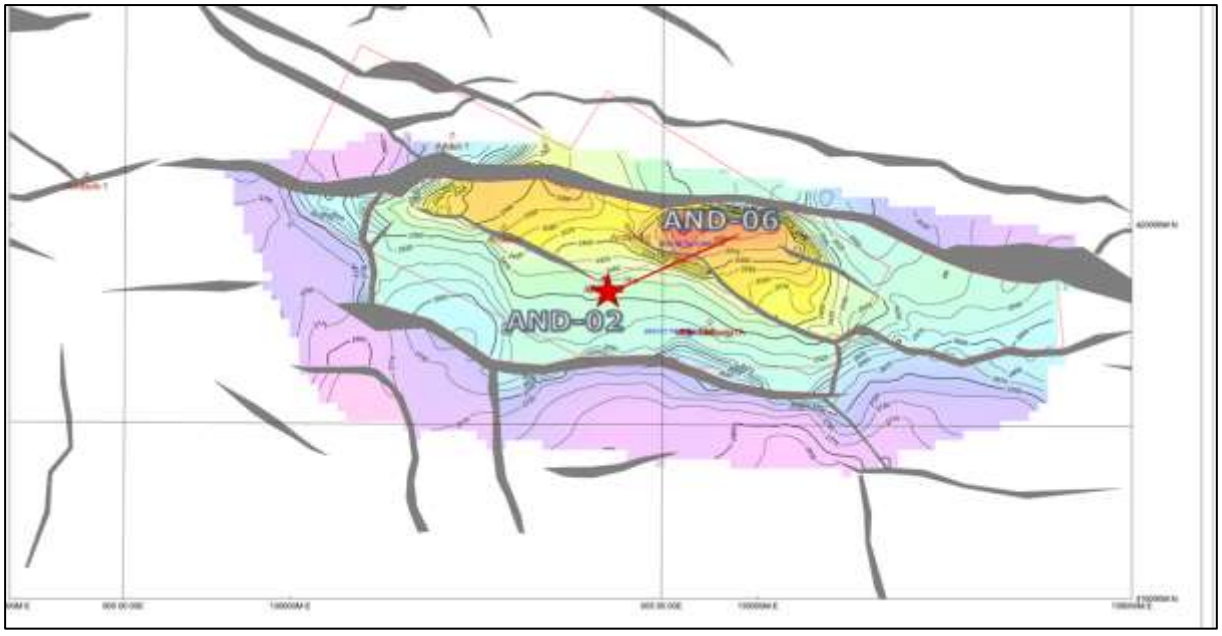

Figure 27 Structural map of the Andel gas field, including wells AND-02 and AND-06. Depth contours indicate top Buntsandstein reservoir. N.B. Only AND-06 penetrated the reservoir. Source: Structural map, Andel field, 2007. NLOG.

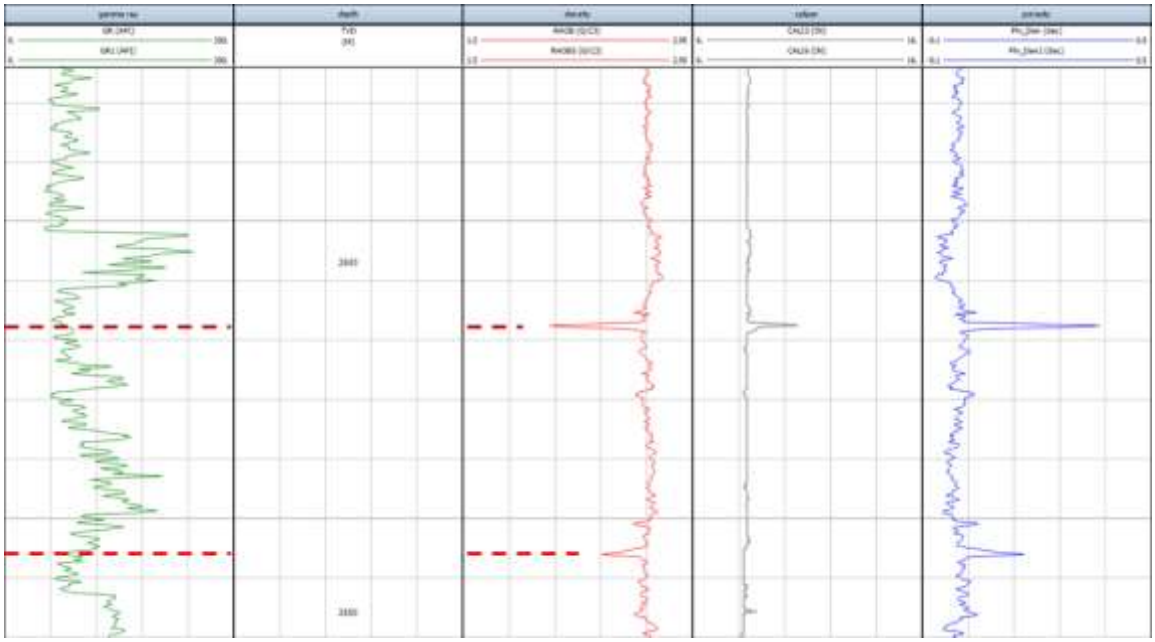

Figure 28 Well AND-06: indications of faults at 2610 m and 2630 m TVD (dashed lines). Caliper log of the lower fault does not indicate a sudden increase.

Region C: KDK-01

In the RVG the main fault zones are located on both sides of the grabens. In this region, three wells are located near these faults: KDK-01, VEH-01-S1 and AST-01. As indicated in table 6, only well KDK-01 contains sufficient logs for the analysis. At this well, a fault is reported at 1620 m AH. Due to the lack of a caliper log, the geometry of the borehole cannot be verified. The density log at this depth also does not indicate any direct suggestion for a fault (see figure 31). However, slightly higher in the well, there is a sudden drop in the density log which may potentially indicate the presence of a fault.

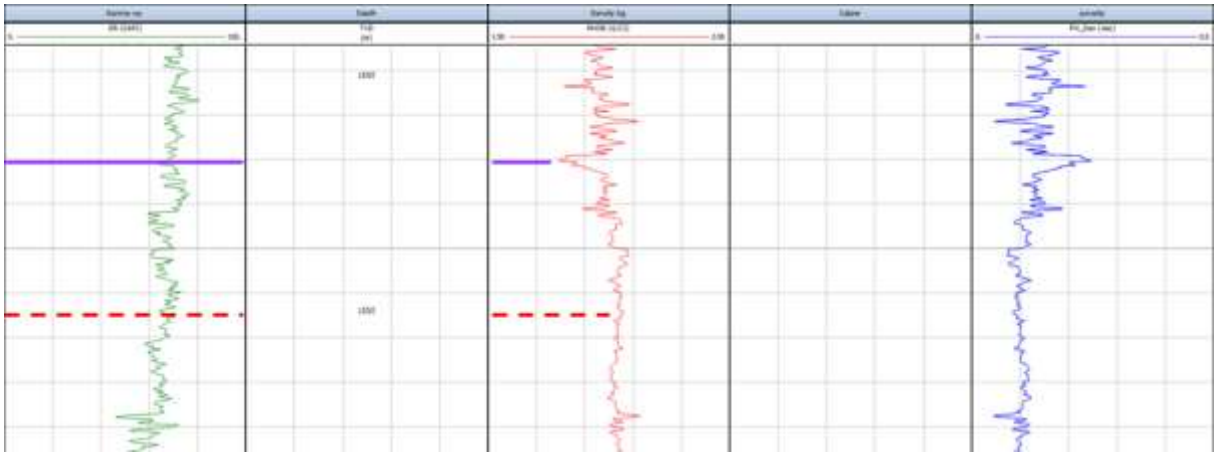

Figure 29 Well KDK-01: the reported fault cannot be identified on the logs (dashed line). Slightly higher in the well density suddenly drops in a clayey interval, suggestion a potential presence of a fault (purple line)

3.6.2.4 Californië geothermal wells

The current geothermal wells in the WNB are not directly targeted at fault zones. However, the wells in the vicinity of Californië drilled to, and produce from a reservoir in a fault zone (CAL-GT wells). The wells are located near Venlo in the northern part of the Limburg province. These wells are not located inside the study area, but on a horst block north of the RVG. Consequently, they are of interest for this research project and are shortly discussed in this paragraph.

A specific difference between the CAL-GT wells and the wells inside the study area is the type of reservoir rock. In contrast to the siliclastic sandstone reservoirs in the WNB and RVG, the CAL-GT wells are drilled to limestones from Dinantian - Early Carboniferous ages (Broothaers, 2013). The encountered Dinantian limestone has a very limited matrix porosity and permeability (Feket et al., 2009; Broothaers, 2013). For this reason, the wells are drilled to a fault zone with potential meteorically and/or hydrothermally karstified zones with increased permeability. Mud losses occurred during drilling and production rates from this limestone reservoir appeared high (Broothaers, 2013).

No density logs are available for the CAL-GT wells, which did not allow complete petrophysical evaluation for this project. Available logs from the CAL-GT-01 and CAL-GT-02 wells are presented in figure 32. These logs are adopted from a report by Broothaers (2013), in which the well logs are described in detail. The main conclusions in this report are:

- At CAL-GT-01 at depths between 1735m to almost 1800m MD, the caliper indicated a large cavity. At this depth interval, total mud losses are encountered.
- At the other zones in which mud losses occurred, small openings are discovered. These are interpreted as open faults and fractures. Mud losses in these intervals are limited, and did only occur for several meters at the time.
- At approximately 2330m MD, the large Tegelen fault (based on seismic data) is interpreted. The caliper log indicates openings and mud losses are encountered at this depth.
- The permeability is based on fractures and karstified zones in CAL-GT-01. In CAL-GT-02 the permeability is entirely based on karstified zones.
- Large faults are not required for sufficient permeability. Smaller faults can either cause sufficient permeability values for geothermal production. These smaller faults may be connected to a larger fault network at greater distance from the well.

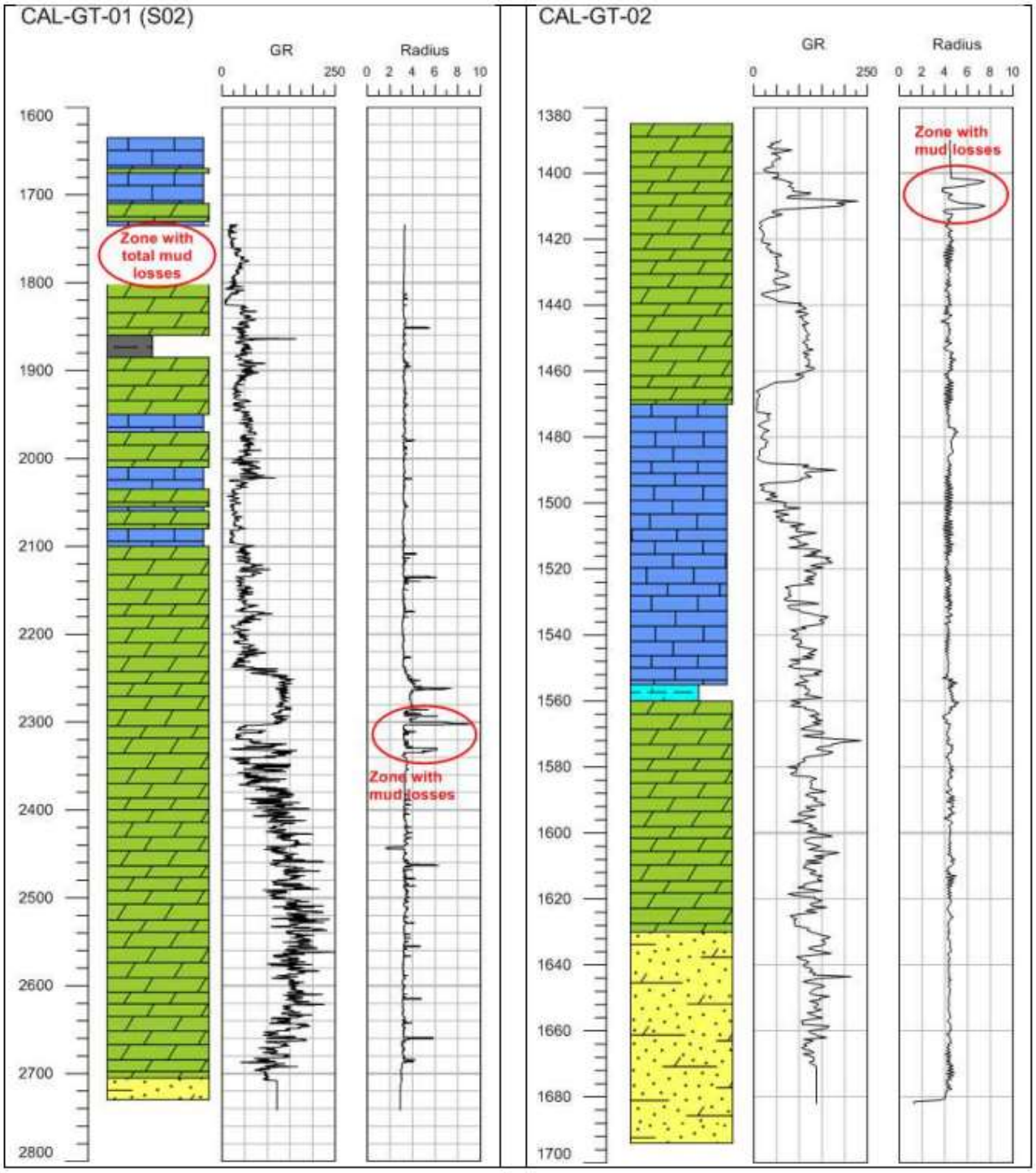

Figure 30: Wireline logs from two Californië geothermal wells, including zones with losses (after Broothaers, 2013).

3.6.2.5 Mud losses

Multiple wells in the study area encountered mud losses during drilling. A dataset was supplied by EBN and subsequently a relationship between geothermal gradient anomalies and mud losses occurrence was analysed. Wells in which mud losses occurred during drilling are plotted in figure 33. If temperature data was available, the calculate geothermal gradient is also indicated. Most of the wells are located in the central part of the study area, in region B. For some wells the expected reason for the mud losses are related to 'unstable sediments'. However, for most wells the exact reason for the losses in unknown (source: EBN Drilling Hazards Database). Only two wells with mud losses indicate a decreased calculated geothermal gradient. All other wells with losses have an average or significantly increased geothermal gradient.

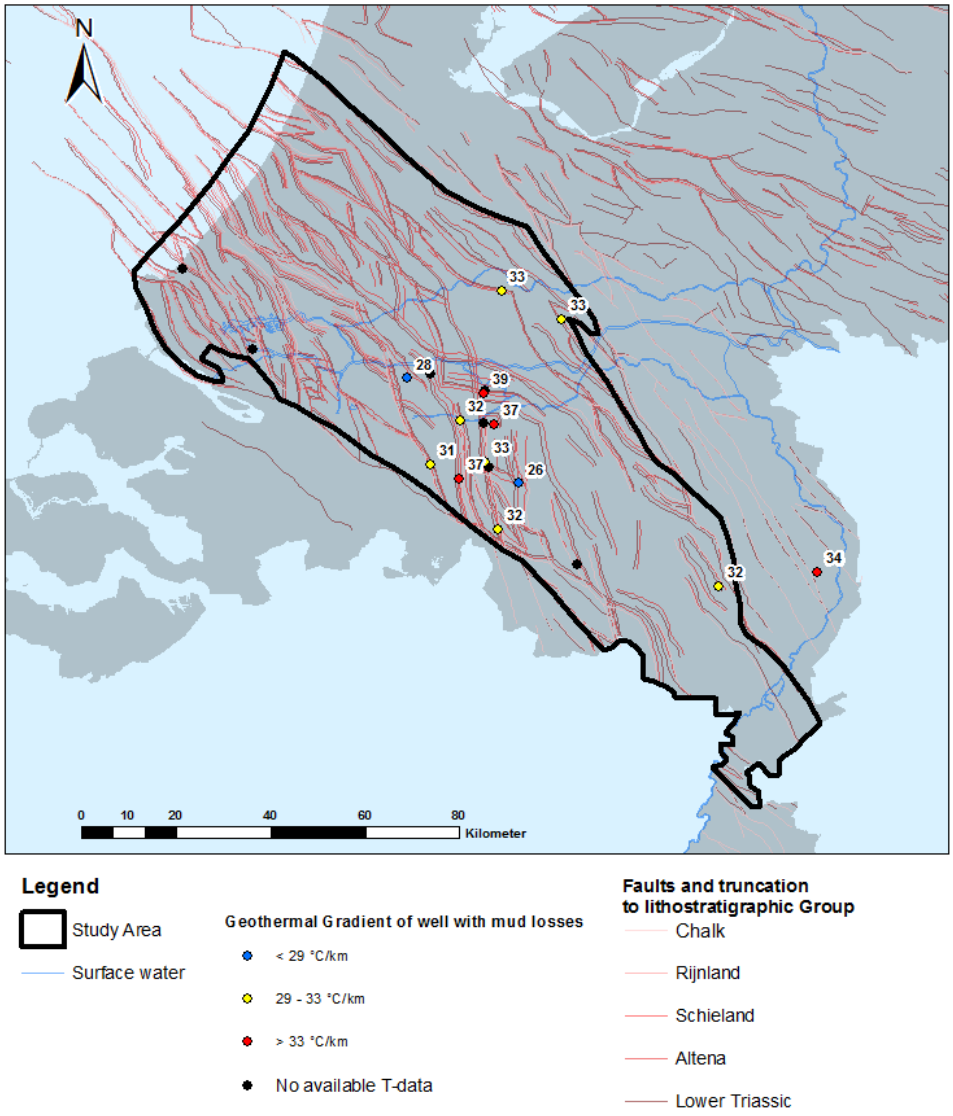

Figure 31: Wells with registered losses and temperature data in the study area. The geothermal gradients are plotted next to the data points.

3.6.3 Seismic analysis

Interpretations are done on selected seismic lines for the three defined regions in the study area, respectively region A, B and C. Selected lines cross geological structures with (a variation in-) geothermal gradient anomalies. Multiple wells along the seismic lines are investigated on their petrophysical properties in the previous paragraph. See figure 34 for location of the seismic lines.

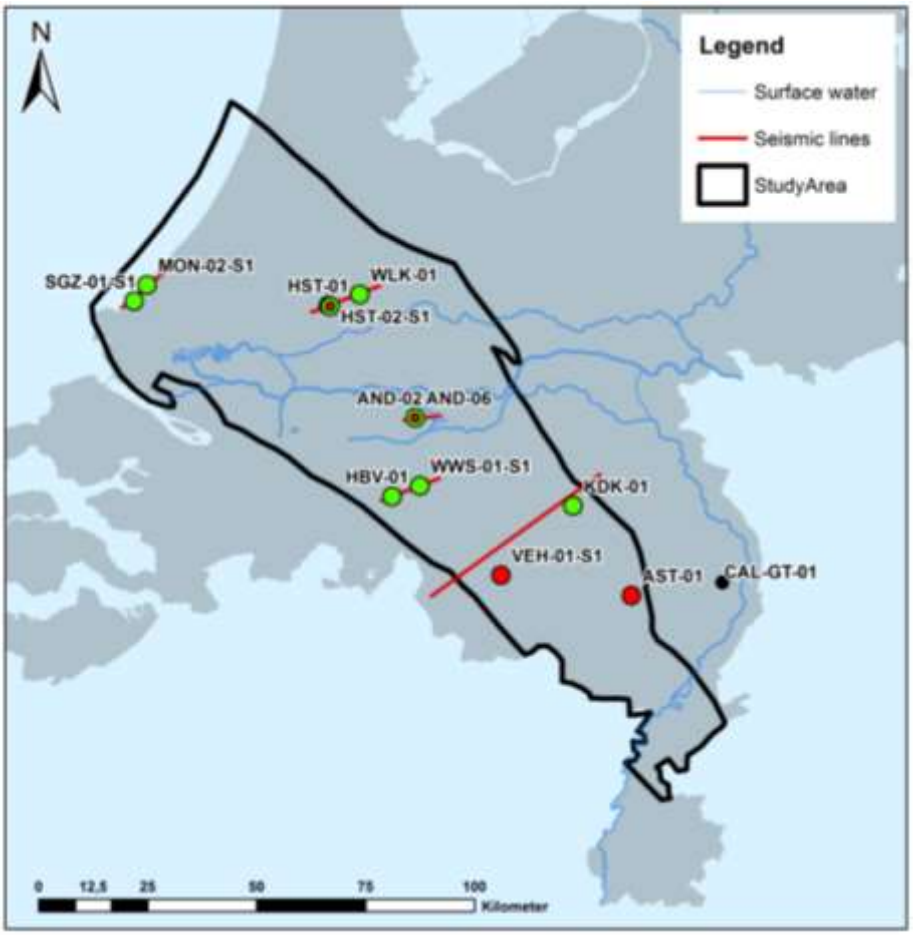

Figure 32 Overview of the location of the seismic lines. Lines are located over the various wells analysed for the petrophysical selection

3.6.3.1 Region A

In region A, three wells in the Westland area have been analysed in the seismic data: wells MON-03, MON-02-S1 and SGZ-01-S1, with average geothermal gradients of respectively 32.3˚C/km, 28.9˚C/km and 35.8˚C/km. Especially well SGZ-01-s1 indicates an increased geothermal gradient. Figure 34 shows a seismic cross-section over these wells, based on a 3D seismic cube that covers the area around Monster and ‘s-Gravenzande. As can be seen on the plan view in the right lower corner of figure 35, the western part of the seismic section is acquired offshore and the eastern part onshore. This may cause the difference in resolution at depths exceeding 2.000ms TWT.

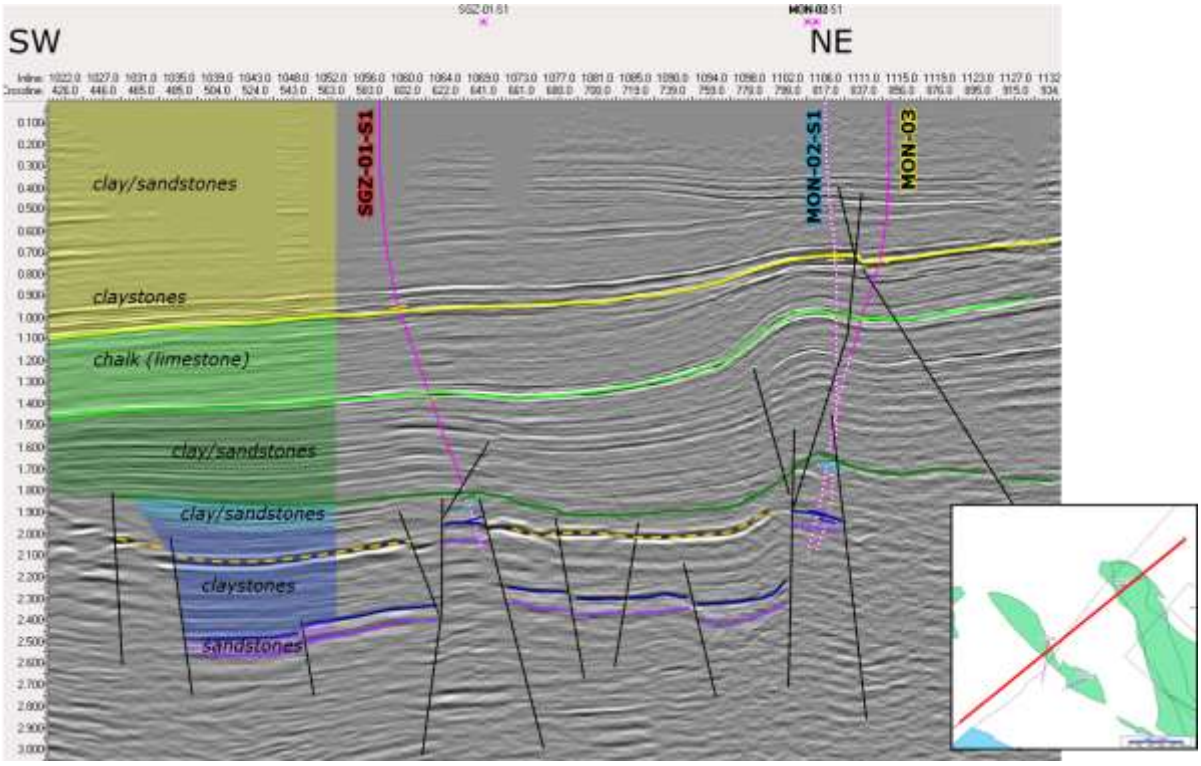

Figure 33: Seismic line (SW-NE) from 's-Gravenzande to Monster in the West Netherlands Basin. Well paths of the three selected wells are projected on the seismic transect with pink lines. Dashed purple well path indicates that the well path is behind or in front of the seismic image. Interpreted formation tops are displayed on the left side of the image.

All three wells target Triassic reservoir in two horst blocks (see figure 35). Hydrocarbons were encountered in both highs.

Remarkably, the faults at the Monster wells show offsets up to the claystone formations in the lower part of the North-Sea Group, which is in contrast to all other interpreted faults in this area. These appear to fade out in the Lower Cretaceous sediments. Additionally, an anticlinal fault-propagation structure is recognized in the reflectors above the horst at MON-02-S1, with a reverse fault on the NE side. The reverse fault is verified within the deposits of the Holland Formation in this well. The anticlinal structure indicates a compressional stress regime, whereas all other faults along this section are normal faults originating from an extensional phase(s).

The fault-propagation structure implicates that the related fault was reactivated during the inversion phase in the Late Cretaceous. Thinning of the upper part of the Ommelanden Formation (chalk) towards this fault also indicates syn-sedimentary tectonism. Movement along a fault plane may cause cataclasis. Cataclasis is a process that makes a fault sealing by a cataclastic gouge of grinded

sediments along the fault plane (see paragraph 3.5.2.1). Whether this also applies to the chalk deposits is not clear. Downward throw along the fault which is penetrated by MON-03 indicates evidence of extensional tectonism during the Tertiary once again.

Synthesis

The fault at MON-02 is the only fault related to a compressional regime in this section. Cataclasis related to the revers faulting may have had a potential sealing effect through cataclasis, which might explain the difference in geothermal gradients between MON-03/02-S1 and SGZ-01-S1. A sealing fault has little chance of allowing vertical fluid flow along the fault, and therefore no 'thermal charging' of porous rocks.

Faults around the horst block of SGZ-01-S1 (see figure 35) do not show a compressional character and appear to be normal faults. The geothermal gradient of the SGZ-01-S1 well is significantly increased in comparison to the Dutch average geothermal gradient.

The high geothermal gradient in SGZ-01-S1 and the low to medium geothermal gradient in MON-03/02-S1 in combination with the normal and reverse faults might imply that normal faults have a better chance for vertical fluid migration. This vertical fluid migration can consequently lead to thermal upwelling and local accumulation of higher temperatures.

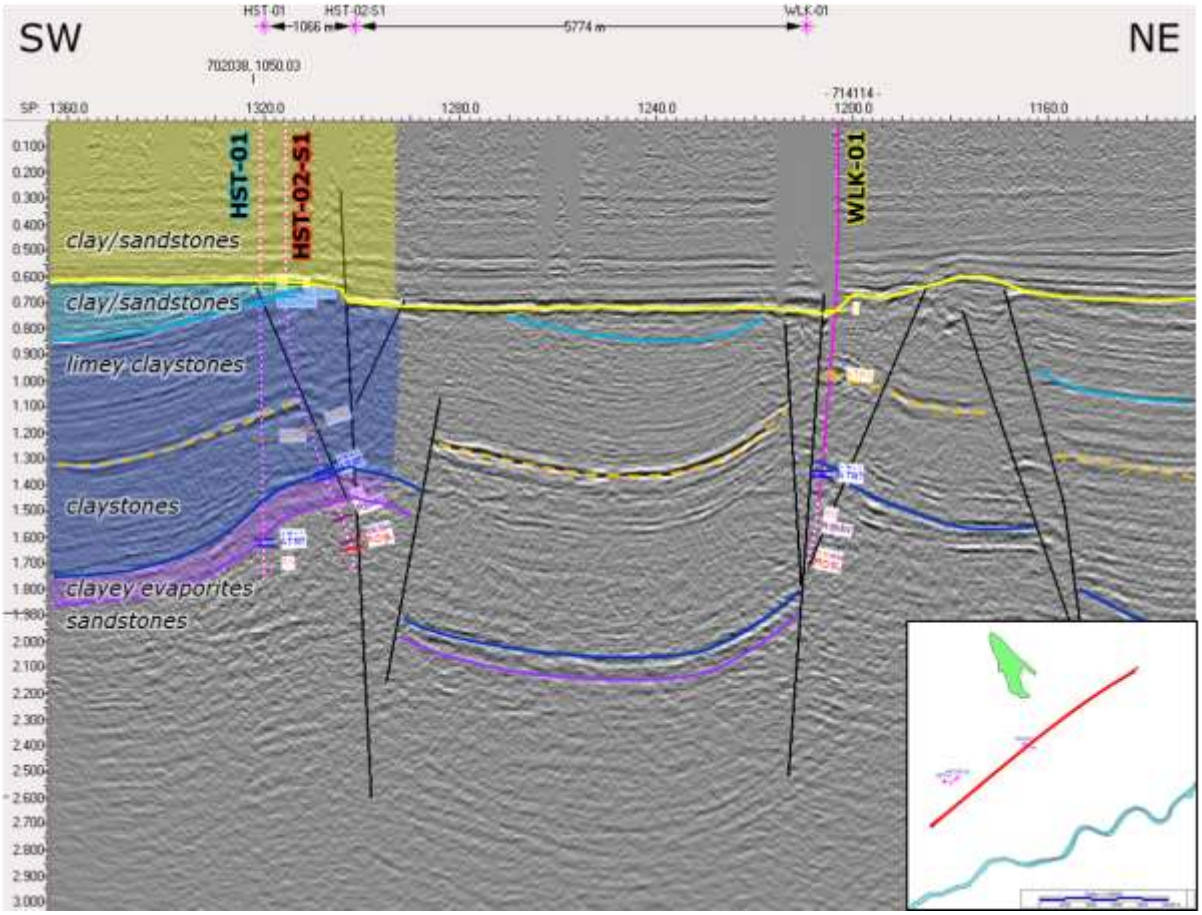

Figure 34 Seismic line (SW-NE) over the Haastrecht and Willeskop wells in the northern part of the West Netherlands Basin. The Haastrecht wells are located ~1500 meters NW of the line and are projected on the seismic section. Dashed purple well path indicates that the well path is behind or in front of the seismic image. Interpreted formation tops are displayed on the left side of the image.

In the northern part of region A, three wells near the Papekop field show three different geothermal gradients: HST-01, HST-02-S1 and WLK-01 with average geothermal gradients of respectively 27.3˚C/km, 33.7˚C/km and 31.7˚C/km. Figure 36 shows a seismic cross-section along these wells. HST-02-S1 and WLK-01 are both targeted at large offset fault zones, whereas well HST-01 is located slightly away from the fault zone. The only fault which show clear offsets far into the sediments of the North Sea group, is located just north of well HST-02-S1.

Seismic data above the big fault directly south of WLK-01 is absent. However, reflections north and south of the absent area do not show significant offsets, indicating that the fault only just penetrates the basal parts of the North Sea Group.

Only one fault has indications of a compressive setting: the most north-eastern fault at the fault complex near HST-02-S1, which relates to the big vertical offset of the Triassic (at shotpoint 1290). The anticlinal feature in the Triassic, which is drilled by the HST wells, appears to be part of a fault propagation structure that is related to a compressive setting. Results of this folding are not recognized in the sediments of the North Sea Group anymore. In fact, the two normal faults penetrating the base of the North Sea Group at HST-02-1 and WLK-01 are indicators of an extensional setting. These arguments indicate that the present faults have possibly been reactivated multiple times in geological history.

3.6.3.2 Region B

The seismic section presented in figure 37 has an W-E orientation and two wells (AND-02 & AND-06) are plotted by purple dashed lines. These wells are located just north of the seismic section and drilled to the pop-up structure. The geothermal gradient of the Andel-06 well (AND-06) is determined at 37,5˚C/km, which is significantly increased. The geothermal gradient of the Andel-02 well (AND-02) is significantly reduced, with 23,0˚C/km. This difference in geothermal gradient on a local scale and therefor of interest to take a closer look at the subsurface structure.

In the seismic section, a heavily faulted pop-up structure is interpreted. The drilled strata is presented on the left hand side in the figure. Andel-06 is drilled to Triassic sediments (purple), whereas the Andel-02 well is drilled to claystones belonging to the Altena Group (dark blue). The Triassic layer is normally faulted and slightly tilted. An anticlinal structure can be recognized from the light blue horizon, the base Schieland Group. The Schieland Group is truncated at the top and overlain by sediments belonging to the North Sea Group (yellow).

The interpreted faults (black lines) fade out at the basal part of the North Sea Group or in the Altena Group. All faults appear to have a normal, rifting character. Though, the anticlinal shape indicates a compressional stress regime. This implicates that the interpreted faults might have been reactivated during multiple tectonic phases.

Synthesis

From the petrophysical study was concluded that the Andel-06 well is drilled through faults of which some are expected to be opened. This fault penetration in the Altena Group can be observed in the seismic section. These opened faults might declare the increased geothermal gradient of AND-06 by vertical fluid flow along fault(damage zone)s. Thermal blanketing is another explanation of the anomaly, since AND-02 is drilled upon insulating claystones of the Altena Group and AND-06 to Triassic sandstones underneath this isolating package.

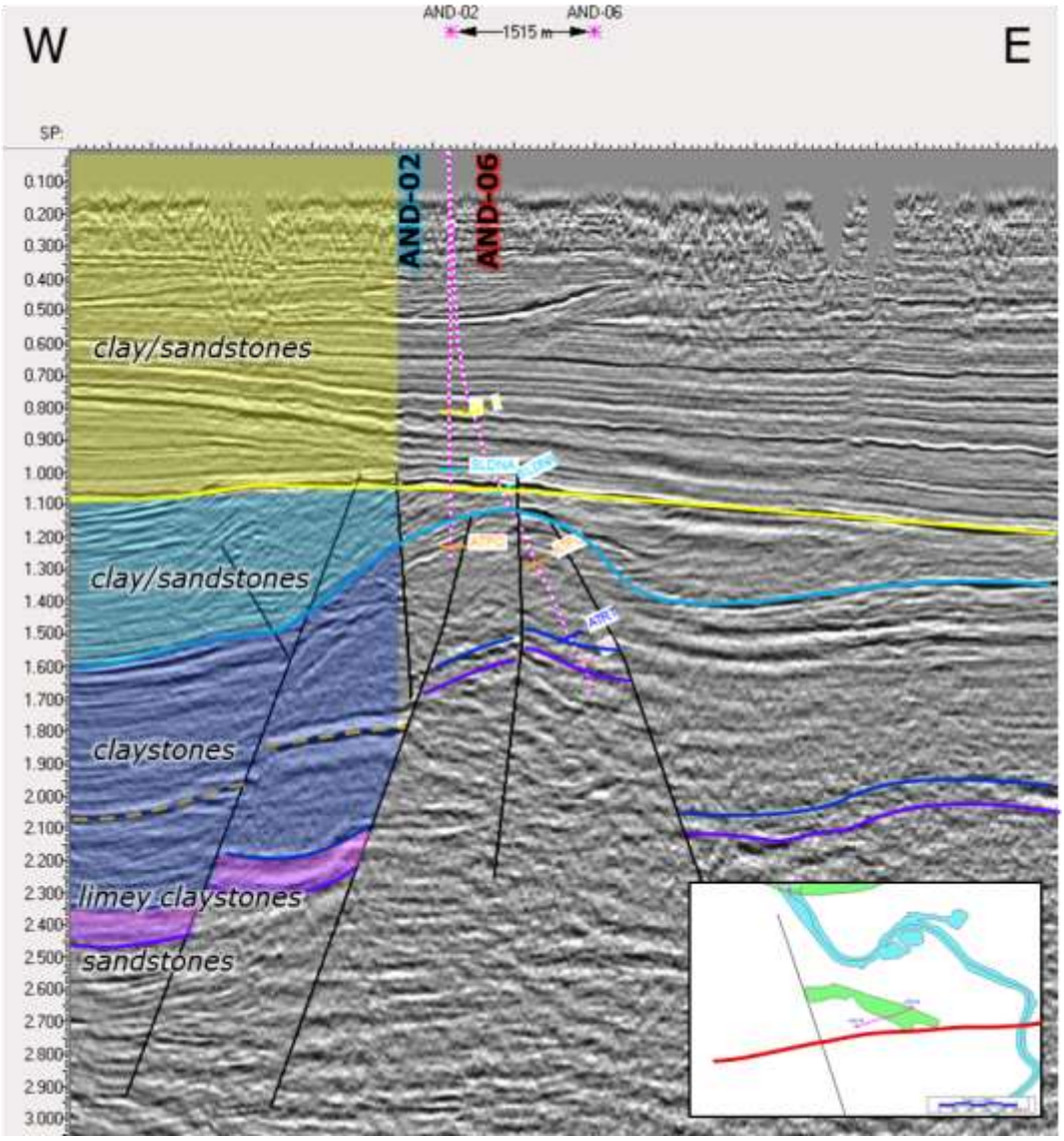

Figure 35 Seismic line (W-E) just south of the Andel wells, located in the central part of region B. The Andel wells are drilled from roughly the same location, though the trajectory of Andel-6 deviates towards the ENE. Interpreted formations and overall lithologies are displayed on the left.

In figure 38, a seismic section with an WSW-ENE orientation along the wells Huibeven-01 (HBV-01) and Waalwijk South-01-S1 (WWS-01-S1) is presented. The section shows zone with a high fault density in which several faults truncate far into the North Sea Group sediments (yellow). The North Sea Group penetrating faults have an normal fault character and indicate a phase of rifting.

Synthesis:

The geothermal gradients that were calculated for HBV-01 and WWS-01-S1 are respectively: 37,0˚C/km and 35,8˚C/km, in which WWS-01-S1 has a clear 'dent' in the temperature profile (see paragraph 3.2.3) . These significantly increased geothermal gradients are remarkable. The normal faults truncating North Sea Group sediments are expected to have been active during the Late Oligocene-recent rifting phase. Besides this, the faults have a slightly different orientation (NNW-SSE) in comparison to most other faults in the study area (NW-SE). Both projected wells (HBV-01 & WWS-01-S1) are drilled through one of these faults. These fault characteristics might be of influence to the origin of the encountered increased geothermal gradients. A fault damage zone could have been formed by the rifting event and thereby increase vertical permeability around the relatively recently activated faults. This increased vertical permeability may allow (convective) fluid flow from deeper and warmer layers, thermally charging the drilled sandstones. Another possible explanation of the increased geothermal gradients is thermal blanketing. The presence of a thick low conductive Altena claystone package on top of the Triassic sandstones may conserve high temperatures underneath these shales. This may also explain the temperature increase in the Triassic, according to the BHT data points of WWS-01-S1.

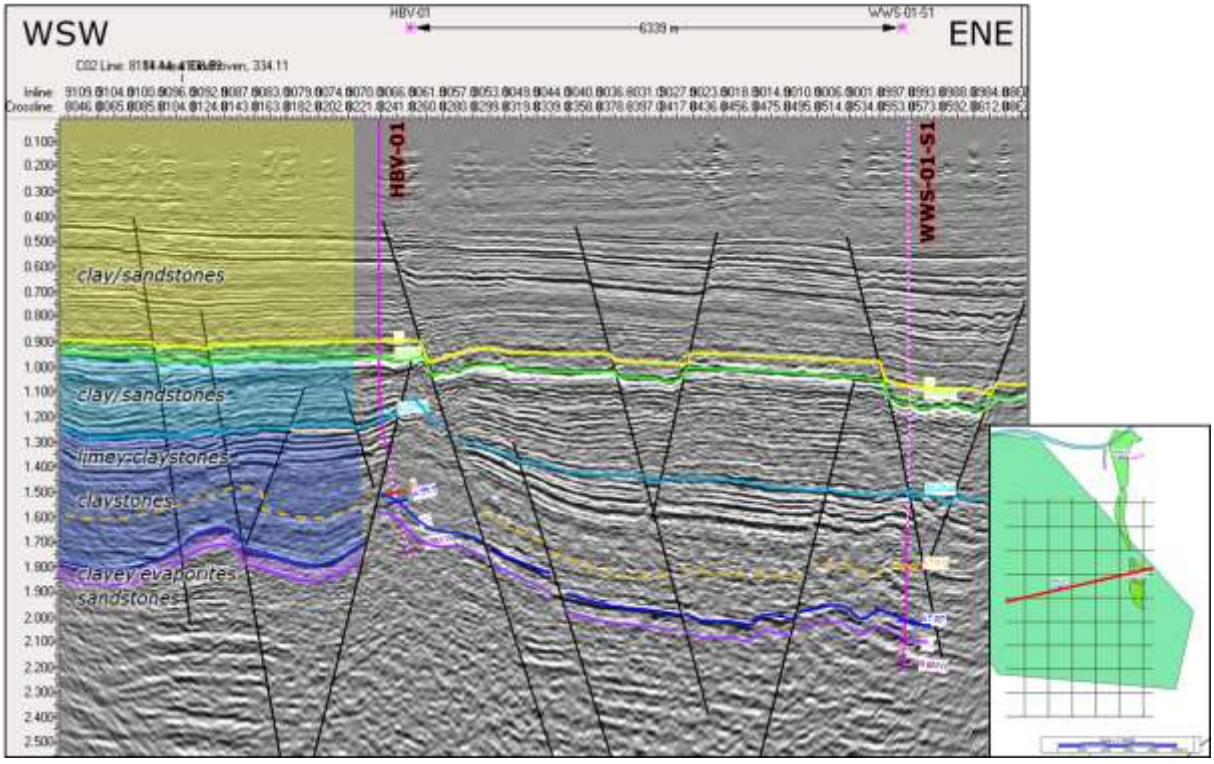

Figure 36 Seismic line (WSW-ENE) over wells HBV-01 and WWS-01-S1, located in the southern part of region B. Note that faults penetrate into the North Sea Group. Interpreted formations and overall lithologies are displayed on the left.

3.6.3.3 Region C

The seismic section through region C has a WSW-ENE orientation and crosses nearly the entire Roer Valley Graben (figure 39). Wells Veldhoven-01-S1 (VEH-01-S1) and Keldonk-01 (KDK-01) are projected in the figure at respectively the western and eastern boundary of the graben structure. The geothermal gradients calculated for wells VEH-01-S1 and KDK-01 are both decreased with respectively 24,8˚C/km and 29.0˚C/km. The interpreted faults at the boundary of the graben show large offsets in the reflectors of the pre-North Sea Group sediments and penetrate far into the thick North Sea Group (yellow), close towards the surface. Interestingly, the faults in the central part of the graben, do not penetrate as far in the sediments of the base of the North Sea group or even stop at the base. All faults appear to be normal faults, relating to an extensional regime.

Synthesis:

The decreased geothermal gradients in these boundary fault zones of the Roer Valley Graben are explained by the modelled topography driven groundwater flows and meteoric water infiltration along surface reaching permeable fault zones as modelled and described by Luijendijk et al. (2012). These processes are expected to locally cool the formation temperature. In the central part of the graben structure temperatures may be average or even increased due to thermal blanketing. However, no temperature data is available of wells drilled in this area to support this thought.

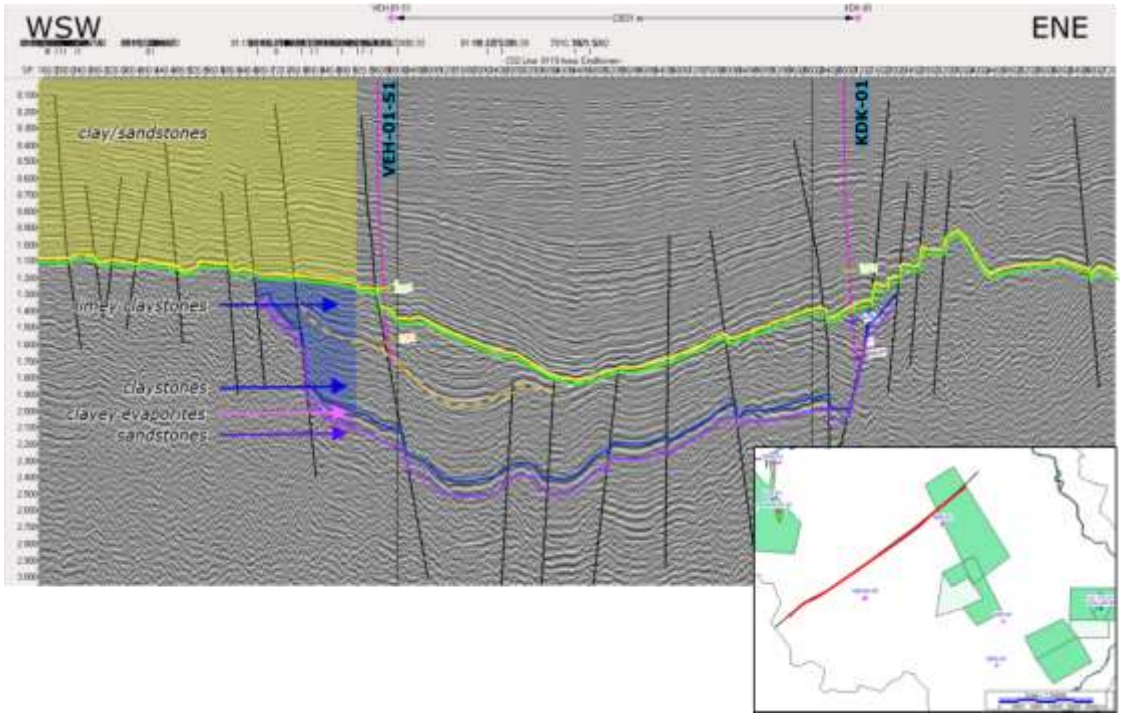

Figure 37 Seismic line (WSW-ENE) just north of VEH-01-S1 and KDK-01, located in the RVG in region C. Note that faults are more abundant at the western and eastern part of the graben and penetrate further into the North Sea Group in respect to the centre. Interpreted formations and overall lithologies are displayed on the left.

SUB-CONCLUSION:

1) Significant deviation on the average geothermal gradient appear to relate to faults penetrating into the sediments of the North Sea Group.
2) In region B a relative high fault density appears to be present with a slightly different fault orientation in respect to the rest of the study area (NNW-SSE versus NW-SE).
3) The faults at the boundaries of the RVG penetrate further into the North Sea Group in respect to the center of the graben.

3.7 Geothermal gradient mapping

So far, anomalies on the average geothermal gradient are plotted on a map (figure 21 in paragraph 3.6.1). In this chapter the encountered geothermal gradients are connected by interpolation to build a regional geothermal gradient map. It was chosen to develop three interpolated maps. One map for wells of at least 1000m deep, one for at least 2000m and one for at least 3000m deep. These maps are presented in the next paragraphs.

The eastern part of the study area has a significantly lower data coverage in comparison to the middle and western part of the area. The amount of data point is directly related to the uncertainty in interpolation. For this reason, it needs to be understands that high uncertainty exists for the geothermal gradient map in the eastern part of the RVG, region C.

In the central part, most wells in the dataset are located along a NNW-SSE fault belt. In the northern and southern part of this area (region B), the data-density is lower. The same is applicable to region A covering the WNB. In the northern part only few wells are present in the dataset, whereas the southern part (including the Westland area) contains a high data-density.

The structural framework of faults is plotted over the interpolation map. These faults are not included in the interpolation process. However, the interpolated zones of increased- and decreased geothermal gradients appear to follow the trend of the fault structures. For example, in the NNW-SSE fault zone through the central part of the study area.

3.7.1 Geothermal gradient map: wells > 1000m

This geothermal gradient interpolation map is based on wells deeper as 1000m (see figure 40). Geothermal gradients calculated from temperature measurements at shallower levels vary strongly from well to well. Therefore, it was decided to exclude these shallow wells from the main dataset.

Zonations of average-, increased- or decreased geothermal gradients can be recognized. Around the structural axis of the WNB a 'cooler' elongated zone can be distinguished, with a NW-SE orientation. In the WNB to RVG transition zone, in the central part of the study area, predominantly increased geothermal gradients are calculated. The zone has a more NNW-SSE treending in comparisson to the 'cooler zone.'

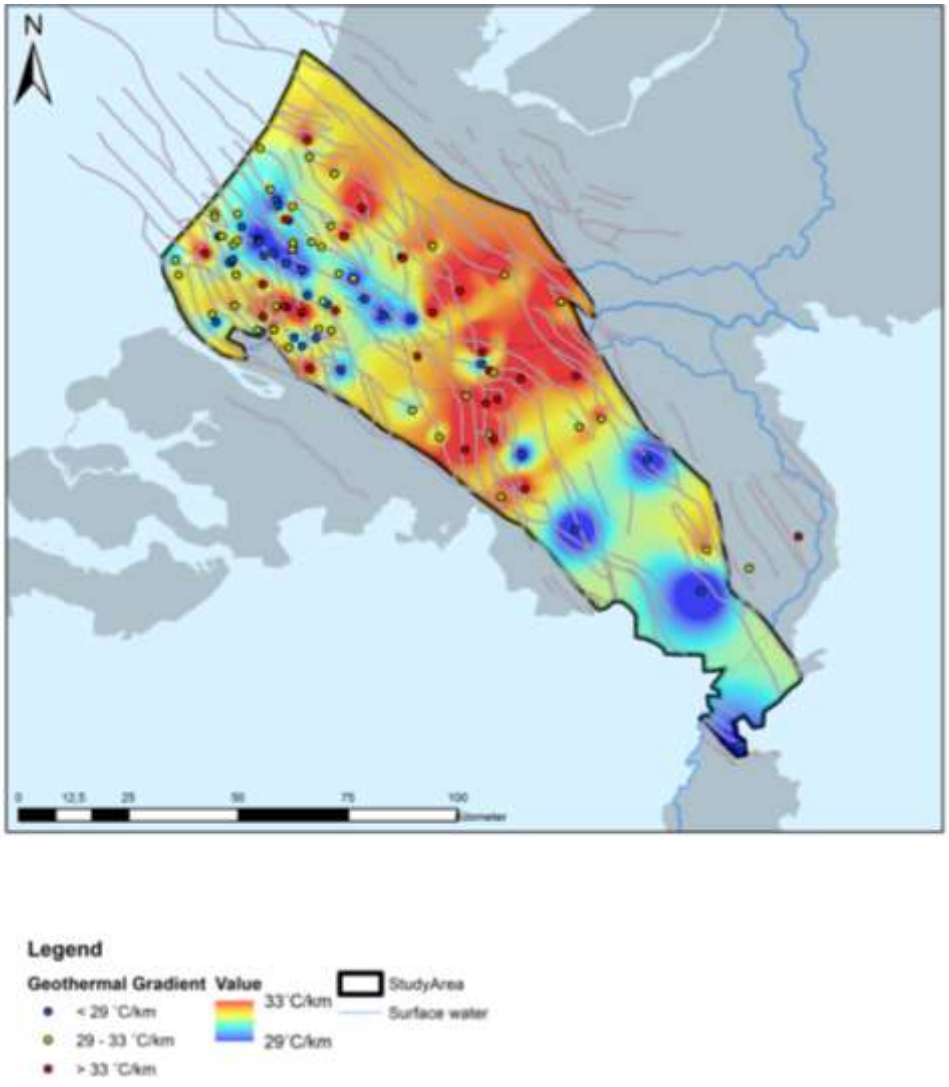

Figure 38: Interpolated geothermal gradient map based on wells deeper as 1000m in the WNB-RVG. Note: At some locations wells with different gradients are located in closed vicinity to each other. Due to the large scale of the map, this may lead to a seeming contradicting visualization between interpolated values versus specific well gradients.

3.7.2 Geothermal gradient map: wells > 2000m

The geothermal gradient map based on wells of 2000m or deeper is maybe the most interesting map for the geothermal projects in this area (see figure 41). Firstly because of the depth, many geothermal doublets are drilled to depths around this order of magnitude and secondly because there is relatively much data in comparisson with the 3000m map.

The clusters of specific average geothermal gradients become morge clear in this map (fig. 40). Whereas the distribution of normal-, increased- and decreased geothermal gradients was more frayed in the 1000m map (fig. 39), the 2000m map shows clears zonations in consequent anomalies (if present) on the geothermal gradient. The eastern part of the Roer Valley Graben has a limited number of temperature data points, however three out of four wells show a significantly reduced geothermal gradient.

In the central part of the study area the geothermal gradients are mostly increased, in which the 'hot' zone seems to follow the fault belt towards the northwest of the WNB. The orientation of this fault belt deviates slightly from the WNB and RVG primary axis. Similar fault orientations are seen in the smaller 'hot' zone around the city of Rotterdam in the southern part of the WNB.
A consistently cooler zone is located in the centre of the WNB, multiple wells with indicate a significantly decreased geothermal gradient. The orientiation of this 'cold' zone is parallel to the basin axis and the dominant fault direction.

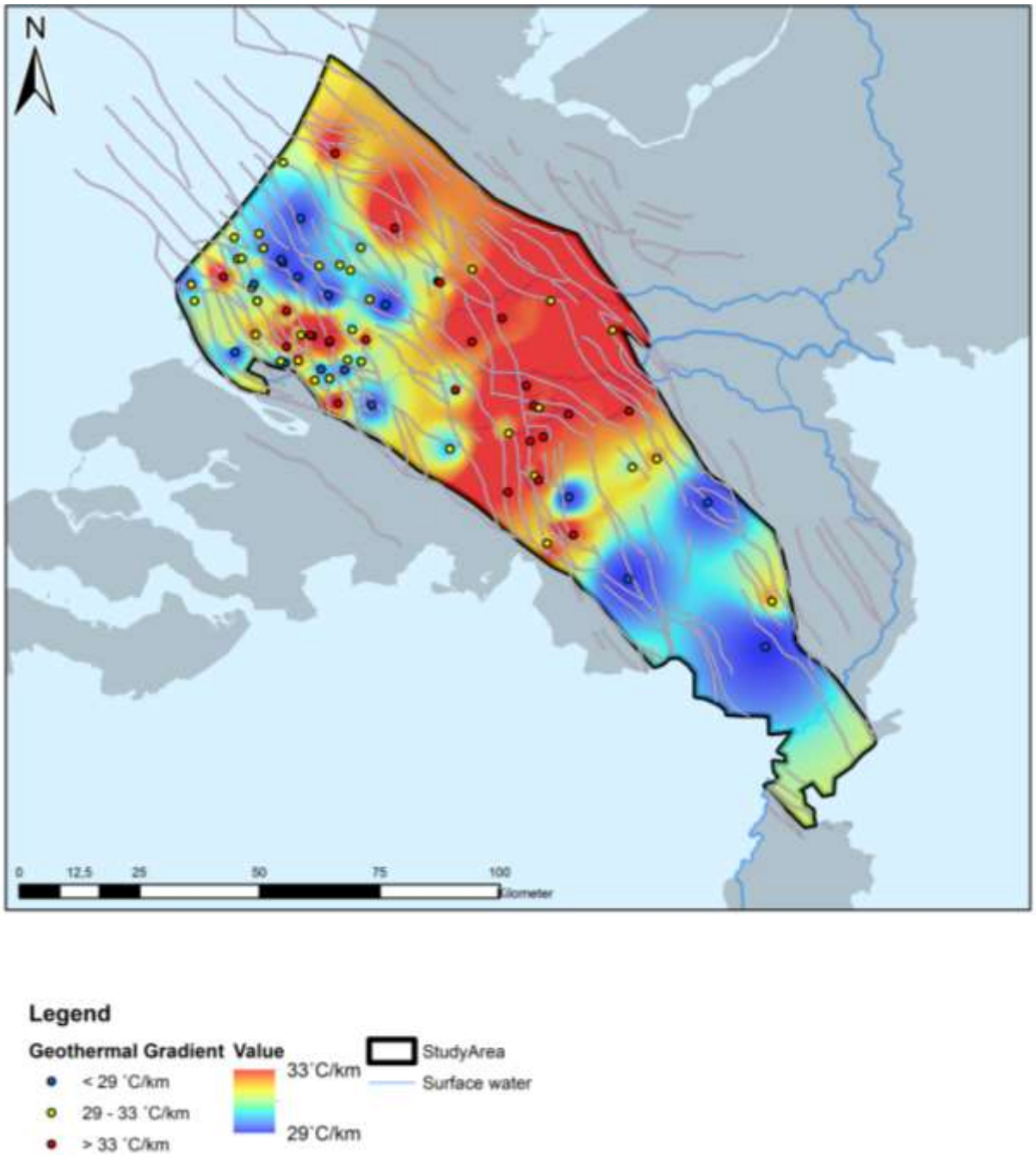

Figure 39: Interpolated geothermal gradient map based on wells deeper as 2000m in the study area.

3.7.3 Geothermal gradient map: wells > 3000m

Figure 42 is the interpolated geothermal gradient map of the study area based on wells deeper as 3000m. As can be noticed, the number of wells penetrating strata at depths exceeding 3000m is significantly less as for the 2000m map, causing 'bullet holes' at different parts of the map. Especially the eastern part of the Roer Valley Graben has a limited number of data points. In the 1000m and 2000m maps this region was interpolated as a relatively 'cold' zone, but in the 3000m map the area is indicated as average due to the interpolation algorithm and the lack of temperature data. This makes the interpolation of this area uncertain.

The south-western part of the West Netherlands Basin has a higher data density. The 'cold' and 'hot' zones in the region are still interpolated from this smaller amount of data points. The maps indicate an increased geothermal gradient in the central part of the study area similar as seen in the 1000m and 2000m map.

The relation between structural framework and the geothermal gradient anomaly zones is not as clear as in the 1000m and 2000m maps. This is mainly caused by the lower data density throughout the study area.

SUB CONCLUSIONS:

1) For the conventional geothermal window of ±1500m-3500m, zones with potentially increased geothermal gradients are interpolated. The most dominant zone with increased geothermal gradients is located in the central part of the study area around the border between the WNB and RVG.
2) In comparison to the 1000m and 2000m geothermal gradient map, the 3000m map is based on a limited dataset. Additional temperature data from depths exceeding 3000m is required to build an accurate geothermal gradient map of the study area.

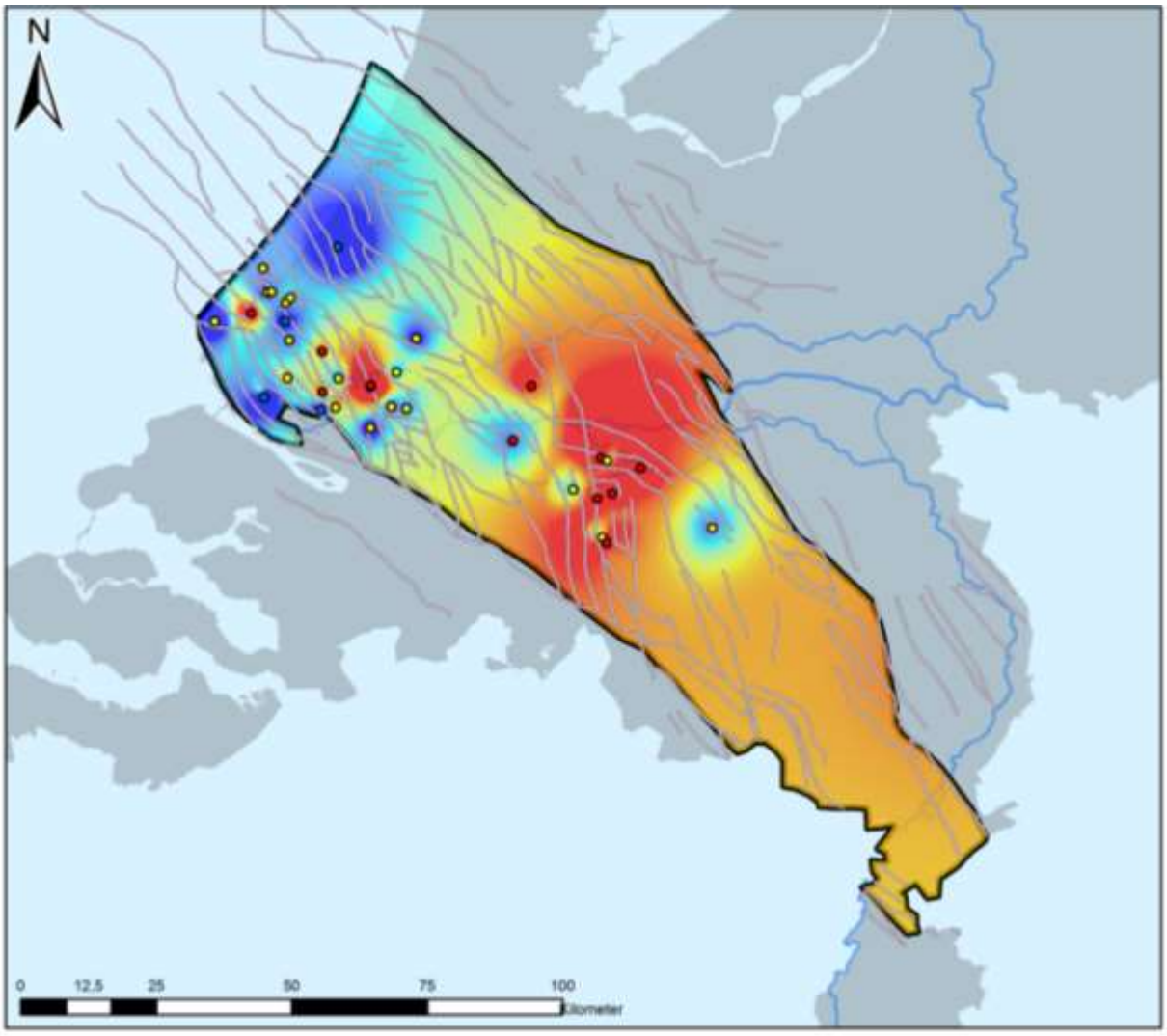

Figure 40: Interpolated geothermal gradient map based on wells deeper as 3000m in the WNB-RVG.

4 Geothermal energy and deviating geothermal gradients

4.1 Geothermal gradients: application example

In the previous chapter, zones with higher and lower geothermal gradients have been identified, indicating gradients from 39 °C/km to as low as 23 °C/km. Though the most extreme gradients may be related to uncertainties in the underlying temperature data, the zonation of higher and lower gradients is very interesting for potential geothermal systems. In figure 43 current and requested licenses (per February 2018) are projected on top of the geothermal gradient map based on wells deeper than 2000 meters. Note that this map is only based on an extrapolation of temperature data points, non-restricted by geological features with a restricted amount of wells. Keeping these uncertainties in mind, some interesting features can be observed from the figure. multiple active geothermal installations are positioned in a decreased geothermal gradient zone in the western part

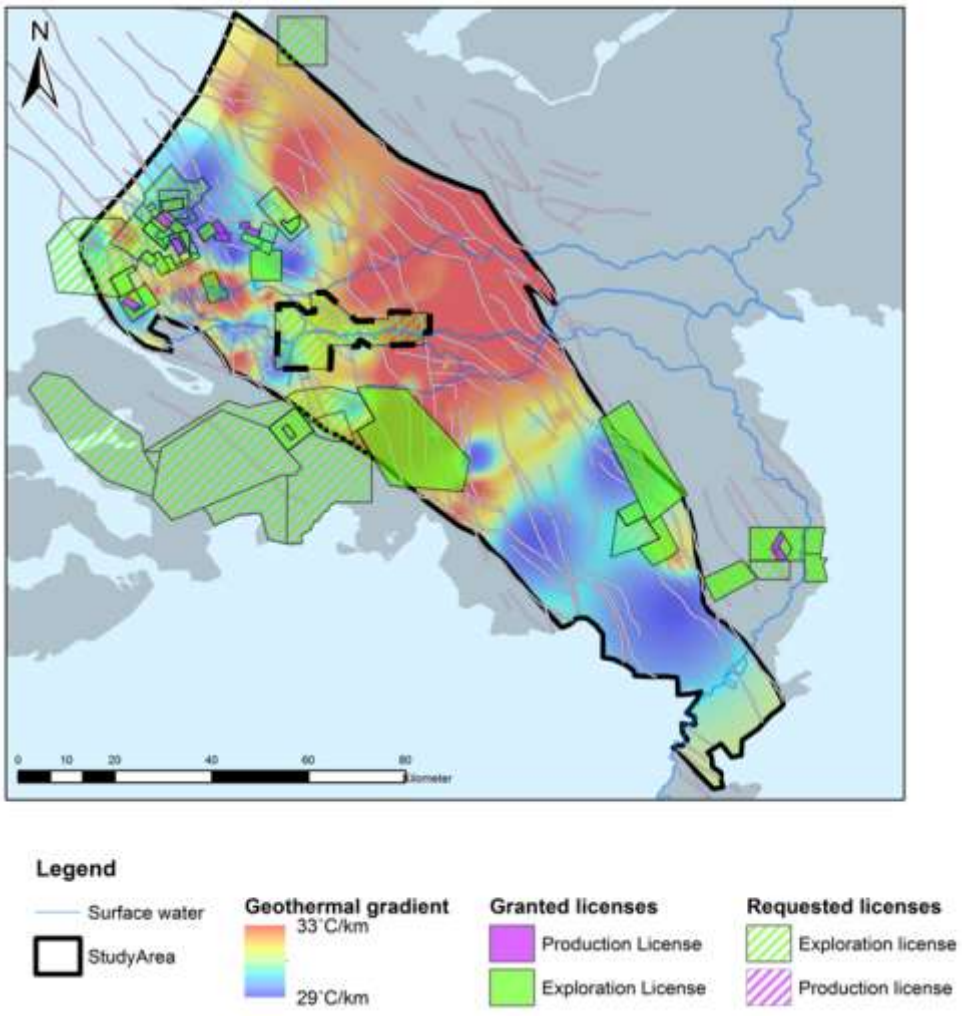

Figure 41: Geothermal gradient map with the granted and requested geothermal exploration and production licenses, as per February 2018. The dashed black line indicates the requested Drechtsteden geothermal exploration license. Source: Dutch Oil and Gas Portal (*www.nlog.nl*)

of the WNB. To the south of this area, a small zone with an increased geothermal gradients is interpolated with no active systems at the moment. In the central area between the WNB and RVG a zone of expected increased geothermal gradients is interpolated, though the amount of licenses here is limited. The eastern part of the geothermal license of Drechtsteden (framed by a dashed black line) lies partly over this zone with elevated gradients, though the western part is located over a zone with decreased gradients. When a geothermal doublet is designed for this license, it could be of interest to know that the forecasted subsurface temperature in the western part of the license is potentially lower and in the east potentially higher in respect to average geothermal temperatures. In the RVG in the southeast (Region C), the map indicates overall lower geothermal gradients. Though this is based on a limited amount of wells in this area, projects in this area should keep lower potential geothermal outputs in mind.

4.2 Effects of varying geothermal gradients on geothermal power output

As an indication, geothermal doublet performance calculations are conducted in DoubletCalc (v1.4.3) to determine the impact on geothermal power by variations in the geothermal gradient. DoubletCalc is a publically available software tool provided by TNO, which enables users to calculate indicative geothermal power of a potential doublet (Mijnlieff et al., 2014). The calculations are based on fictive default numbers provided by TNO and do not represent an exact example. The only adjustment in respect to the default values is an increased Kh/Kv ratio to 2. Figure 44 presents the input and output values for a fictive geothermal doublet with a reservoir at 2000 meters and an average geothermal gradient of 31.3 ^{o}C/km. Based on these values, there is a 50% chance (P50) to install a geothermal system with a geothermal power of 5.72 MW_{th}.

To assess the effects of varying geothermal gradients, multiple calculations have been performed with increased and decreased gradients from 27.3 to 35.3 ^{o}C/km. Based on the results in previous chapters, these are realistic values which may occur in different parts of the study area. To see whether depth affects the calculations, the same values have been applied to scenarios at 2000 and 3000 meters depth. The P50 power output is used as a reference value for the different scenarios. See table 7 for the results of the calculations of these scenarios.

Doublet Calculator 1.4.3

number of simulation runs (-) 1000 | Calculate ! | Open Scenario | Save Scenario | Exit Program

file: j:\werk\6425\doubletcalc\6425_lc_default2000_31-3.xml

Geotechnical input

A) Aquifer properties

Property	min	median	max
aquifer permeability (mD)	150	250	500
aquifer net to gross (-)	0.75	0.8	0.85
aquifer gross thickness (m)	95	105	115
aquifer top at producer (m TVD)	1800.0	2000	2200.0
aquifer top at injector (m TVD)	1800.0	2000	2200.0
aquifer water salinity (ppm)	100000	120000	140000

Property	value
aquifer kh/kv ratio (-)	2
surface temperature (°C)	10
geothermal gradient (°C/m)	0.0313
[mid aquifer temperature producer (°C)]	0.0
[initial aquifer pressure at producer (bar)	0.0
[initial aquifer pressure at injector (bar)]	0.0

B) Doublet and pump properties

Property	value
exit temperature heat exchanger (°C)	35
distance wells at aquifer level (m)	1500
pump system efficiency (-)	0.61
production pump depth (m)	500
pump pressure difference (bar)	40

C) Well properties

calculation length subdivision (m) 50

Producer	
outer diameter producer (inch)	6.125
skin producer (-)	0
penetration angle producer (deg)	45
skin due to penetration angle p (-)	-0.69

Segment	pipe segment sections p (m AH)	pipe segment depth p (m TVD)	pipe inner diameter p (inch)	pipe roughness p (milli-inch)
1	500	500	8	1.2
2	1050	1050	12.25	1.2
3	1930	1833	8.625	1.2
4	2166	2000	6.625	1.2
5				

Injector	
outer diameter injector (inch)	6.125
skin injector (-)	0
penetration angle injector (deg)	45
skin due to penetration angle i (-)	-0.69

Segment	pipe segment sections i (m AH)	pipe segment depth i (m TVD)	pipe inner diameter i (inch)	pipe roughness i (milli-inch)
1	50	50	5	1.2
2	1054	1054	12.375	1.2
3	1930	1833	8.625	1.2
4	2166	2000	6.625	1.2
5				

Geotechnics (Output)

Monte Carlo cases (stochastic inputs)	P90	P50	P10
aquifer kH net (Dm)	16.17	21.32	32.68
mass flow (kg/s)	32.28	41.61	60.25
pump volume flow (m³/h)	109.0	140.5	203.8
required pump power (kW)	198.6	255.9	371.2
geothermal power (MW)	4.26	5.72	8.34
COP (kW/kW)	20.2	22.2	24.0
aquifer pressure at producer (bar)	192.51	204.3	216.63
aquifer pressure at injector (bar)	193.08	204.37	215.94
pressure difference at producer (bar)	15.02	15.83	16.29
pressure difference at injector (bar)	24.21	25.45	26.31
aquifer temperature at producer * (°C)	70.75	74.23	77.69
temperature at heat exchanger (°C)	68.97	72.43	75.57

Figure 424 Input (above) and output (below) values in DoubletCalc, for a fictive geothermal system with a reservoir at 2000 meters and a geothermal gradient of 31.3 °C/km.

Table 7 Results of geothermal power (P50) calculations in DoubletCalc with a reservoir at 2000 and 3000 meters, for different geothermal gradients

Geothermal gradient (°C/km)	**27.3**	**29.3**	**31.3**	**33.3**	**35.3**
Geothermal output, 2000 m (P50, MW_{th})	4.26	4.97	5.72	6.48	7.33
Geothermal output, 3000 m (P50, MW_{th})	9.24	10.64	12.12	13.67	15.30

The results in table 7 show that the impact of the geothermal gradient is significant on the geothermal output. When related to the average geothermal gradient, the geothermal power of a system at 2000 meter increases ~27% if the local geothermal gradient is 35.3 °C/km and decreases ~25.5% if the gradient is 27.3 °C/km. That relates to an average 6.7 % increase or decrease per MW/ °C/km. As can be expected the power outputs at 3000 meter are higher in respect to the scenarios for 2000 meter. For a system at 3000 meter the geothermal power increases ~26% if the local geothermal gradient is 35.3 °C/km and decreases ~24% if the gradient is 27.3 °C/km. That relates to an average 6.25% increase or decrease per MW/ °C/km. The geothermal power increases and decreases with roughly the same percentage amount at both depths. That suggests a rule of thumb of roughly 6-7% increase or decrease per MW/ °C/km.

SUB-CONCLUSION:

1) The geothermal gradient has strong influence on the geothermal power output of a system. A variation in geothermal gradient should be taken into account during geothermal energy performance calculations.
2) General rule of thumb: geothermal output increases or decreases with 6-7% per MW/ °C/km

5 Discussion

The different outcomes of the study are combined and interpreted in this part of the report. One or more potential explanations for the variations in geothermal gradients are discussed.

5.1 Limitations BHT data

The main part of the temperature database is comprised by BHT data points. Many uncertainties around measured BHT values exist. Both surface and subsurface conditions as well as measuring methods and timing are expected to influence BHT data strongly. The main concerns around the reliability of BHT data are listed below.

- *Method;* What type of method was used for measuring the BHT. Was it done digitally or analogue? What is the vintage of the data? Different measuring methods through the years can have potential effects on the data.
- *Timing;* When was the BHT was measured? It is often unclear from drilling reports or well logs if a BHT was measured shortly after drilling or after a longer period of time in which the formation might have recovered partly from cooling. Sometimes multiple BHT measurements are done at the same depth with different periods of times after drilling. During this time span formation temperature recovery could have started. When these naturally increased BHT measurements are consequently corrected by the same BHT correction method, overcorrection can occur.
- *Circulation;* Was the borehole circulated for a short or long period of time? Longer mud circulation times can cool the formation significantly more than short circulation times.
- *Borehole diameter;* What was the diameter of the borehole during measurement? Larger borehole diameters contain larger volumes of drilling fluid and are expected to cool the formation more.
- *Mud temperature;* What was the initial drilling fluid or mud temperature? Lower mud temperatures are expected to cause more formation cooling during drilling and circulation.
- *Seasonality;* Does seasonality influence BHT measurements? For example, mud temperatures might be lower in winter times in comparison to summer times.
- *Reporting of measurements;* BHT data is sometimes difficult to trace back, mostly depth intervals are noted instead of depth points. Not to mention archiving of temperature recording times, which is expected to be the result of different focus, temperature was not of main interest for most wells.

All of these uncertainty parameters put questions to the reliability of comparing BHT data in general. However, BHT data is the only temperature dataset that has good coverage over the area of the Netherlands.

5.2 Possible explanations for deviations in geothermal gradients

The average geothermal gradient of the Dutch subsurface is described as a linear function in which the temperature increases with 31,3˚C/km plus the average surface temperature (Bonté et al., 2012). However, BHT data reveals a significant irregular pattern in temperature increase over depth. Part of the explanation may relate to 1) uncertainty in the BHT data, 2) analysis uncertainty due to different correction methods (analytical versus statistical), 3) uncertainties in applied methods and 4) potential differences between data type (BHT versus DST). Potential geological explanations for this phenomenon:

- *Faults;* open faults or fractures could potentially allow vertical fluid flow from deeper (higher temperature) levels to more shallow levels with lower ambient temperatures due to density or pressure differences. If a fault is opened or closed is a much discussed issue. One of the explanations on predictability of open or closed faults is fault-orientation with respect to the main stress regime (Nieuwland, 2012).

  Another potential explanation for the discovered temperature anomalies is the presence of a fault damage zone (Bense et al., 2013) as discussed in paragraph 3.5.2.1. Depending on the truncated lithology, a fault damage zone with increased permeability (fracture based) can have a significant extent. Fault damage zones can become of equal width as the offset of a fault in pure sandstones (Bense et al., 2013). Locations with large offset faults and a high sand column could potentially have a good fracture network as result of a well-developed fault damage zone. Such a fracture network could potentially allow fluid flow around a fault. Besides its potential effect on the geothermal gradient, this phenomenon is also of interest because of potential local reservoir improvement.

  Asides this phenomenon, the 'hot' zone of increased geothermal gradients in the central part of the study area corresponds to the south-western boundary of the defined basin during the Cenozoic (Worum et al., 2005), see figure 45. The most recent tectonic activity in the basin is the Late Oligocene–recent rifting phase (Van Balen et al., 2002). The defined Cenozoic basin area with potential fault (re-)activation is expected to be the explanation of faults truncating North Sea Group sediments in region B and C. In the central and southern part of the WNB (region A) faults do not truncate these Upper North Sea sediments (see figure 45, cross section 1-1'and 2-2').

  The rifting event is expected to relate to the increased geothermal gradients in the central part of the study area. The extensional stress regime caused dominantly normal faulting, in which the faults are potentially (partly-) opened since its last activity is recent and f.e.

processes as cementing have not taken place yet (Van Balen, 2002; Worum et al., 2005; Bense et al., 2013). This is supported by the mud losses data presented in figure 33. Even when faults itself are sealing, chances of a developed fault damage zone with enhanced fracture based permeability exists with large offset faults (Bense et al., 2013).

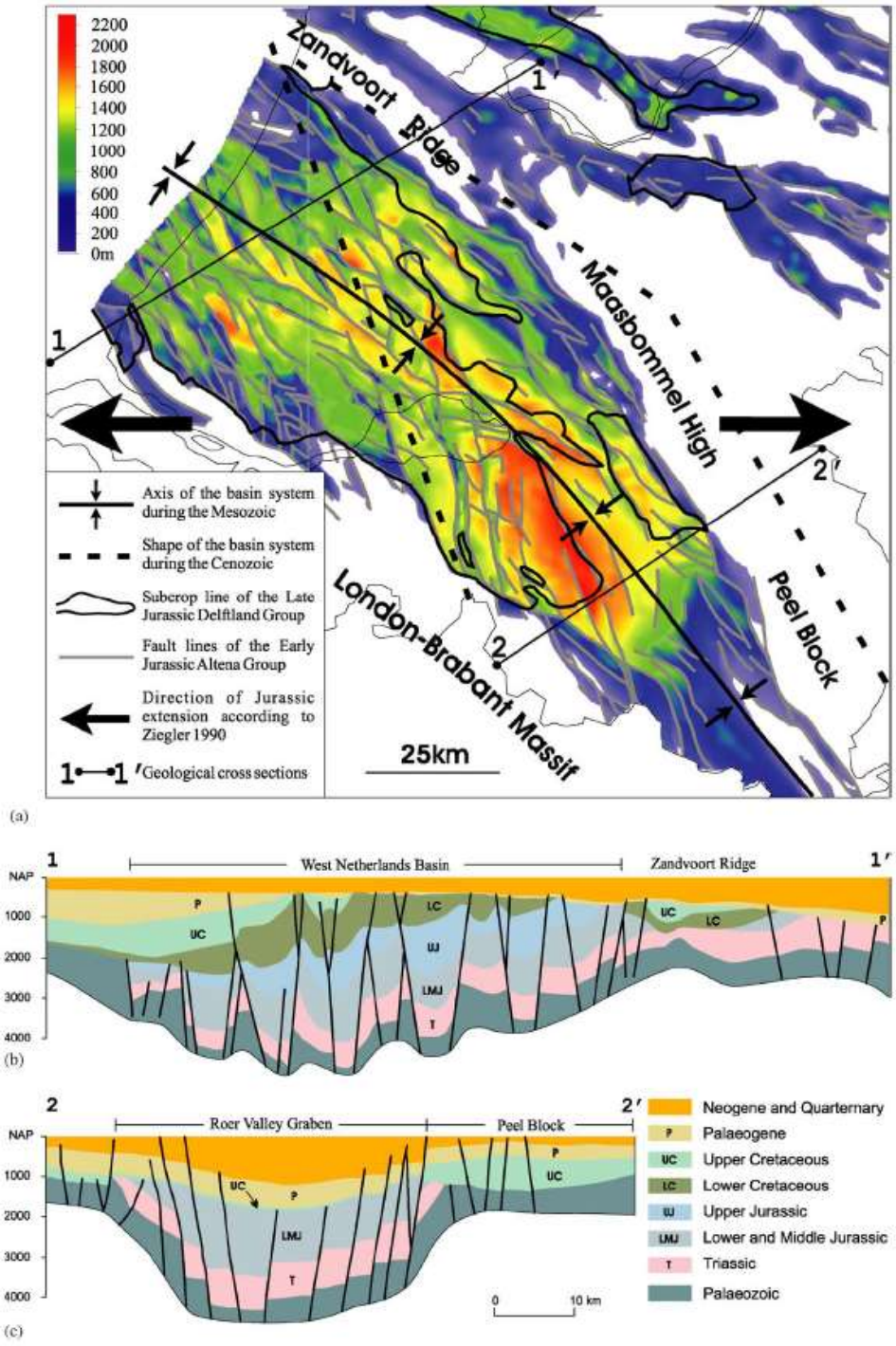

Figure 43: a) a thickness map of the Altena Group, which consists mainly out of shales. b) NE-SW Cross section 1-1' through the WNB. c) NE-SW Cross section 2-2' through the RVG. Source: Worum et al. (2005)

- *Thermal blanketing;* different lithologies have different heat conductive capacities. This may lead to insulation or conduction of heat in particular lithologies. For example, shales have better insulating capacities in respect to sandstones. Thick packages of shale could therefore potentially conserve heat underneath the package, resulting in a reduced geothermal gradient in the section above the shales and an increased geothermal gradient below the thick shale package.

  This principle is illustrated in figure 46, where two wells (AND-06 and AND-02) are displayed on the interpreted geological structure. AND-02 is drilled to a depth of 1980m TVD in the Altena Group and has a decreased geothermal gradient of 23,0˚C/km. AND-06 is drilled to the Lower Germanic Triassic sandstones at a depth of 2670m TVD and has an increased geothermal gradient of 39.0˚C/km. These significant differences in temperature at this small scale are remarkable. One of the probable causes in this deviation might be thermal blanketing. However, fluid migration or convection along the fault zone (red arrows) and thermally charging the Triassic sandstones (pink) might also play a role.

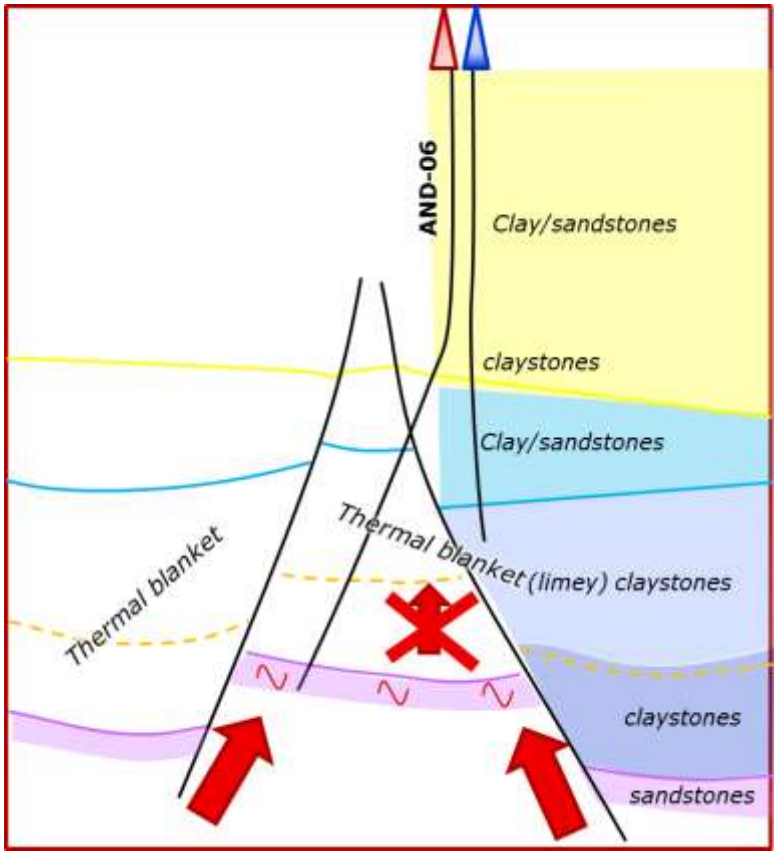

Figure 44: Schematic of geological setting around the AND-02 (blue, reduced geothermal gradient) and AND-06 (red, increased geothermal gradient) wells. The interpreted lithostratigraphic units and their main type of sediments are given on the right side in the image. The red arrows indicate potential heat migration along fault zones.

The occurrence and thickness of the Altena Group in the study area is presented in figure 45. Multiple regions with high thicknesses of Altena are corresponding to zones with increased geothermal gradients. For example, the reddish (thick) area NW of transect 2-2' and the reddish zone E of the 1-1' line. See figure 40, the geothermal gradient anomaly map.

- *Convection;* formations with high vertical permeability or open faults and fracture networks can accommodate convective fluid movement. For example, density driven convection due to temperature differences in a reservoir rock. This convection can create heat upwelling and cold down welling at specific locations. This can lead to an increase or a decrease in geothermal gradient at the specific location. Another result can be a homogenous temperature throughout a thick reservoir due to temperature mixing by the convective fluid flow. This is only possible in reservoirs with a homogeneous character and high vertical permeability (Kühn et al., 2004).

- *Ground water flow and meteoric infiltration;* As mentioned by Luijendijk (2012), topography driven ground water flow can significantly alter subsurface temperatures in the Roer Valley Graben. In his study cooling effect of 14˚C on average was determined with maximum cooling values of 40˚C with a topographic relief of only 130m (Luijendijk et al., 2012). Besides the topography-driven ground water flow that is assumed to cool formation temperatures, infiltration of meteoric water in fault(zones) in the Roer Valley Graben might also cause reduced geothermal gradients in wells in the area of large surface reaching faults. These surface reaching faults are mainly located in the Roer Valley Graben as described in the seismic result chapter of this report. These faults are expected to have been active during the Late Oligocene-recent rifting phase (Van Balen et al., 2002). Isotope dating and salinity measurements revealed inflow of fresh water into deeper situated layers (>1000m) (Luijendijk et al., 2012).

- *Magmatic rocks;* Multiple wells in the WNB and RVG encountered igneous rocks, which mainly consisted out of intrusive rock bodies. The distribution of these known magmatic rocks is presented in figure 47, as published in *Geology of the Netherlands* by Wong et al. (2007).

Table 8: geothermal gradients in wells that encountered igneous rocks in the study area.

Well code	Name	Geothermal gradient [˚C/km]
AND-02	Andel 2	23,0 ˚C/km
BRTZ-01	Barendrecht-Ziedewij 1	31,0 ˚C/km
HEI-01	Heinenoord 1	27,7 ˚C/km
IJS-64	IJsselmonde 64	31,7 ˚C/km
LOZ-01	Loon op Zand 1	33,4 ˚C/km
SPC-01	Sprang Capelle 1	31,6 ˚C/km

Wells in which magmatic rocks were discovered do not seem to correspond to the discovered positive deviations on the average geothermal gradient. Wells that are included in the temperature dataset are presented in table 8. The temperature measurements from these wells do not indicate significantly increased geothermal gradients, only one wells (LOZ-01) does have an increased geothermal gradient. In fact, several of the mentioned wells have decreased geothermal gradients.

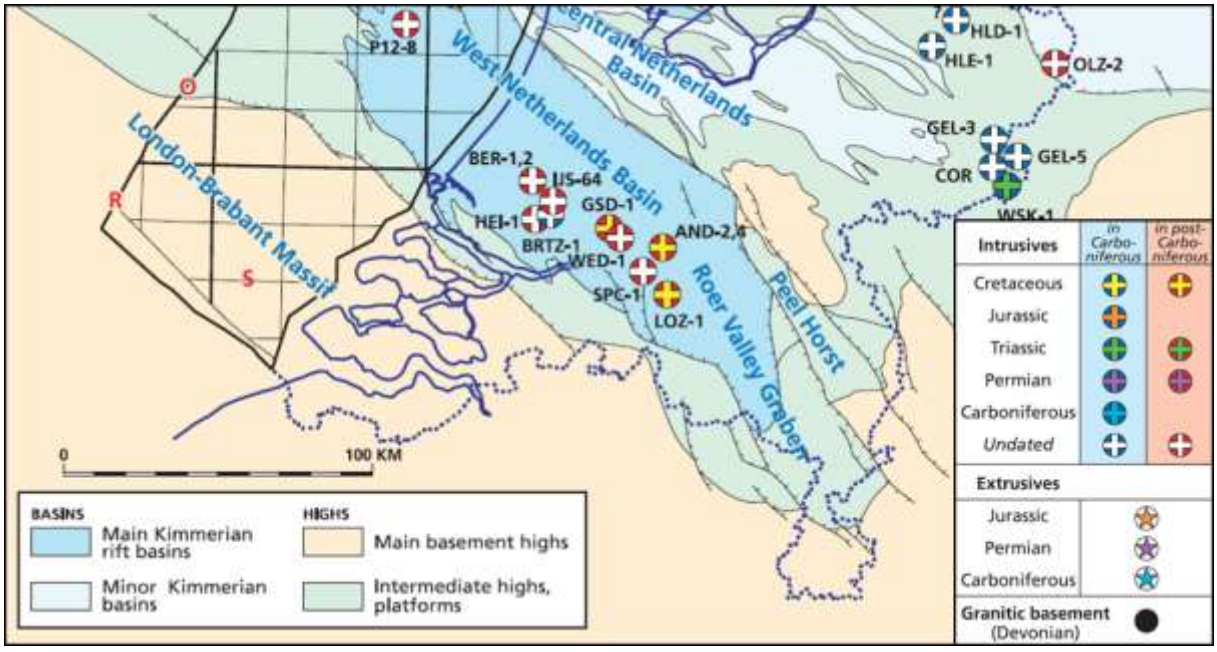

Figure 457: Magmatics in and around the study area encountered by wells. Source: Wong et al. (2007)

6 Conclusion

The main objective of this research project:

Investigate geothermal potential of fault zones in the West Netherlands Basin and Roer Valley Graben.

To solve this problem, a temperature data set is built and temperature data is analysed. Bottom Hole Temperature (BHT) data is the most common type of temperature data. This data is less accurate then Drill Stem Test (DST) data, which are measured over a longer period of time. During drilling, the formation temperature decreases due to cooling by the drilling fluid. To compensate for the temperature uncertainty in BHT measurements, the AAPG statistical BHT correction method was applied. After computing the geothermal gradients, it was concluded that significant [±2,0˚C/km] deviations on the Dutch average geothermal gradient exist in multiple. Applying one single geothermal gradient of 31,3 ˚C/km for the WNB and RVG does not seem to be adequate.

Geothermal gradient anomalies were divided into three groups, respectively: increased [> 33˚C/km], decreased [< 29˚C/km] and average [29 - 33˚C/km]. A map is made presenting the geographical location of anomalies. Clusters of wells with specific geothermal gradient anomalies can be distinguished. These geothermal gradient anomaly clusters are visible in wells with minimum depths of 1000m, 2000m and 3000m. Deeper wells do not have significantly higher geothermal gradients in general. The distribution of geothermal gradient anomalies over the three classes in the study area remains in the approximate same ratio in all three well depth groups, respectively >1000m, >2000m and >3000m.

Besides depth grouping, the calculated geothermal gradients were divided over the lithostratigraphic units in which the temperatures were originally measured. Though the distribution of BHT measurements over the stratigraphic intervals is not even, the results indicated significantly decreased geothermal gradients in the Schieland Group and significantly increased geothermal gradients in the Triassic Group. These variations on the average geothermal gradient might be explained by differences in heat conductivity between the lithostratigraphic units or potential thermal charging of porous rock layers by ‘hot’ fluid migration via permeable pathways.

Overall, no evidence for one main cause of the variations in geothermal gradient was found. However, a combination of the following factors is expected to influence the discovered anomalies:

- *Faults*; open faults and fault damage zones may cause increased geothermal gradients by hydrothermal fluid flow from deeper situated layers. Via permeable pathways a shallower positioned reservoir rock could be thermally charged by the hydrothermal current. The predictability of open faults or permeable fault zones presence is complex.

  Though, various indicators were interpreted or extracted from seismics, petrophysics and literature. reactivated faults have higher chance to be sealing due to multiple phases of fault plane movement. This movement can cause a sealing cataclastic gouge along the fault plan. The amount and extent is highly dependent on the type of host rock which is truncated by the fault and the offset of the fault.

  The Late Oligocene-recent rifting phase is interpreted as the most important tectonic activity for the contemporary measured anomalies on the average geothermal gradient. Recent faults are sometimes not yet cemented and might therefor allow fluid migration along a permeable fault (damage zone). The mud losses data indicates a high density of wells with encountered losses in the central part of the study area, where an overall increased geothermal gradient is interpolated.

- *Thermal blanketing;* thermal conductivity depends from lithology to lithology. Sandstones have more conductive properties in comparison with shales. Shales have an isolating capacity. This isolating capacity may cause heat conservation in layers below thick shale packages.

- *Ground water flow and meteoric infiltration;* Topography driven groundwater flow and the infiltration of meteoric water via permeable, surface reaching faults are two of the suggested causes of the decreased geothermal gradients in the eastern part of the Roer Valley Graben (Luijendijk et al., 2012). This anomaly in geothermal gradient is encountered in multiple wells throughout the area, but the data density is low. Most of the wells in this eastern part of the Roer Valley Graben are located nearby large offset (boundary) faults. Most of these large faults reach the surface, and they are expected to have been active during the Late Oligocene-recent rifting phase.

- *Magmatic bodies;* Magmatic bodies were drilled in several wells in which temperature measurement are conducted. Geothermal gradients calculated from this temperature data did not indicate specific anomalies. It is concluded that the drilled magmatic bodies do not have influence on the measured temperatures in the selected wells in the study area.

Petrophysics

From the petrophysic evaluation the following conclusions were made:

- In several wells sudden changes in caliper and density logs potentially indicate presence of faults
- The damage zone of a fault is difficult to establish with logs. Only well WLK-01 presents indications of such a zone.
- Many wells have penetrated faults. From the selected wells only well AND-06 contains log information of faults at reservoir level.

Seismics

- Significant deviation on the average geothermal gradient appear to relate to faults penetrating into the sediments of the North Sea Group.
- In region B a relative high fault density appears to be present with a slightly different fault orientation in respect to the rest of the study area (NNW-SSE versus NW-SE).
- The faults at the horst blocks of the RVG penetrate further into the North Sea Group in respect to the center of the graben. Some faults even reach close to the surface

Main conclusion

One geothermal gradient for the West Netherlands Basin and Roer Valley Graben does not exist.

The application of a single linear geothermal gradient is expected to under- and overestimate formation temperatures in the study area on a frequent base. Subsurface temperature increase over depth appears to be highly dependent on location, depth, structural framework and variety and thicknesses of different geological formations. A graphical presentation on the interpolated variation geothermal gradient in the subsurface of the study area is created (see figure 40, 41 and 42).

Elevated geothermal gradients appear to relate to NNW-SSE trending faults.

The increased geothermal gradients in the central part of the study area appear to relate to NNW-SSE trending faults. These faults appear to have been activated in the Late Oligocene-recent rifting phase.

Relation to geothermal exploration and production

Currently only a few geothermal installations have increased geothermal gradients. One of the practical applications for the outcome of this study is to check whether new geothermal wells can be placed in areas with elevated gradients, resulting in higher production temperatures. Following the geothermal gradient anomaly map, areas with increased geothermal gradients do overlap with current geothermal exploration licenses (as per February 2018). Calculations are conducted on the effect of a variation in geothermal gradient on the geothermal power output. The results indicated that 1 ^{o}C / kilometre extra can relate to an increase of approximately 6-7% in geothermal power output.

7 Recommendations

According to the findings and things that were run into during the project, the following recommendations are done:

- In order to give a correct representation of expected geothermal output power it is advised to add a P10/P50/P90 bar for the expected geothermal gradient in DoubletCalc. Currently only one geothermal gradient can be inserted in the TNO tool. This study indicated that the geothermal gradient can vary strongly between different locations. Subsequently, a single geothermal gradient does not seem to be applicable to the subsurface of the West Netherlands Basin and Roer Valley Graben.
- More research is advised on the exact causes of geothermal gradient anomalies in order to use the heat stored in the subsurface in the most efficient way.
- When geothermal exploration is conducted on local scale in the Roer Valley Graben, the temperature dataset presented by Luijendijk (2012) is expected to present the most accurate subsurface temperature prediction. However, the average geothermal gradient of 35,9 ˚C/km reported by Luijendijk deviates quite strongly from the average gradients in this study. This is remarkable as the uncertainty range of the Bottom Hole Temperature Recovery Model is significantly smaller as the statistical method that is used for this study. Further analysis should indicate how these difference can be explained.
- Future research is advised on the fault behavior during late Oligocene-recent rifting phase.
- The correlation between areas with increased geothermal gradients and geothermal reservoir presence will create a better insight in high potential geothermal energy locations. The development of such a map is recommended.
- An alternative method for formation temperature predictions could be developed by constructing a location specific geothermal gradient out of temperature building units. These building units (stratigraphic dependent geothermal gradients) with specific average geothermal gradients over their depth interval, added up to the total depth of the expected stratigraphic column. This could be integrated into existing 3D subsurface models, such as DGM Deep (TNO). This could provide a better indicative temperature prognosis on all onshore locations in the Netherlands in respect to the average geothermal gradient. To develop this technique further, more research is required.
- The study indicates clear zones in the study area with deviating geothermal gradients in respect to the average gradient of the Netherlands. It is likely that similar patterns may be identified in other basins in the Netherlands. Consequently, comparable studies may be of interest in basin areas where geothermal exploration is planned, such as the Noord-Holland Platform and the Friesland Platform.

8 Acknowledgements

The execution of this project is made possible by the Kennisagenda Aardwarmte (R&D initiative for geothermal energy) which is supported by the Dutch Ministry of Economic Affairs, LTO Glaskracht and Kas als Energiebron. We would like to thank these institutions for the financial support and trust that was granted for the project. Besides this, we would like to thank all data suppliers which were essential for the execution of the project. Special attention for: Damien Bonté, Eelco Luijendijk, Pieter Wijnen, TNO-AGE and EBN. At last we would like to thank the members of the *Begeleidingscommissie.*

9 References

1. Van Adrichem Boogaert, H. A., & Kouwe, W. F. (1997). Stratigraphic Nomenclature of the Netherlands, Revision and Update by RGD and NOGEPA, Meded. Rijks Geol. Dienst, 50.
2. Agemar, T., Alten, J.-A., Kühne, K., Kuder, J., Suchi E., Weber, J. and Schulz, R. (2015). A new geothermal approach to estimating the geothermal potential of faults in Germany. Proceedings World Geothermal Congress 2015, Melbourne, Australia, pp. 6
3. Van Balen, R.T., Verweij, J.M., , Van Wees, J.D., Simmelink, H., Van Bergen, F. & Pagnier, H. (2002). Deep subsurface temperatures in the Roer Varlley Graben and the Peelblock, the Netherlands – new results. Netherlands Journal of Geosciences / Geologie en Mijnbouw 81 (1): p. 19-26.
4. Bense, V.F., Person, M.A. (2006). Faults as conduit-barrier systems to fluid flow in siliciclastic sedimentary aquifers. Water Resources Research 2006; Vol. 42, W05421, pp. 18
5. Bense, V. F., Gleeson, T., Loveless, S. E., Bour, O., & Scibek, J. (2013). Fault zone hydrogeology. Earth-Science Reviews, 127, 171-192.
6. Blackwell D.D., Steele J.L. (1989) Thermal Conductivity of Sedimentary Rocks: Measurement and Significance. In: Naeser N.D., McCulloh T.H. (eds) Thermal History of Sedimentary Basins. Springer, New York, NY
7. Bonté, D., Van Wees, J.-D., Verweij, J.M. (2012). Subsurface temperatures of the onshore Netherlands: new temperatures dataset and modelling. Netherlands Journal of Geosciences – Geologie en Mijnbouw, 914, p. 491-515
8. Bonté, D., Struijk, M., Békési, E., Vrijlandt, M., and van Wees J.-D., (in prep). Thermal structure of the Netherlands subsurface.
9. Broothaers, M., 2013. Aanvullende toelichtingen voor de SEI aanvraag AARD03001 CLG BV. Vito rapport ETE/N13L1/MB/N13-01, p. 5,6,7 & 8
10. Caine, J. S., Evans, J. P., & Forster, C. B. (1996). Fault zone architecture and permeability structure. Geology, 24(11), 1025-1028.
11. Chester, J. S., & Chester, F. M. (1990). Fault-propagation folds above thrusts with constant dip. Journal of Structural Geology, 12(7), 903-910.
12. Childs, C., Manzocchi, T., Walsh, J. J., Bonson, C. G., Nicol, A., & Schöpfer, M. P. (2009). A geometric model of fault zone and fault rock thickness variations. Journal of Structural Geology, 31(2), 117-127.
13. Deming, D. (1989). Application of bottom-hole temperature corrections in geothermal studies. Geothermics, 18(5-6), 775-786.
14. Faulkner, D. R., Jackson, C. A. L., Lunn, R. J., Schlische, R. W., Shipton, Z. K., Wibberley, C. A. J., & Withjack, M. O. (2010). A review of recent developments concerning the structure, mechanics and fluid flow properties of fault zones. Journal of Structural Geology, 32(11), 1557-1575.
15. Ferket, H., Laenen B. & van Tongeren P.C.H., 2009. Diagenesis and reservoir characteristics of the Lower Carboniferous carbonates around Venlo. VITO rapport 2009/SCT/R/007, 45p.
16. Garibaldi, C. (2011) Détermination des températures profondes du Bassin du Sud-Est de la France et relations entre anomalies thermiques, géologie et circulations hydrothermales par modélisation 3D.Sciences de la Terre. Université Nice Sophia Antipolis, 2010. Français.
17. Hermanrud, C., Cao, S., & Lerche, I. (1990). Estimates of virgin rock temperature derived from BHT measurements: bias and error. Geophysics, 55(7), 924-931.

18. Houwers, M. E., Heijnen, L. J., Becker, A., & Rijkers, R. (2015). A workflow for the estimation of fault zone permeability for geothermal production: A general model applied on the ROER Valley Graben in the Netherlands. In Proceedings of the World Geothermal Congress (pp. 19-25).

19. Kombrink, H., Doornenbal, J. C., Duin, E. J. T., Den Dulk, M., Ten Veen, J. H., & Witmans, N. (2012). New insights into the geological structure of the Netherlands; results of a detailed mapping project. Netherlands Journal of Geosciences, 91(4), 419-446.

20. Kühn, M. (2004). Reactive Flow Modeling of Hydrothermal Systems (Vol. 103). Springer Science & Business Media.

21. Lipsey, L., Pluymaekers M., Goldberg T., van Oversteeg K., Ghazaryan L., Cloetingh S., van Wees J.D. (2016). Numerical modelling of thermal convection in the Luttelgeest carbonate platform, theNetherlands. Geothermics v64, p135- 151.

22. Loveless, S., Pluymakers, M., Lagrou, D., de Boever, E., Doornenbal, H. and Laenen, B. (2014). Mapping the geothermal potential of fault zones in the Belgium-Netherlands border region. Energy Procedia 59, pp. 351-358

23. Luheshi, M. N. (1983). Estimation of formation temperature from borehole measurements. Geophysical Journal International, 74(3), 747-776.

24. Luijendijk, E. (2012). The role of fluid flow in the thermal history of sedimentary basins: Inferences from thermochronology and numerical modeling in the Roer Valley Graben, southern Netherlands. PhD thesis, VU University Amsterdam, pp. 217

25. Mijnlieff, H.F., Obdam, A.N.M., van Wees, J.D.A.M., Pluymaekers, M.P.D. and Veldkamp, J.G. (2014) DoubletCalc 1.4 manual: English version for DoubletCalc 1.4.3., TNO.

26. Nieuwland, D. A., (2012). Prediction of Fault Sealing by Cataclasis: a calibrated quantitative geo-mechanical method. Presentation PGK D.A. Nieuwland, NewTec Internationaal B.V. (ppt)

27. Sclater, J., and P. Christie (1980), Continental stretching: An explanation of the post-mid-Cretaceous subsidence of the central North Sea Basin, Journal of Geophysical Research, 85(B7), 3711–3739.

28. Shen, P. Y., & Beck, A. E. (1986). Stabilization of bottom hole temperature with finite circulation time and fluid flow. Geophysical Journal International, 86(1), 63-90.

29. Vondrak, A. G. (2016). (Bio-) stratigraphic correlation of geothermal aquifers in the West Netherlands Basin. Kennisagenda Aardwarmte, Panterra report G1185, pp. 76

30. Ter Voorde, M., & Bertotti, G. (1994). Thermal effects of normal faulting during rifted basin formation, 1. A finite difference model. Tectonophysics, 240(1-4), 133-144.

31. Walsch, J.J., Watterson, J., Bailey, W., Childs, C. (1999) Fault Relays, Bends and Branchlines. Journal of Structural Geology 21, 1019–1026.

32. Wong, T.E., Batjes, D.A.J. and De Jager, J., (2007). Geology of the Netherlands. Royal Netherlands Academy of Arts and Sciences, 354 pp.

33. Worum, G., Michon L., van Balen, R.T., van Wees, J.D., Cloetingh, S., Pagnier, H. (2005) Pre-Neogene controls on present-day fault activity in the West Netherlands Basin and Roer Valley Rift System (southern Netherlands): role of variations in fault orientation in a uniform low-stress regime, Quaternary Science Reviews, Volume 24, Issues 3–4, pp. 473-488

10 Disclaimer

Het onderzoek waarover hier wordt gerapporteerd is op zorgvuldige wijze uitgevoerd volgens algemeen gebruikelijke inzichten en methoden.
Middels een ISO-9001:2000 en VCA** gecertificeerd kwaliteitssysteem waarborgt T&A de kwaliteit van haar diensten.

De bevindingen van de uitgevoerde studie berusten op petyrofysische analyse van gegevens van een reeks zorgvuldig geselecteerde diepe boringen binnen en in de directe nabijheid van het onderzoeksgebied en op de seismische interpretatie van 3D en 2D seismische surveys binnen het onderzoeksgebied. Dit betekent dat de studie is gebaseerd op een beperkt archiefonderzoek.

T&A acht zich niet aansprakelijk voor de schade die mogelijk voortvloeit uit het gebruik van haar onderzoeksresultaten.